Pathogenesis of 2009 Pandemic Influenza A Virus (H1N1) Infection in the Ferret Model

Beatriz Vidaña Mateo

Ph. D. thesis

Bellaterra, 2015

Pathogenesis of 2009 Pandemic Influenza A Virus (H1N1) Infection in the Ferret Model

Tesi doctoral presentada per la **Beatriz Vidaña Mateo** per optar al grau de Doctora en Veterinària dins del programa de doctorat de Medicina i Sanitat Animals del Departament de Sanitat i d'Anatomia Animals de la Facultat de Veterinària de la Universitat Autònoma de Barcelona, sota la direcció de la Dra. **Natàlia Majó i Masferrer** i el Dr. **Jorge Martínez Martínez.**

Departament de Sanitat i d'Anatomia Animals

Universitat Autònoma de Barcelona

Bellaterra, 2015

La Dra. NATÀLIA MAJÓ I MASFERRER, professora titular del Departament de Sanitat I d'Anatomia Animals de la Facultat de Veterinària de la Universitat Autònoma de Barcelona (UAB) i investigadora adscrita al Centre de Recerca en Sanitat Animal (CReSA), i el Dr. JORGE MARTÍNEZ MARTÍNEZ, professor adjunt del Departament de Sanitat I d'Anatomia Animals de la Facultat de Veterinària de la UAB i investigador adscrit al CReSA,

Certifiquen:

Que la memòria titulada "**Pathogenesis of 2009 Pandemic Influenza A Virus (H1N1) Infection in the ferret model"**presentada per la Beatriz Vidaña Mateo per a l'obtenció del grau de Doctor, s'ha realitzat sota la seva direcció i supervisió i , considerant-la acabada, n'autoritzen la seva presentació per tal de ser avaluada per la comissió corresponent.

I per tal que consti als efectes oportuns, signen el present certificat a Bellaterra, a 9 de Març de 2015

Dra. Natàlia Majó i Masferrer	Dr. Jorge Martínez Martínez	Beatriz Vidaña Mateo
Directora	Director	Doctoranda

Els estudis de doctorat de la Beatriz Vidaña Mateo han estat finançats per una Beca per a Personal Investigador en Formació, concedida pel Departament de Sanitat i Anatomia Animal de la Universitat Autònoma de Barcelona i el Centre de Recerca en Sanitat Animal, referència BPIF-1/2010-DEP.SAA-CReSA.

Aquest treball ha estat finançat pel projecte coordinat RTA-2011-00111-C03 del Instituto Nacional de Investigación y Tecnología Agraria y alimentaria (INIA), pel Instituto de Salud Carlos III ("Programa especial de investigación sobre la gripe pandémica" GR09/0023, GR09/0040, GR09/0039) i el Servei de Diagnòstic de Patologia Veterinària (SDPV) de la Universitat Autònoma de Barcelona.

Abbreviations……i

Summary/Resumen.....vii

PART I: GENERAL INTRODUCTION AND OBJECTIVES.....1

CHAPTER 1: GENERAL INTRODUCTION……3

1. Influenza Virus……5

1.1. History of Influenza.....5

1.2. Etiology.....5

1.2.1. Classification and Nomenclature.....5

1.2.2. Morphology and Molecular Organization.....6

1.3. Replication Cycle.....8

1.4. Antigenic Diversity.....10

1.4.1. Antigenic Drift.....10

1.4.2. Antigenic Shift.....10

1.5. Host Range and Species Adaptation..... 11

1.6. Viral Factors in Influenza Pathogenicity.....12

1.7. Host Immune Response to Influenza Virus Infection.....14

1.7.1. Viral Detection and Activation of the Innate Immunity.....15

1.7.2. Cellular Innate Immune Response.....17

2. Swine Origin Influenza A virus H1N1 and the 2009 Pandemic.....18

2.1 History of Influenza A Pandemics.....18

2.1.1 Influenza A Pandemics of the 20th Century.....18

2.2 The 2009 H1N1 Virus Pandemic.....19

2.2.1 Genetic Characteristics and Formation of H1N1v……..20

2.2.2 Antiviral Resistance.....22

2.2.3 Epidemiology and Transmission……22

2.2.4 Clinical Disease……24

2.2.5 Gross and Microscopic Lesions……24

2.2.6 H1N1v Pathogenesis.....25

3. Animal Models for Human Influenza.....29

3.1 Mice.....31

3.2 Cynomolgus Macaques.....32

3.3 Ferrets.....33

CHAPTER 2: HYPOTHESIS AND OBJECTIVES.....39

PART II: STUDIES.....41

CHAPTER 3. STUDY I: ***Immune System Cells in Healthy Ferrets. An Immunohistochemical Study***.....43

3.1 Introduction.....45

3.2 Material and Methods.....45

3.3 Results.....52

3.4 Discussion.....63

CHAPTER 4. STUDY II: ***Experimental Infection of Ferrets with Two Wild Type H1N1v Viral Isolates from Patients Presenting Different Pathological Outcomes of Disease***.....67

4.1 Introduction.....69

4.2 Material and Methods.....70

4.3 Results.....77

4.4 Discussion.....85

CHAPTER 5. STUDY III: ***Experimental Infection of Ferrets Infected with a Wild Type and an Oseltamivir-Resistant H1N1v Viral Isolates from Patients Presenting Fatal Pathological Outcomes***.....91

5.1 Introduction.....93

5.2 Material and Methods.....94

5.3 Results.....99

5.4 Discussion.....107

CHAPTER 6. STUDY IV: ***Involvement of the Different Lung Anatomic Compartments in the Pathogenesis of H1Nv1 Influenza Virus Infection in ferrets***.....111

6.1 Introduction.....113

6.2 Material and Methods.....114

6.3 Results.....119

6.4 Discussion.....125

PART III: GENERAL DISCUSSION AND CONCLUSIONS.....129

CHAPTER 7: GENERAL DISCUSSION.....133

CHAPTER 8: CONCLUSIONS.....145

REFERENCES.....149

ANNEX.....173

A

ABC: avidin-biotin-peroxidase complex

Ag: antigen

APP: acute phase proteins

ARDS: acute respiratory distress syndrome

B

BALT: bronchus associated lymphoid tissue

BAX: BCL2-associated X protein

bp: base pairs

BSA: bovine serum albumin

BSL-3: biosafety level 3

C

CASP8: caspase 8

CCL: C-C motif ligand

CCR: chemokine receptor type

CD55: complement decay-accelerating factor

CDC: Centre for Disease Control and Prevention

CNM: Centro Nacional de Microbiología

COPD: chronic obstructive pulmonary disease

CReSA: Centre de Recerca en Sanitat Animal

cRNA : complementary RNA

cRNA: complementary RNA

Ct: threshold cycle

CTL: cytotoxic T cells

CXCL : C-X-C motif ligand

D

DAB: 3,3'-diaminobenzidine tetrahydrochloride

DAD: diffuse alveolar damage

DC: dendritic cell

DIP: defective interfering particles

dpi: days post infection

E

EDTA: ethylenediaminetetraacetic acid

ELISA: enzyme-linked immunosorbent assay

eRNA: extracellular RNA

F

Fc: fragment crystallizable

FFPE: formalin-fixed paraffin-embedded

G

GEC: genome equivalent copies

GISAID: Global Initiative on Sharing Avian Influenza data

H

h: hour

H1N1v: 2009 H1N1 influenza a virus

HA: hemagglutinin

HE: haematoxylin and eosin

HI: hemagglutination inhibition assay

HLA: human leukocyte antigen

Hp: haptoglobin

HPAI: highly pathogenic avian influenza

hpi: hours post infection

I

IAV: influenza A virus

ICU: intensive care unit

IFITM: interferon-inducible transmembrane

IFN: interferon

IFNR: interferon receptor

Ig: immunoglobulin

IHC: immunohistochemistry

IL: interleukin

ISCIII: Instituto de Salud Carlos III

L

LCM: laser capture microdisssection

M

M1 : matrix protein

M2: membrane ion channel protein

MDCK: Madin Darby Canine Kidney

MHC: major histocompatibility complex

min: minutes

mRNA: messenger RNA

N

NA: neuraminidase

NBT-BCIP: nitroblue tetrazolium- 5-Bromo-4-chloro-3-indolyl phosphate

NCBI: NCBI nucleotide data base

NEP: nuclear export protein

NF-kB: nuclear factor Kappa Beta

NI: neuraminidase inhibitor

NK: natural killer

NOS2: nitric oxide synthase 2

NP: nucleoprotein

NS1: non-structural protein 1

NS2: non-structural protein 2

O

OCT: optimum cutting temperature medium

OR: Oseltamivir-resistant

P

PA: polymerase acid protein

PAMP: pathogen-associated marker pattern

PB1: polymerase basic protein 1

PB1-F2: polymerase basic protein 1- frame 2

PB2: polymerase basic protein 2

PBS: phosphate buffered saline

PFU: plaque forming unit

PRRs: pattern-recognition receptors

R

RBC: red blood cells

RDE: receptor destroying enzyme

RIG-I: retinoic acid inducible gene-I

RNA: ribonucleic acid

RNP: viral ribonucleoprotein

RRT-PCR: real time reverse transcription polymerase chain reaction

RT: room temperature

S

SA: sialic acid

SAA: serum amyloid A

SARS: severe acute respiratory syndrome

SELPLG: selectine P-ligand

SEMs: standard errors of the mean

SNP: single nucleotide polymorphism

svRNA: small viral RNA

T

$TCID_{50}$: 50% tissue culture infective dose

Th: T helper

TLR: toll-like receptor

TNF: tumor necrosis factor

TRAIL: tumor necrosis factor related apoptosis-inducing ligand

U

UAB: Universitat Auntonoma de Barcelona

V

vRNA: viral ribonucleic acid

W

WHO: World Health Organization

Wt: wild type

Influenza A virus (IAV) infection is an acute and recurring respiratory disease which has an elevated effect on public health worldwide. IAV infection is highly contagious and unique among human viruses, having two epidemiological modes, as seasonal epidemics, or over longer time periods, as pandemics. The first pandemic of the 21st century occurred in 2009 by an H1N1 type virus, causing high rates of morbidity and more than 250.000 deaths around the world. Overall, the case fatality rate was similar to that of seasonal influenza. However, previously healthy young adults and children were disproportionally affected, accounting for more than 60% of the reported cases. The pandemic H1N1 virus has now been established itself worldwide, replacing the previous seasonal H1N1 virus. Currently, the infection causes predominantly mild disease, but it can develop onto severe illness in some cases. Severe pandemic H1N1 outcomes have been related to high viral replication capacities and exacerbated host inflammatory immune responses.

The pathogenesis of pandemic H1N1 infection results from various processes involving the host immune system and their response to virus-induced changes. Understanding both virus and host response characteristics in severe and mild infection cases is important for the future development of therapeutic strategies. Several investigations have been carried out in order to understand the physiopathology of pandemic H1N1 infection. Among influenza animal models, the ferret is an attractive model due to the fact that they share similar lung physiology with humans and demonstrate a similar disease entity, without prior viral adaptation. However, the immune system of ferrets has not been very well characterised.

In **study I** of this dissertation, we characterised different immune system cells in ferret tissues in order to then characterise viral-host interactions, occurring in the lungs of H1N1v infected ferrets. In **study II**, we used the ferret model to study the differences in virulence of two human viral isolates, presenting similar genetic characteristics, yet resulting in different disease outcomes in human patients (death vs. mild symptoms). In **study III**, we studied two human viral isolates with different genetic characteristics (one wild type virus and one virus with the H275Y mutation,

conferring resistance to Oseltamivir antivirals) in patients who developed the same disease outcome (death).

The experimental infection of ferrets with human H1N1 viral isolates was associated with different degrees of lung damage. More severe lung lesions correlated with viral replication in alveolar areas, higher proinflammatory cytokine release in the lungs, and higher lung inflammatory infiltrates, as observed in human patients. Our results revealed that the presence of viral replication in alveolar areas was not only related to viral capacities, but also to the type of host immune response triggered by the infection. In the case of viral strains with similar viral capacities, the development of severe or mild disease depended on the type of immune response triggered by the host. Infected animals showed different pathological outcomes, depending on the type/magnitude of the host immune response, and independently of the viral strain inoculums. On the contrary, in the presence of viral mutations affecting viral growth, pathogenicity was related to viral kinetics. Ferrets infected with the Oseltamivir resistant virus (presenting slower viral kinetics) presented milder pathological lesions, when compared with ferrets infected with the wild type isolate.

In both studies, more severe lung lesions correlated with viral replication in alveolar areas and higher expression of the proinflammatory cytokines IL-6, CXCL10, CCL5, CCL3, IL-8, TLR3, and apoptotic markers (BAX and CASP8). These cytokine profiles correlated with the inflammatory phenotype observed in the lungs, characterised by high numbers of macrophages and neutrophils in apoptosis, accompanied by large numbers of cytotoxic T, and NK cells. In contrast, milder lung lesions correlated with viral replication, mainly occurring in bronchiolar areas, and with a higher induction of type I IFN and RIG-I genes, suggesting that IFN induction is beneficial for the host, after IAV infection.

From the above mentioned observations, we hypothesized that the different expression of proinflammatory genes, and therefore, the income of leukocytes to the lungs, plays a role in the development of severe pathology after influenza infection.

The income of leukocytes into the lungs is mediated through the signalling effects of innate immune molecules, like cytokines and chemokines, induced by different cell types in the lungs. In **the study IV**, we studied the induction of different innate immune molecules in different lung anatomic compartments (bronchiolar, alveolar and vascular), in response to pandemic H1N1 infection in the ferret model, by means of laser capture microdissection. Our results showed that bronchiolar areas initiate the innate immune response and the first influx of inflammatory cells after viral infection, through the expression of IFNα, IL-6, TNFα and IFNγ. However, TLR3 and CCL2 expression was mainly observed on vascular areas throughout infection, and vascular areas also presented an up-regulated expression of IL-6 and IFNγ, indicating its contribution to the innate immune response during early stages of infection. Interestingly, viral RNA was also detected by real time RT-PCR in vascular areas, but no viral replication by immunohistochemistry was observed. From these results, we hypothesized that vascular areas induce an innate immune response at early stages post infection, through the recognition of viral RNA or a crosstalk with infected cells.

The present dissertation highlights the notion that viral replication location and the correct orchestration of the early inflammatory immune response are key factors in the development of severe influenza. We believe that this thesis provides new data which aids in clarifying the role of the host immune response in the divergent pathogenesis observed in pandemic H1N1 infection. Understanding the interactions between both viral genetic characteristics within the host immunogenetic context is of great importance to the development of future therapeutic strategies, against influenza infection.

La infección causada por el virus influenza A (VIA) causa una enfermedad aguda y recurrente con graves consecuencias sobre la salud pública mundial. El VIA es altamente contagioso y único entre las infecciones humanas presenta dos patrones epidemiológicos. Uno como epidemias estacionales anuales y otro como pandemias cada largo periodo de tiempo. En el 2009 se produjo la primera pandemia del siclo XXI, la cual presentó alta morbilidad causando más de 250.000 muertes alrededor del mundo. La mortalidad observada durante la pandemia fue similar a la observada en previas epidemias estacionales. Sin embargo, adultos jóvenes y niños resultaron desproporcionalmente afectados, resultando en un 60% de los casos descritos. Desde el inicio de la pandemia, el virus H1N1pandémico se ha establecido alrededor del mundo desplazando al anterior virus H1N1 estacional. Actualmente, la infección causada por el virus H1N1 pandémico resulta primordialmente en enfermedad leve, no obstante puede resultar en enfermedad grave en algunos casos. Los casos severos descritos se han relacionado con altos niveles de replicación viral acompañados de respuestas inflamatorias exacerbadas.

La patogénesis causada por la infección del virus pandémico H1N1 es el resultado de varios procesos los cuales involucran tanto las capacidades infectivas virales como la respuesta inmunitaria del huésped. Por lo tanto, el entendimiento de ambas características y sus interacciones es importante para el desarrollo de futuras estrategias terapéuticas contra la infección.

Varias investigaciones se han llevado a cabo para entender la patofisiología de la infección de los VIA. Entre los modelos animales utilizados, el hurón es uno de los modelos más atractivos ya que hurones y humanos comparten una fisiología pulmonar y una enfermedad clínica similar. Sin embargo, el hurón presenta varios inconvenientes, entre los cuales se encuentra la limitada caracterización de su sistema inmune.

En el **estudio I** de esta tesis, se han caracterizado diferentes aspectos del sistema inmune del hurón para posteriormente utilizar el modelo de hurón en la

infección experimental de diferentes aislados humanos del virus pandémico H1N1 para finalmente estudiar las interacciones ocurridas entre el virus y la respuesta inmune del huésped.

En el **estudio II**, se han estudiado las diferentes virulencias de dos aislados virales con características víricas semejantes, pero que resultaron en patología de diferente gravedad, en los respectivos pacientes humanos (síntomas leves versus fallecimiento). En el **estudio III**, se han estudiado la diferentes virulencias de dos aislados virales con diferentes características víricas (un virus natural y un virus resistente a Oselamivir portador de la mutación "H275Y"), los cuales fueron aislados de pacientes humanos que desarrollaron infecciones fatales.

La infección experimental en hurones con diferentes virus pandémicos H1N1 humanos se asoció a daño pulmonar de diferentes grados. En general, las lesiones pulmonares más severas correlacionaron con replicación viral en aéreas alveolares, elevada expresión de genes inductores de citoquinas a nivel pulmonar y presencia de infiltrados inflamatorios pulmonares. Nuestros resultados han revelado que la presencia de replicación viral en áreas alveolares no está únicamente relacionada con las capacidades infectivas virales sino también con el tipo de respuesta inmune inducida por el huésped. Animales infectados con cepas virales de similares características, desarrollaron diferentes grados patológicos dependiendo del tipo/magnitud de la respuesta inmune del huésped e independientemente de la cepa vírica inoculada. Por el contrario, en el caso de animales infectados experimentalmente con cepas virales con diferentes mutaciones afectando la velocidad de replicación viral, la patogenia observada en los animales se relacionó con la cinética viral del inoculo. Los hurones infectados con el virus resistente al antiviral Oseltamivir presentaron una patología más leve en comparación con los hurones infectados con un aislado vírico natural.

En ambos estudios, las lesiones pulmonares severas correlacionaron con la presencia de replicación viral en pneumocitos y con un aumento en la expresión de los

genes de la inmunidad innata TLR3, IL-6, CXCL10, CCL5, CCL3, IL-8 además de los marcadores apoptóticos (BAX y CASP8). Estos perfiles de expresión genética, a su vez se correlacionaron con el fenotipo de células inflamatorias observadas en los pulmones. El fenotipo celular se caracterizó por altos números de macrófagos y neutrófilos en apoptosis acompañados de elevados números de células T citotóxicas y células NK. Por el contario, las lesiones pulmonares leves se correlacionaron con la presencia de replicación viral restringida a áreas bronquiolares además de un aumento en la expresión génica de los genes de la inmunidad innata IFN tipo I y RIG-I, sugiriendo que la inducción de IFN tras la infección por VIA es beneficiaria para el huésped.

La entrada de leucocitos a los pulmones está marcada por la señalización de moléculas de la inmunidad innata, como las citoquinas y las quemoquinas, las cuales inducen la migración de diferentes tipos celulares a los pulmones. En el **estudio IV**, hemos utilizando la técnica de microdisección de captura láser para estudiar la expresión génica y por lo tanto la señalización de la inmunidad innata en diferentes compartimentos anatómicos pulmonares (bronquiolar, alveolar y vascular), en respuesta a la infección por el virus pandémico H1N1 en hurones. Los resultados obtenidos han identificado a las áreas bronquiolares y alveolares como las primeras inductoras de la respuesta inmune innata tras la infección y por tanto responsables del primer influjo de células inflamatorias, a través de la expresión génica de IFNα, IFNγ, IL-6 y TNF. Sin embargo, la expresión de TLR3 y CCL2 fue principalmente observada en áreas vasculares durante la infección. Asimismo, las áreas vasculares también presentaron una elevada expresión de los genes IFNγ e IL-6, apuntando a su importante contribución en el influjo de células inflamatorias al pulmón y en la inducción de la respuesta innata en los primeros estadios de la infección. A pesar de que no se observó la presencia de antígeno vírico y por tanto de replicación activa del virus en áreas vasculares. Sí, se detectaron elevados niveles de ARN viral por RT-PCR a tiempo real en áreas vasculares. Estos resultados indican que las áreas vasculares pulmonares podrían contribuir a la inducción de la respuesta inmune innata a través

del reconocimiento de RNA viral o a través de la comunicación con células infectadas en otras áreas pulmonares.

La presente tesis subraya la importancia de la localización de replicación viral junto con la correcta orquestación de la respuesta inflamatoria inmune temprana como factores determinantes en el desarrollo de patología severa, tras la infección con el VIA. Creemos que esta tesis proporciona datos nuevos para clarificar el rol del la respuesta inmune en la patogenia divergente observada tras la infección del virus H1N1 pandémico del 2009. El entendimiento de las interacciones entre las características víricas genéticas y la respuesta inmunológica del huésped son importantes para el desarrollo de futuras estrategias terapéuticas contra la infección por el virus influenza.

The results presented in this dissertation have been published in international scientific peer-reviewed journals:

Vidaña, B., Majo, N., Perez, M., Montoya, M., Martorell, J. & Martinez, J. (2013). Immune System Cells in Healthy Ferrets: An Immunohistochemical Study. *Vet Pathol*. 17;51(4):775-786.

Vidaña, B., Martinez, J., Martinez-Orellana, P., Garcia Migura, L., Montoya, M., Martorell, J. & Majo, N. (2014). Heterogeneous pathological outcomes after experimental pH1N1 influenza infection in ferrets correlate with viral replication and host immune responses in the lung. *Vet Res* 45, 85.

Vidaña, B., Martorell, J., Baratelli, M., Martinez, J.; Martinez-Orellana, P., Migura, L.G., Cordoba, L., Perez, M., Casas, I., Pozo, F., , Majo, N. & Montoya, M. (2015). Oseltamivir-resistant A(H1N1) pdm09 influenza virus exhibited lower pathogenicity than its wild type counterpart in ferrets. *Under revision at Journal of General Virology.*

Vidaña, B., Martínez, J., Martorell, J., Fraile, L., Córdoba, L., Pérez, M., Montoya, M. & Majó, N. (2015) Involvement of the different lung compartments in the pathogensis of pH1N1 influenza virus infection in ferrets. *In preparation.*

PART I

GENERAL INTRODUCTION AND OBJECTIVES

CHAPTER 1

GENERAL INTRODUCTION

1. Influenza Virus

1.1 History of Influenza

Influenza virus infection affects several animal species as well as humans, and has done so since antiquity [1]. The disease was probably first described by Hippocrates in 412 B.C [2], although the term Influenza was coined by the Italians much later on. The Italians used the expression "*ex influenza colesti"* in allusion to the widely held belief that the epidemic was of celestial influence[3], and references can be found in scientific and lay publications from 1650 onwards [4]. The first convincing report of an influenza pandemic was written by Molineux [5] in the 17th century. Numerous reports of influenza epidemics followed from the 17th to the 19th century, across America and Europe, appearing in several publications [6,7]. In 1930's, the agent which causes human influenza was discovered and isolated for the first time [8]. Today, human influenza occurs annually as seasonal influenza, mainly in the winter months of temperate climates; every several years as inter-pandemic epidemics; and sporadically at an average of 35 year intervals, as pandemics [9].

1.2 Etiology

1.2.1 Classification and Nomenclature

All human influenza viruses belong to the *Orthomyxoviridae* family which includes three influenza genera; Influenza A, B and C [10]. Influenza viruses are enveloped viruses that contain single-stranded ribonucleic acid (RNA) of negative polarity, contained in 7 or 8 gene segments (Figure 1) [11]. The three influenza genera differ in host range and pathogenicity, and have probably diverged evolutionarily over several thousand years [11]. Influenza B- and C-type viruses are adapted to, and isolated almost exclusively from, humans [12]. In contrast, influenza A viruses (IAVs) infect a wide range of warm-blooded animals [13].

Type A is the most important of the influenza viruses, causing alternate annual outbreaks and epidemics worldwide [14]. IAVs are divided into subtypes based on major

antigenic specificities of their hemagglutinin (HA) and neuraminidase (NA) proteins, by which they are classified. Eighteen types of HA and ten types of NA have been reported. Most HA and NA subtypes have been described in avian species, whereas, subtypes reported in mammals are more restricted in their host range, with HA 17, HA 18 and NA 10 having only been reported in bats [15-17].

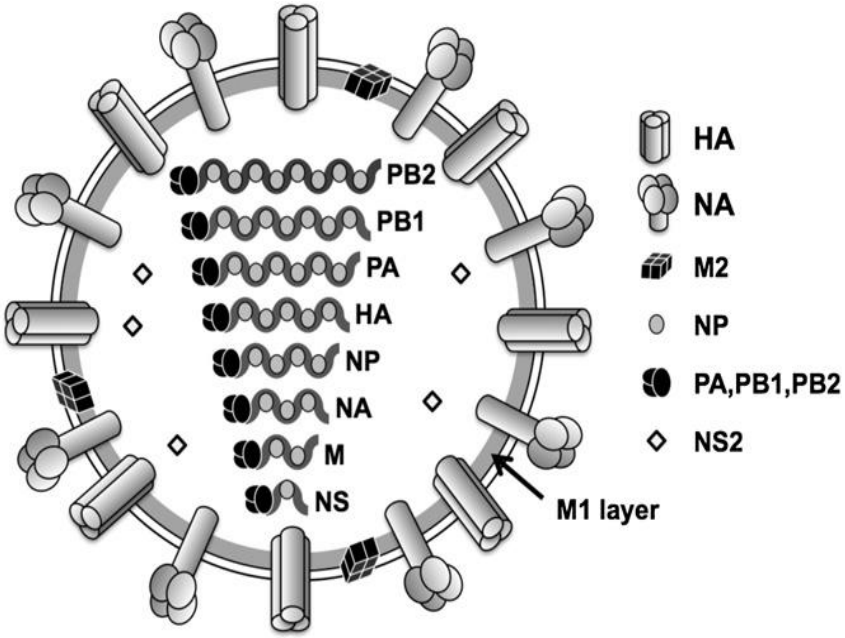

Figure 1. Diagrammatic representation of an Influenza A Virus. The two major surface glycoproteins, hemagglutinin (HA) and neuraminidase (NA), along with small numbers of the matrix 2 (M2) ion channel protein, are embedded in a lipid bilayer. The matrix 1 (M1) protein underlies the envelope and interacts with the surface proteins and also with the ribonucleoproteins (RNPs). RNPs consist of the eight negative-stranded RNA segments and nucleoprotein (NP) and the polymerase complex heterotrimer (PA, PB and PB2). The nuclear export protein (NEP, or nonstructural protein 2, NS2) is contained within the virion, but the nonstructural protein 1 (NS1) is not. Adapted from Taubenberger & Kash, 2010 [18].

1.2.2 Morphology and Molecular Organization

IAVs are pleomorphic RNA encapsulated virus of 80-120 nm, which contain eight gene segments, encoding at least 11 proteins with different functions (Table 1) [19]. The envelope of the virus consists of a host cell membrane lipid bilayer, covered with projections of the three surface proteins: HA, NA, and membrane ion channel protein (M2) (Figure 1).

Of the surface proteins, HA is a glycosylated type I integral membrane protein which binds the virus to sialic acid (SA) receptors in the host cell. IAVs have HAs with different specificities for SAs [20]. For example, IAV adapted to humans have higher specificity for α2,6 SA, whilst avian-adapted viruses present higher specificity for α2,3 SA receptors [20]. NA is a type II integral membrane glycoprotein, with sialidase enzymatic activity, which is required for cleavage from host cell SAs. In addition, NA allows the release of newly produced virions from infected cells, and prevents aggregation of new viral particles. Finally, the tetramer (M2) membrane protein is a small proton channel which forms an ion channel between the interior of the virus and its environment[21].

IAVs internal proteins include the matrix protein 1 (M1), and the viral ribonucleoprotein (RNP) complexes. RNPs consist of eight negative-stranded RNA segments, the nucleoprotein (NP) and the polymerase complex proteins which classically consist in: the polymerase basic protein 2 (PB2), the polymerase basic protein 1 (PB1), and the polymerase acidic protein (PA) (Figure 1). Additionally, another small viral protein, polymerase basic protein 1- frame 2 (PB1-F2), is variably encoded within the PB1 gene in some IAVs [21].

Segment	Size	Protein	Function
1 (PB2)	2341	Polymerase basic 2	Transcriptase: cap binding
2 (PB1)	2341	Polymerase basic 1 PB1-F2 (frame 2)	Transcriptase: elongation Virulence
3 (PA)	2233	Polymerase acidic	Transcriptase: protease activity
4 (HA)	1778	Hemagglutinin	Binding the virus to the host cell
5 (NP)	1565	Nucleoprotein	RNA binding: part of transcriptase complex
6 (NA)	1413	Neuraminidase	Release of mature virions from the host cell
7 (M or MP)	1027	M1, matrix protein 1 M2, matrix protein 2	Component of viral envelope Integral membrane protein: ion channel
8 (NS)	890	NS 1 (non-structural 1) NS2/NEP (non-structural /nuclear export protein)	Counters interferon, a product of the host immune system Effects on cellular RNA transport from the host cell nucleus to the cytoplasm, splicing, translation

Table 1. The eight segments of IAV encoding eleven proteins, lengths and functions. Adapted from Christman *et al.* 2011 [21].

Besides the internal and surface proteins, IAVs posses two non-structural proteins named nonstructural protein (NS)1 and NS2, also referred as nuclear export proteins (NEP), which are essential for the migration of the viral RNP out of the nucleus [11].

1.3 Replication Cycle

IAVs are dependent on the host RNA processing machinery for their replication. In order to achieve the replication cycle, the virus needs to infect the host cell, get imported into the nucleus, be replicated and then exported back out to the cytoplasm [22]. The infective process of IAVs starts with the binding of the HA glycoproteins to the SA host cell receptors. Upon binding to the host cell's SAs, receptor-mediated endocytosis occurs and the virus enters the host cell in an endosome. The acidic pH in the endosomal compartment leads to a conformational change in the HA protein, which then expresses a fusion peptide. This fusion peptide inserts itself into the host cell endosomal membrane, bringing both the viral and the endosomal membranes into contact with each other. Here, the M2 protein plays a key role in this process, as it allows H^+ ions to enter the virion, promoting an acidic pH in the endosomal compartment. Then, the acidic environment in the virion-endosome compartment releases the viral RNPs from M1, to enter the host cell's cytoplasm (Figure 2) [12,23].

Once the viral RNPs are liberated into the cytoplasm, they are imported into the nucleus [22]. In the nucleus, the viral RNA (vRNA) is copied by the polymerase complex, resulting in three types of vRNA; i) The complementary RNA [(+)cRNA], which serves as a template to generate more vRNA; ii) small viral RNAs (svRNAs) which regulate the switch from transcription to regulation; and iii) the viral messenger RNAs [(+)mRNAs] [24,25], which migrate from the nucleus to begin viral protein translation in the cytoplasm [24] (Figure 2).

Afterwards, some of the newly synthesized cytoplasm viral proteins are transported to the nucleus, where they bind to vRNA to form viral RNPs. Other

proteins are processed in the endoplasmic reticulum, where glycosylation of the three integral membrane proteins (HA, NA and M2) occurs [26]. HA, NA and M2 are then folded and trafficked to the Golgi apparatus for post-translational modification, to be eventually transported to the cell membrane, where they stick in the lipid bilayer [26].

Nuclear localization of M1 and NEP/NS2 proteins are essential for the migration of the vRNP out of the nucleus, and assembly into progeny viral particles in the cytoplasm [27]. Finally, when all the new viral proteins are formed, the M1 protein brings the complex RNP-NEP into contact with the envelope-bounded HA, NA and M2 proteins for packaging at the host cell membrane [24] (Figure 2). Then, NA releases progeny from host cells by using its destroying activity to cleave the terminal SA residues of the cell surface, and removes the SA from the virus envelop, preventing viral aggregation [28].

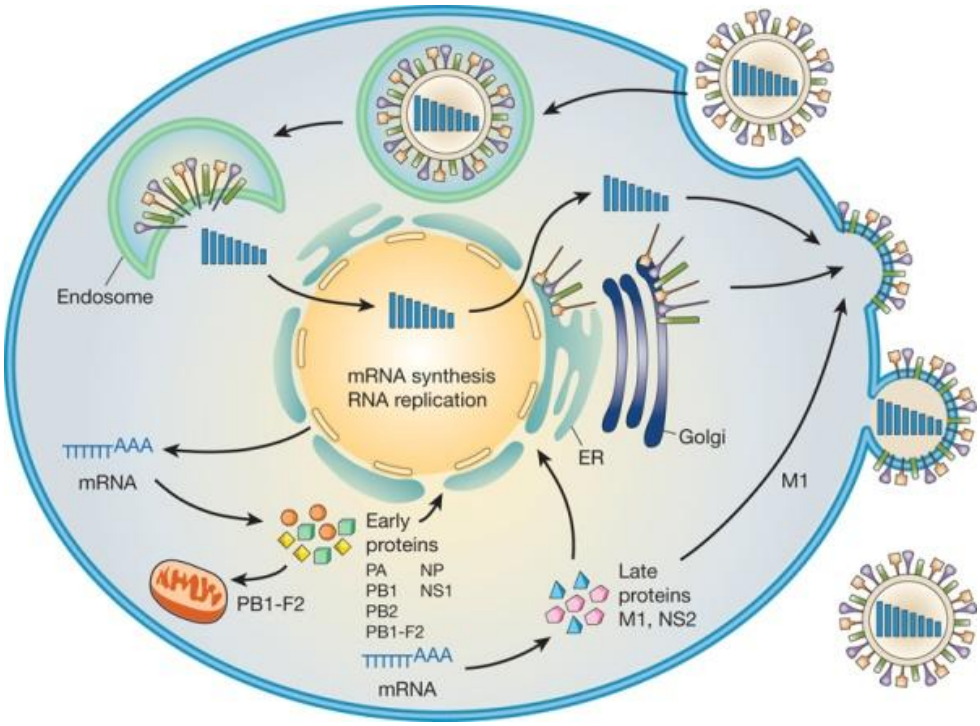

Figure 2. Schematic diagram of the influenza viral life cycle. The HA protein is critical for binding to cellular receptors and fusion of the viral and endosomal membranes. Replication and transcription of vRNAs are carried out by the three polymerase subunits PB2, PB1 and PA, and the nucleoprotein NP. Newly synthesized viral RNP complexes are exported from the nucleus to the cytoplasm by NS2 and the matrix protein M1, and are assembled into virions at the plasma membrane. The NA protein facilitates virus release from infected cells by removing sialic acids from cellular and viral HA and NA proteins. Adapted from Neumann *et al.* 2009 [23].

1.4 Antigenic Diversity

The major aim of viral pathogens is to ensure their multiplication in the host, avoiding host specific immunity and obtaining a long-term survival. The IAV strategy to achieve long-term persistence in its host is to maintain antigenic heterogenicity. This is accomplished via two distinct mechanisms: i) the existence of many different subtypes based on the surface proteins, and ii) high and rapid mutation genetic rates, particularly in the HA and NA surface proteins [29].

1.4.1 Antigenic Drift

IAVs are evolutionary dynamic viruses that have high mutation rates (ranging from approximately 1 x 10^3 to 8 x10^3 substitutions per site per year) [30]. Viral mutations are especially important for IAVs adapted to humans because they are subjected to strong immunologic population pressures. Antibodies against the HA protein prevent receptor binding, they can also neutralize, as well as being effective at preventing reinfection by the same strain [31]. Viral mutations often change amino acids in the antigenic portions of the surface proteins HA and NA, producing selective advantages and allowing viral strains to evade preexisting immunity. These selective mutations in the antigenic domains of HA and NA have been referred to as antigenic drift [18]. These selective mutations explain annual epidemics, since the antibodies acquired by previous infections are less efficient in protecting against mutated viruses. As mutations accumulate, there is a tendency towards no protection whatsoever throughout the various epidemics [18].

1.4.2 Antigenic Shift

Co-infection of one host cell with two different IAVs is possible as IAV genome consist of eight single RNA segments, resulting in progeny viruses containing gene segments of both parental viruses, in a process called genetic reassortment. Genetic reassortment has been shown to be common and important in IAV evolution [32,33]. When genetic reassortment involves the gene segments encoding the HA and/or NA

genes, antigenic shift occurs, and a complete and genetically new viral subtype emerges [29].

1.5 Host Range and Species Adaptation

IAVs have been isolated from a wide range of both mammal and avian species [15,34] (Figure 3). Almost all antigenic forms of IAV have been reported in avian species, while only some have been isolated from mammals [35]. Phylogenetic studies have shown that all mammalian IAV strains derive from the avian IAV pool [12] .

In general, IAVs are distributed around the world in wild avian species, which are considered viral reservoirs. Stable host switch events from wild birds to novel hosts, including domestic gallinaceous poultry, horses, swine and humans, have lead to the emergence of viral lineages which are transmissible in the new host. The emergence of these new lineages involves the acquisition of a variable number of mutations, which evolve in an eight distinct segment genome with the new host [32,36], and separate the derived IAV strain from the large wild bird IAV gene pool. As it becomes fully adapted to a new host, the virus becomes more species specific and less efficient to replicate in the original host species [37]. Domestic poultry are not natural reservoirs of avian IAV, but are the most frequent hosts susceptible to infection with wild-bird-derived IAV after adaptation [12].

In mammals, IAVs have been consistently isolated from pigs, horses and humans, which are permanent hosts with species specific viral strains [18]. IAVs of different subtypes have been isolated globally, especially in swine. Swine possesses both α2,6 and α2,3 SA linkages on tracheal epithelial cells, conferring this species dual susceptibility to avian and human IAVs [13]. For that reason, swine has been considered a key intermediate host for the generation of IAVs of pandemic potential to humans [13].

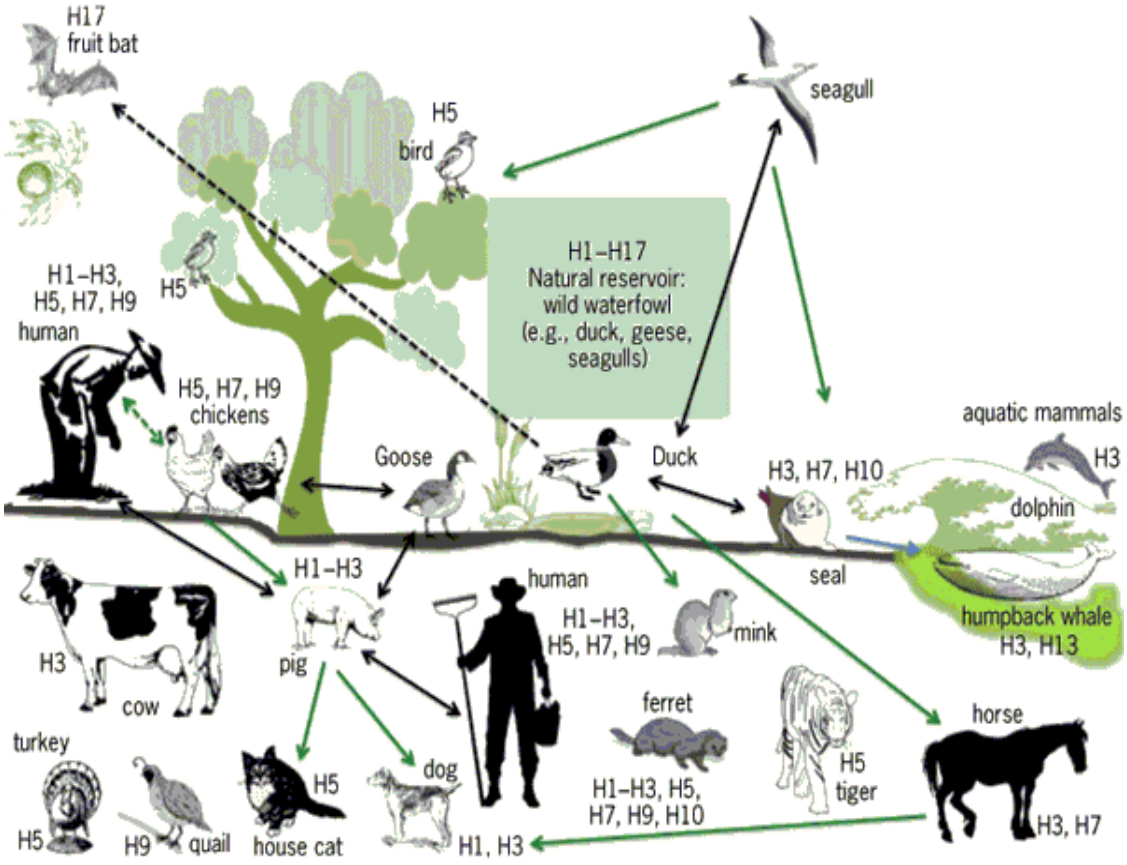

Figure 3. Ecology and host range species of influenza a viruses. Adapted from Shors *et al.* 2013 [38].

Direct influenza virus infections of zoonotic origin and without reassortment, can occur in humans, although this is not common. These zoonotic agents derive mainly from pigs, poultry and horses, and typically show low virulence for humans [18,39,40]. Nevertheless, zoonotic infections from poultry and swine have also resulted in severe illnesses in humans [41-45], or the generation of new host specificity, as was the case of the 2009 H1N1 pandemic virus.

1.6 Viral Factors in Influenza Pathogenicity

Influenza viral pathogenicity has been linked to particular genetic mutations in specific viral proteins of influenza viruses [23] (Table 2). A major virulence determinant in IAVs, is the presence of multiple basic amino acids around the cleavage sites of the **HA** protein. This mutation has only been found in viruses of the H5 and H7 subtypes [46-48], and confers these viruses the capacity to be recognized by ubiquitous host proteases,

allowing systemic infection in poultry [49]. However, no human influenza virus with a multi-basic cleavage site in the HA has as yet been isolated [50]. Differences in the SA binding site of the HA protein determine the receptor binding specificity for human and avian IAVs [51]. Human influenza viruses predominantly bind to α2,6 SA host receptors which are expressed in the human upper respiratory tract. Meanwhile, avian influenza viruses predominantly bind to α2,3 SA receptors, expressed in the avian respiratory and intestinal tract [52-54].

The viral replication complex **PB2** has been recognized as a contributor to viral pathogenicity by affecting viral growth. The best described marker of pathogenicity is a lysine residue at position 627 of the PB2 protein [55]. This residue enhances the growth efficiency of IAVs in mammals. Notably, almost all human influenza viruses posses lysine in this position, whereas, most avian viruses posses glutamic acid [23]. Additionally, the amino acidic change D701N at position 701 of PB2 has also emerged as a determinant of virulence in mammals [56,57]. Interestingly, the pandemic 2009 H1N1 virus has neither the PB2 627, nor the 701 mutations, which are usually associated with high pathogenicity (Table 2). However, second-site compensatory mutations in PB2 (590S and 591R) have been identified [58].

Protein	Position	Pathogenicity		Pandemic 2009 H1N1 virus	Function
		Low	High		
PB2	627	Glu	Lys	Glu	Replicative ability in some mammals, including humans
	701	Asp	Asn	Asp	Nuclear import kinetics affecting replicative ability in mice
PB1-F2	66	Asn	Ser	Truncated (11 aa)	Induction of apoptosis
HA	Cleavage site	Single basic aa	Multi basic aa	Single basic aa	HA cleavage
NS1	92	Asp	Glu	Asp	Unknown (interferon response?)
	C terminus	Arg-Ser-Glu-Val, deletion	Glu-Ser-Glu-Val	11 C terminal aa truncated	Unknown

Table 2. Genetic determinants of viral pathogenicity. Adapted from Neumann *et al.* 2009 [23].

The PB1 gene of most avian and human influenza A viruses encodes a second protein, the **PB1-F2**. The PB1-F2 is expressed by nearly all avian influenza viruses, but it becomes truncated, following introduction to humans or pigs [50]. The amino acid change in position 66 of the PB1-F2 protein (Table 2) was found to be responsible for the high virulence of both the 1918 pandemic and H5N1 viruses [59], by increasing the secretion of pro-inflammatory cytokines, inducing apoptosis, and increasing the frequency of secondary bacterial infection [23].

The **NS1** protein is an interferon (IFN) antagonist [60] which blocks the activation of transcription factors of important players in the innate immune response as retinoic acid inducible gene-I (RIG-I), and toll-like receptors (TLRs). The NS1 proteins in H5N1 viruses confer resistance to the antiviral effects of IFN and are associated with high levels of pro-inflammatory cytokines. Several amino acids in NS1 have been shown to affect virulence (Table 2) [23]. The pandemic 2009 H1N1 virus posses the low-pathogenic type amino acid in these positions, [23] and lack C-terminal amino acids of NS1, which have also been associated with enhanced virulence [23]. However, recent data suggests that NS1 biological activity may contribute to pathogenesis in a strain-specific, host species-dependent manner [50].

1.7 Host Immune Response to Influenza Virus Infection

In addition to the physical epithelial damage, influenza virus infections evoke host immune responses which ultimately result in abortion of virus replication. When influenza virus invades a host, the immune system responds with the innate immunity that provides an immediate, but non-specific response, followed by an adaptive immune response. In the course of the innate immune response, cells like macrophages, dendritic cells (DCs), natural killer (NK), and cytotoxic T cells (CTLs), are recruited with the objective of controlling and blocking virus replication and dissemination. These cells secrete different types of chemical mediators that will elicit an adaptive immune response, with the production of specific influenza virus-antibody responses [61]. The adaptive immune response is highly specific but relatively slow upon

first encounter with the virus. It consists of humoral (virus-specific antibodies) and cellular (virus-specific CD4+ and CD8+ T cells) immunity.

As innate immunity is one of the topics of this thesis, only this part of the immune response will be reviewed in more detail, in this introduction.

1.7.1 Viral Detection and Activation of the Innate Immunity

The primary targets for influenza viruses are the epithelial cells that line the respiratory tract, and which initiate the antiviral immune response upon detection of the virus. The first line of defence is formed by the innate immune system, which is quick but lacks specificity and memory. Innate immunity is formed by physical barriers (e.g., mucus and collectines) and innate cellular immune responses [62]. Cell pattern recognition receptors (PRRs), which include TLRs, as well as the RNA helicase receptor RIG-I, recognize and initiate a signalling cascade which results in the transcription of pro-inflammatory cytokines, chemokines and IFNs. This induction activates the antiviral response and the recruitment of neutrophils, activation of macrophages, and maturation of DCs [63].

TLRs and RIG-I receptors are expressed in macrophages, DCs, epithelial, endothelial and stromal cells [63] and are the first receptors which recognize the influenza virus. RIG-I receptors recognize double stranded RNA and mediates the production of antiviral type I IFNs, as well as, nuclear factor Kappa Beta (NF-κB)-dependent induction of inflammatory cytokines. TLR7 and TLR3 are intracellular receptors that recognize single and double stranded viral RNA respectively [64,65]. In addition, TLR3 is activated by endogenous mRNA released from necrotic cells [63]. TLR2 and TLR4 are cell surface receptors which recognize viral surface glycoprotein HA and NA [66,67].

Cell recognition of influenza viruses starts intracellular signalling cascades that induce the expression of type I IFNs (IFNα and IFNβ), which play an important role in limiting viral replication by, inhibiting protein synthesis in host cells [68]. In addition to

IFN's response, the production of early-response cytokines, like tumour necrosis factor (TNF) α, or interleukin (IL)-1β, act upon inflammatory cells to initiate the cascade of secondary cytokines [69]. Critical among these cytokines are those acting on neutrophils and monocytes, like chemokine IL-8, C-C motif ligand (CCL) 2 or CCL3, which serve both to activate and to recruit these cells [70] (Figure 4).

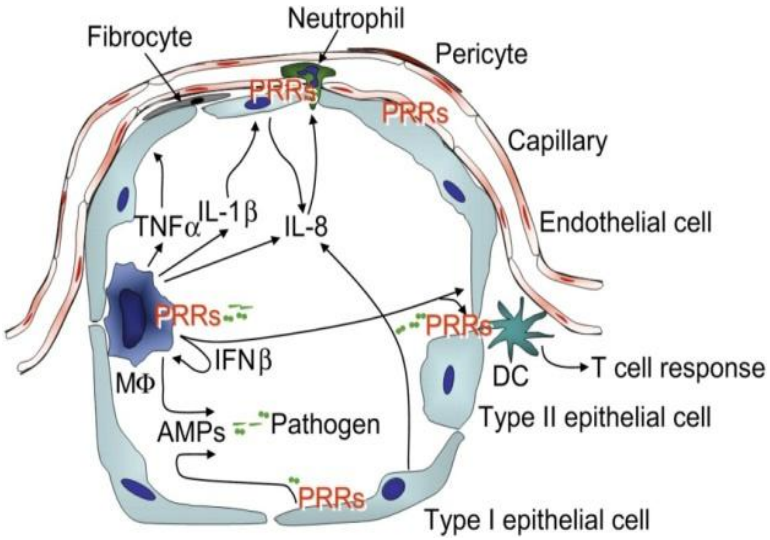

Figure 4. Overview of the role of pattern recognition receptors (PRRs) in the innate defence to infections in the alveolus. PRRs: pattern recognition receptors; MΦ: macrophages; AMPs: antimicrobial peptides; DC: dendritic cells. Adapted from Opitz *et al.* 2010 [63].

The innate immune response is crucial for the protection of the host against IAV infection. Therefore, a lack of type I IFN results in an increase in virus dissemination and susceptibility to IAV infection [71,72]. Even though TLR activation induces signals that restrict viral replication, the unregulated response of proinflammatory cytokines and chemokines induced by TLR signalling, can harm respiratory organs as well [59]. Influenza virus infection induces the upregulation of several inflammatory cytokines and chemokines, such as IL-1β, IL-6, IL-8, TNFα, CCL2, CCL3, CCL5, C-X-C motif ligand (CXCL) 1, and CXCL10, [73] which are known chemoattractants for neutrophils and monocytes [74]. The upregulation of these proinflammatory cytokines corresponds with the observation of a high number of neutrophils and monocytes in pulmonary lung lesions, after severe IAV infections in humans and animal models [73,74].

1.7.2 Cellular Innate Immune Response

After influenza virus infection, innate immune cells are recalled to block virus propagation, either by phagocytosis of virus and infected cells, or, by producing cytokines that will activate NK or CTLs to kill infected cells. Neutrophils are recruited to the lung through the release of soluble mediators such as cytokines, which activate these cells through cell surface receptors [75]

Activation of both circulating neutrophils and the vascular endothelium leads to the rapid sequestration of neutrophils to the microvascular beds of the lung [76,77]. This mechanism is accentuated by the release of immature marrow neutrophils, which are larger and less deformable [78]. Additionally, the infiltration of neutrophils results in a release of lytic enzymes that cause further necrosis of epithelial cells, and the infiltration of CTLs, which results in necrosis of infected epithelial cells [79].

High levels of neutrophil chemoattractants and regulators such as IL-8 and IL-6, have been widely associated with IAV pathogenicity [80-82]. In addition, neutrophils are the predominant cell type in bronchoalveolar lavages of patients who developed severe IAV infection, and the consistency of this finding seems to correlate with increased mortality [73,83].

The other major inflammatory cell observed in pulmonary lesions after IAV infections are macrophages [84]. During homeostasis, alveolar macrophages exhibit a relatively quiescent state, producing only low levels of cytokines, and suppressing the induction of innate and adaptive immunity [85,86]. CCL2, produced by infected epithelial cells during the initial phase of the influenza virus infection, attracts alveolar macrophages and monocytes via their chemokine receptor type (CCR) 2 receptor [87-89]. Then, macrophages become activated, phagocytise influenza virus infected cells to limit viral spread [90], and produce Nitric oxide syntase (NOS2), IL-6 and TNFα, thus contributing to influenza-induced tissue damage [87,91]. In addition, CCL2 up-regulation has been related with alveolar epithelial cell apoptosis, via tumour necrosis factor related apoptosis-inducing ligand (TRAIL), which is produced by macrophages [92]. Thus,

macrophages which migrate to influenza-infected lungs play a major role in pulmonary inflammation [88].

NK cells are cytotoxic lymphocytes of the innate immune system. They are able to lyse infected cells in a major histocompatibility complex (MHC) class I independent manner [93,94]. They can recognize antibody-bound influenza virus infected cells, and lyse them in a process called antibody-dependent cell cytotoxicity. This process has been associated with acute lung injury after influenza infections in various studies [93-95], yet its pathological role in IAV induced pneumonia is still unknown.

2. Swine Origin Influenza A Virus H1N1 and the 2009 Pandemic

IAVs, unique among human viruses, have two epidemiological modes, as seasonal epidemics, or over larger time periods, as pandemics. IAV pandemic viruses have emerged sporadically throughout history as entirely novel subtypes with a new subset of genes, particularly those coding for HA and NA. When one or more of these characteristics appears in a virus (antigenic shift), then worldwide pandemics occur, with major economic and general health implications [96].

2.1 History of Influenza A Pandemics

Throughout history, several influenza pandemics have been recorded, as far back as the 16th Century [36]. It is generally agreed that the first influenza pandemic occurred in 1580, and that it came from Asia, rapidly spreading across the world, with high rates of illness [2,97]. Since then, several influenza pandemics have been recorded; i) the 1729 influenza pandemic which broke out in Russia [6,97-99]; ii) the 1781 pandemic that started in China [97,98,100]; and iii) the 1830 pandemic which also began in China [99,100].

2.1.1 Influenza A Pandemics of the 20th Century

The first pandemic of the 20th century, referred to as the **"Spanish flu"** caused by an H1N1 virus, was the worst pandemic ever recorded [101,102]. It started in Europe in

1918, and killed around 50 million people worldwide [103,104]. After 1920, the virus became seasonal and remained "drifted" antigenically for the next 40 years. The novel 2009 H1N1 pandemic virus is a fourth-generation descendant of the 1918 virus [105].

The influenza pandemic of 1957 named "**Asian influenza**" was caused by an H2N2 virus which emerged from China [106]. The new H2N2 virus was a lineal descendant of the 1918 H1N1 pandemic virus, where HA and NA were replaced by an avian-like H2, N2 and PB1 subtypes [107,108]. After two years, the virus became seasonally endemic and circulated worldwide until the next pandemic [109]. The H3N2 pandemic arose in Southeast Asia around 1968 and acquired the sobriquet **"Hong Kong influenza"** [109]. It was caused by a reassortment between the circulating human H2N2 virus and an avian H3 subtype [107,108]. The relative mildness observed was the result of the retention of the previously circulating NA [109], the virus quickly became endemic and seasonal.

Russian or later named **"Red influenza"** of the H1N1 subtype, came in November 1977, in the Soviet Union [109]. The epidemic was almost restricted to persons <25 years of age, which was attributed to the absence of H1N1 viruses in humans after 1957[109]. As had happened with the other pandemic viruses, H1N1 became seasonal and like H3N2, it continues to be isolated nowadays, despite the emergence of the novel 2009 H1N1 virus [29].

2.2 The 2009 H1N1 Virus Pandemic

The first pandemic of the 21st century occurred in 2009, by an H1N1 IAV with the acronym of pH1N1, H1N1pdm or H1N1v [110]. The nomenclature for the new 2009 pandemic virus has lead to some confusion, and the World Health Organization (WHO) currently recommends the abbreviated form: H1N1v [111]. Surprisingly, the new 2009 pandemic virus arose from an HA1 subtype, which contrasts with past pandemic viruses, which arose from an HA subtype completely different from the contemporary endemic virus [111]. The infection broke out in Mexico and rapidly spread across the

world. By June 2009, nearly 30.000 cases of H1N1v virus had been confirmed across 74 countries and the WHO declared the start of the 2009 influenza pandemic [112].

Recently, the Centre for Disease Control and Prevention (CDC) has estimated H1N1v's global death toll as standing at more than 250.000 (based upon the estimate that 201.000 respiratory deaths and another 83.300 deaths from cardiovascular H1N1v associated disease occurred). They also calculated that Africa and Southeast Asia, which represent 38% of the world's population, accounted for a disproportionate 61% of the deaths [113], until the end of the pandemic in August 2010 [114].

2.2.1 Genetic Characteristics and Formation of H1N1v

The H1N1v arose from the reassortment of two unrelated swine IAV, a North American H1N2 and a Eurasian H1N1, each of which had themselves arisen from reassortments [41,115]. The North-American swine H1N2 `triple' reassortment lineage was derived from the classical H1N1 swine virus (of H1N1 1918 pandemic origin), a human H3N2 virus and a North-American avian H1N1 virus (Figure 5).

As a result, the H1N1v possess the PB2 and PA genes of North American avian virus origin, the PB1 gene of human H3N2virus origin and the HA, NP and NS gene segments derived from the classical swine H1N1 virus (1918 origin) [23]. Besides, the other direct parent virus "Eurasian avian-like H1N1" lineage contributed with its NA and M gene segments [116] (Figure 5).

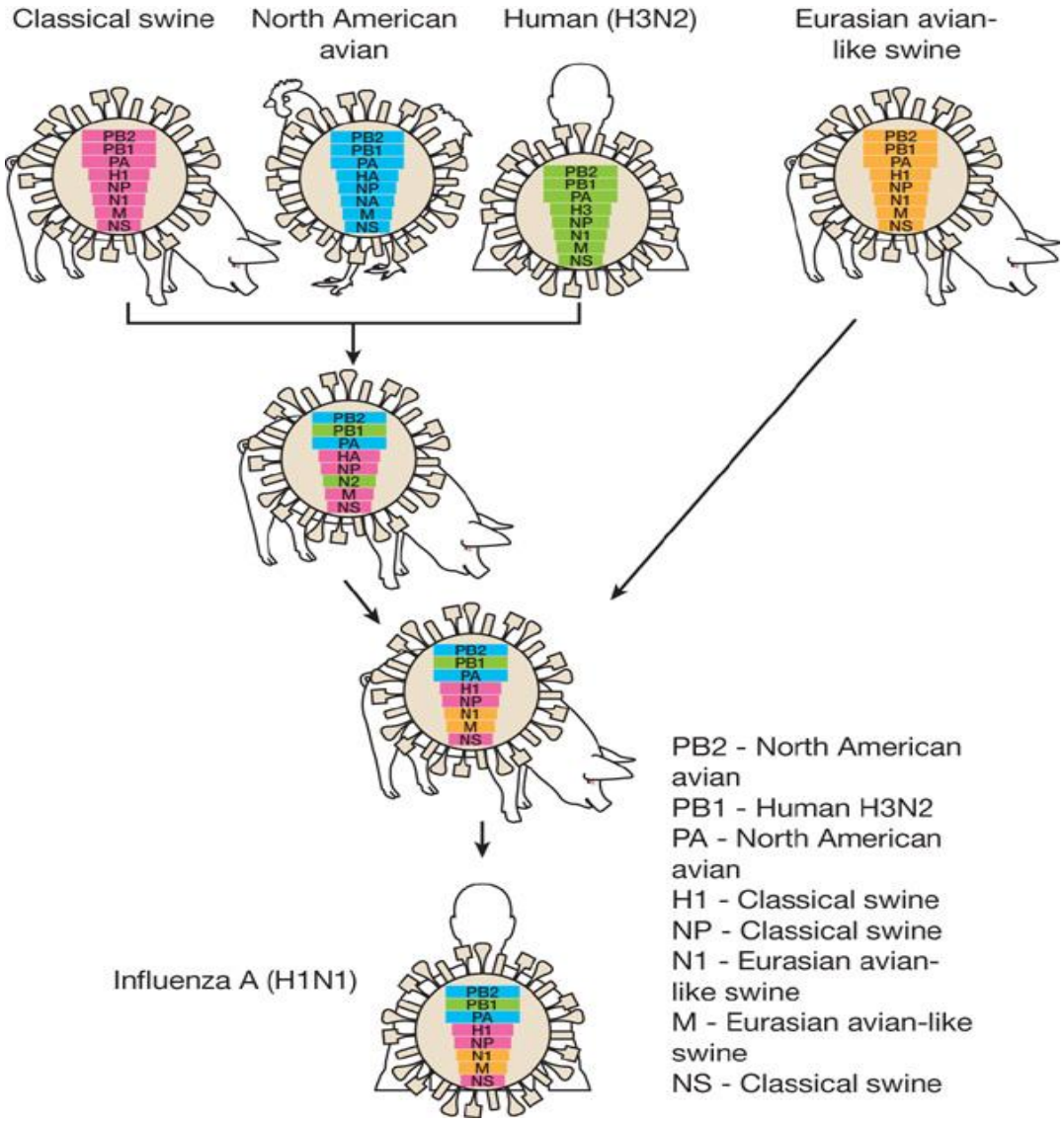

Figure 5. Generation of the pandemic H1N1v. In the late 1990s, reassortment between human H3N2, North American avian, and classical swine viruses resulted in triple reassortant H3N2 and H1N2 swine viruses that have since circulated in North American pig populations. A triple reassortant swine virus, reassorted with a Eurasian avian-like swine virus, resulting in the H1N1v that are now circulating in humans. Adapted from Neumann *et al.* 2009 [23].

Although human and swine H1N1 viruses are all of avian origin, they have evolved in different host species. Swine influenza A viruses are antigenically very similar to the 1918 human influenza A virus, and they may all have originated from a common ancestor [117]. However, antigenic drift has occurred amongst different lineages of H1N1 viruses in different host-species, and therefore, cross-protection antibodies against avian, swine, and human H1N1 viruses, are not supposed to exist between species [118].

2.2.2 Antiviral Resistance

Eurasian swine viruses are sensitive to the antiviral effects of neuraminidase inhibitors (NI) but resistant to the antiviral amantadine. Therefore, H1N1v has inherited resistance to amantadine [119], making NIs the primary antiviral agents currently recommended for the prevention and treatment of influenza infection [120]. NIs bind to the active site of NA present on infected cells, preventing it from removing SA residues and causing virus aggregation [121]. There are two NIs licensed globally, for the prevention and treatment of influenza; *Relenza®* (Zanamivir) and Tamiflu® (Oseltamivir). The latter is one of the most common antiviral treatments used for influenza infection. During 2007–2008, increased resistance to oseltamivir was associated with a specific mutation causing a histidine to tyrosine substitution (H275Y) in NA. This mutation was reported in seasonal H1N1 in many countries and became prevalent worldwide [122,123]. Sporadic oseltamivir-resistant (OR) H1N1v virus infections have been identified [124,125], and nearly all sporadic cases of oseltamivir-resistant H1N1v virus infections identified to date have also been associated with the H275Y mutation in NA. However, two novel NI resistance-associated mutations, I222R and S247N, have been identified recently in clinically derived H1N1v viruses [126], raising concerns about the effects on these mutations in viral fitness. The transmissibility and pathogenicity of oseltamivir-resistant H1N1v have been studied *in vitro* and *in vivo,* showing inconsistent results according to the isolates tested [127-132]. It, therefore, remains debatable whether NI resistant viruses nowadays have a decreased or equal transmission capacity.

2.2.3 Epidemiology and Transmission

H1N1v first emerged in Mexico and was unnoticed until the first two hospitalized cases were reported in California [133]. The virus quickly spread around the world, through human-to-human transmission, in an epidemiological pattern characterised by local outbreaks, transmitted and spread locally by school children, and spread internationally through dissemination by air travel [134]. In temperate areas

the spread was gradual, whilst in tropical climates the infection appeared to move far more rapidly, and very little epidemiological data is available regarding the African continent [133]. By June 2010, more than 214 countries were laboratory-confirmed for H1N1v infection cases [135].

The actual number of H1N1v cases worldwide remains unknown as most cases were diagnosed clinically and were not laboratory-confirmed [136]. However, it is likely that the total number of H1N1v cases worldwide was in the order of several tens of millions. Overall, the case fatality rate for H1N1v was estimated as similar to that of seasonal influenza, and was lower than the 1918 pandemic [137,138]. Conversely, young adults and children were disproportionally affected, when compared to other groups within the population, with more than 60 % of the reported cases occurring amongst people aged 10-29 years of age [139-142].

This age distribution has led to the hypothesis that there exists a partial immunity amongst older generations. This was later confirmed by epidemiological studies, which showed that 33% of humans over 60 years of age had cross-reacting antibodies, and were thus better prepared for H1N1v [143,144]. In addition, a strong conservation of more than the 50% of the T cell epitopes (whether T-helper or CTL epitopes) was described, between the H1N1v and the seasonal H1N1 virus strains, which were used in 2007 and 2008 influenza vaccines. This provided some level of cross-reactive cellular immunity in the vaccinated human population [145].

The transmission model of H1N1v appeared to be similar to those of seasonal influenza viruses, mainly characterised by close, unprotected contact, with respiratory droplets, and with contaminated fomites [146]. RNA has been also detected in the faeces of many infected patients, although the possibility of faecal transmission remains to be proven [133]. The incubation period is comparable to that of seasonal influenza viruses, varying from 1 to 7 days post-infection [138]. Viral shedding begins approximately 1 day prior to the onset of symptoms [147], with a median disease duration of between 4 and

8.5 days. The peak of viral load tends to occur one day after symptoms manifest, and decline gradually thereafter [148].

2.2.4 Clinical Disease

H1N1v illness in humans has been found to be indistinguishable from common viral respiratory infections. In general, the spectrum of disease caused by H1N1v ranged from a non-febrile, mild upper respiratory tract illness, to severe or fatal pneumonia [140,149].

The severity of symptoms tends to be highest during the first 4 days, with a systemic symptoms peak on day 2. Respiratory symptoms tend to resolve gradually over a 2-week period [150]. In general, the most commonly described symptoms are fever and coughing, followed by headache, runny nose, myalgia, and sore throat. A mild illness without fever was also reported in up to 32% of confirmed cases of H1N1v infection. In addition, conjunctivitis, epistaxis, and acute otitis media were also frequently reported, together with gastrointestinal symptoms, especially diarrhoea.

Among hospitalized and intensive care unit (ICU) cases, diffuse viral pneumonia leading to hypoxemia and acute respiratory distress syndrome (ARDS), were found to be the most common clinical conditions, accounting for approximately 49-72% of the hospitalized cases [151].

2.2.5 Gross and Microscopic Lesions

In contrast to clinical and epidemiological studies, histopathological changes associated with H1N1v infection in humans have only been described in a limited number of studies [137,152-155]. In general, patients died between 7-13 days post infection, after the onset of influenza symptoms.

Macroscopic lesions associated to H1N1v infection in humans were mainly characterised by oedema, haemorrhage, or necrosis in the upper respiratory tract, particularly on the internal surface of the larynx and trachea [152]. Commonly, the lungs

appeared heavy and consolidated, diffusely oedematous, with variable degrees of haemorrhage and peribronchial, accompanied by hilar lymphadenopathy [137].

In the upper respiratory tract, **histopathologic lesions** in humans consisted of tracheitis and bronchitis of a local to extensive nature. In general, lesions were characterised by denuded or ulcerated epithelial layers, and submucosal inflammatory infiltrates with glandular epithelial necrosis [154]. Histopathological findings observed in the lower respiratory tract were strikingly similar to those of published autopsy studies from the 1918 and 1957 pandemics [156].

As happened in precedent pandemics, influenza viral pneumonia with focal to extensive diffuse alveolar damage (DAD) was the most common and consistent autopsy finding in H1N1v fatal cases [153]. Focal to mild bronchiolitis were also regularly observed, sometimes associated with squamous metaplasia. Lung histopathological lesions were characterised by diffusely expanded alveolar septa, accompanied by a mild to severe inflammatory infiltrate. In general, interstitial inflammation was characterised by predominant neutrophilic or mononuclear infiltrates, along with increased numbers of myofibroblasts and hyperplasia of type II pneumocytes. Associated hyaline membranes were also present in most cases accompanied by pulmonary oedema, and /or, acute diffuse alveolar haemorrhage [137].

Along with respiratory tract lesions, lesions in other organs were observed in H1N1v fatal patients. In general, mild to moderate kidney tubular necrosis and thrombotic angiopathy were seen fairly often, reflecting some degree of skeletal muscle injury. In some cases, the liver showed erythrophagocytosis as well, accompanied by centrilobular necrosis, and sinusoid mild inflammatory infiltrates [137].

2.2.6 H1N1v Pathogenesis

The susceptibility to severe influenza in humans is polygenic, and it is determined by pathogen genetic characteristics, and the interaction between those

and multiple host factors, which include prior infection history, comorbidities, and host genetic characteristics [157,158].

Severe cases after H1N1v infection have been linked to the spread of H1N1v infection from bronchial to alveolar areas. In contrast to the damage caused by the virus infection to the tracheobronchial epithelium in uncomplicated influenza, damage to the alveolar epithelium has severe consequences for the gas exchange function [159]. In the case of H1N1v, it has been suggested that a D222G substitution in the HA changes the receptor binding specificity of the virus, from α2,6 to α2,3 SA receptors [54], infecting both ciliated bronchial cells and alveolar epithelial cells, and consequently increasing the severity of pneumonia [59]. In human autopsy cases, viral NP antigens detected by immunohistochemistry (IHC) have been localized in the nuclei and cytoplasm, of epithelial and inflammatory cells in the airways. In the lungs, the antigen was mainly observed in the pneumocytes (predominantly type II), occasionally in alveolar macrophages [153], regularly observed in the submucosal bronchial glands, and associated with hyaline membranes, and endothelial cells in rare cases [154]. Several studies have suggested that different mutations affecting the polymerase complex, and the HA subunit of certain H1N1v strains, may contribute to their pathogenicity. These substitutions confer to most virulent strains the ability to produce higher titres, and to replicate over a prolonged period of time. However, the importance of these mutations in H1N1v pathogenicity still needs to be clarified [160,161].

In addition to viral respiratory epithelial damage, detrimental host immune responses have been strongly associated with H1N1v infection fatalities [55,79,162,163]. During fatal infection with H1N1v, high viral titres and severe illness correlated with robust host immune responses [163], leading to the hypothesis that influenza lethality is linked to an excessive innate immune response, especially common in young healthy adults [83]. Several reports have revealed that severe disease caused by H1N1v was characterised by the presence of high systemic levels of cytokines, chemokines and other immune mediators, from the early stages of disease [80,164]. The recruitment of

inflammatory cells like macrophages and neutrophils, is known to cause severe damage to lung structures favouring the cytokine storm [55,79,162].

Underlying conditions which are associated with complications from seasonal influenza are also risk factors in terms of potential complications in H1N1v infection. Chronic obstructive pulmonary disease (COPD), asthma, cardiovascular disease, hypertension and diabetes have been reported as critical illness risk factors following infection with the H1N1v virus [139,151]. In the case of H1N1v, two emerging risk groups (in addition to those previously described), include the pregnant and the obese [165,133]. This increased mortality rate has been associated with increased inflammatory cell infiltration in the lungs and higher levels of chemokines and pro-inflammatory cytokines in animal models [166-169]. Therefore, basal immune alterations, and/or, the presence of a previous-inflammatory state, may impact upon the normal development of specific immune response against H1N1v, and increase the risk of developing severe forms of the infection.

Close to one third of the hospitalised influenza patients who died, had no known underlying medical conditions, due to which, they could have been predisposed to severe infection [133]. Genetic variations in immune-related genes has now been shown to account for disparate susceptibility of numerous infectious agents, and also for the variation observed in H1N1v susceptibility, and disease severity [170]. To date, polymorphisms in the CCR5, TLR3 and interferon-inducible transmembrane (IFITM) genes, [171-174] and a deficiency in the immunoglobulin (Ig) G2 response, amongst others, [175,176] have been correlated with more severe courses of H1N1v infection. Some of these host genetic variations are summarized hereafter.

The ***CCR5Δ32*** **allele** encodes for the CCR5 protein, which plays a pivotal role in mediating leukocyte chemotaxis. Mutations in the CCR5 allele have been associated with an increased risk of developing symptomatic and fatal viral infections, including disease severity in the case of H1N1v infection [171,177,178].

IFITM3 plays a role in restricting influenza virus replication, by inhibiting viral replication, using several orthologous genetic approaches [179]. When examining the role of IFITM3 in human IAV infection, a minor allele with a single nucleotide polymorphism (SNP) was found to be more prevalent in patients who had been hospitalized due to H1N1v infection [174].

Recently, *in vitro* assays showed that a **TLR3** receptor containing the F303S mutation was less effective in activating the transcription factor, NF-κB, as well as triggering downstream signalling via the IFNβ receptor, which suggests that this variant may allow enhanced IAV replication [180]. In addition, a SNP in the *TLR3* gene was identified in a study of 51 children with confirmed H1N1v infection [172], further demonstrating the association between TLR3 and IAV pathogenicity. However, the role of TLR3 in initiating innate immunity, through the recognition of IAV, still remains obscure [181].

Complement decay-accelerating factor (CD55) is a complement pathway regulatory protein, which inhibits the formation of C3 and C5 convertase, two proteases involved in complement activation and inflammation [182]. A recent study investigated SNPs in the *CD55* genes of Chinese patients, for their association with influenza disease outcomes. It showed that individuals homozygous for a specific *CD55* SNP, presented more robust complement activation during IAV infection, resulting in worse outcomes, secondary to enhanced inflammation [183,184].

NK activity is determined by a balance between activating and inhibitory receptors [185]. One of the classes of inhibitory receptors, the **Killer-cell immunoglobulin-like receptors**, form a large family of receptors that recognize human leukocyte antigen (HLA) Class I ligands, and induce an inhibitory response, which is thought to be important in preventing damage to healthy tissue. Recent studies have found that a specific allotype of the *3DL1/S1* gene diversity, which encodes for the Killer-cell immunoglobulin-like receptor, was determined to be common in most severe H1N1v cases [186].

IgG2a and **IgG2b** are thought to be important in the protection against influenza infection, given that they are able to bind to fragment crystallisable (Fc) surface receptors expressed in several inflammatory cells. Human severe cases after H1N1v infections were found to present low levels of IgG2 [176] and a recent study related these IgG2 low levels with one SNP in IgG. These results suggest the involvement of immune complexes and complement activation in determining the risk for severe pneumonia due to H1N1v influenza infection [176].

These studies pointed the potential role of host genetics in susceptibility to severe influenza infection. For this reason, the WHO identified studies into the role of host genetic factors in susceptibility to severe influenza, as a priority [187,188].

3. Animal Models for Human Influenza

Animal models aid a better understanding of human influenza, and the development of medical counter measures, against disease. Forms of influenza in human beings, for which animal models have been developed, include uncomplicated influenza, influenza pneumonia, influenza-associated bacterial sepsis, influenza-associated neurological disease, influenza in immune compromised hosts, and viral transmission [189]. There are many animal models which have been used to study influenza virus infection: mouse, ferret, macaque, guinea pig, syrian hamster, chinchilla, hedgehog, chicken, pig, and rat [190].

Attachment of viral HA to SAs, is the first step in IAV infection. As explained previously, different IAVs use different SAs as their receptor, and because the expression of SAs differs across the respiratory tract, and across species, this step influences the pattern of respiratory disease and host range of virus infection [191]. Consequently, SA distribution pattern also influences the usefulness of different animal models to study IAVs induced pneumonia. The respiratory tract of ferrets and pigs, most closely resemble that of humans, with regards to SA receptor distribution for human IAVs (Figure 6).

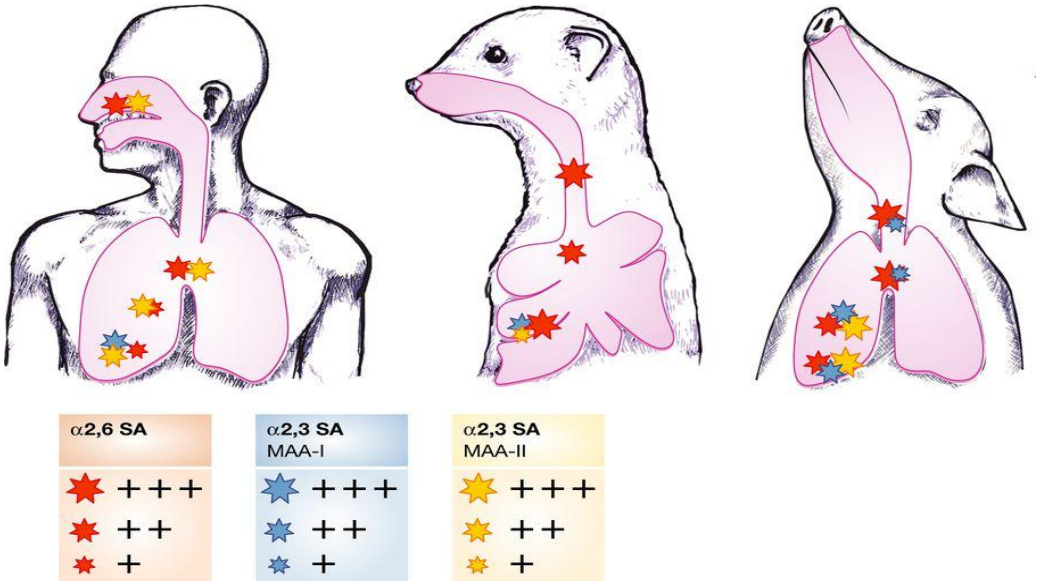

Figure 6. Receptor binding specificity of influenza A virus. Adapted from de Graaf and Fouchier, 2014 [192].

The pig respiratory epithelium has α2,6 and α2,3 SAs receptors that can bind avian, swine, and human influenza viruses [193]. However, pigs infected with the H5N1 high pathogenic avian influenza (HPAI) virus, and with the H1N1v [194,195], present mild respiratory signs and mild bronchiolitis, similar to the clinical signs and respiratory lesions presented by humans infected with seasonal IAVs [196].

In ferrets, α2,6 SA receptors are located in the upper respiratory tract, as far as the bronchioles and α2,3 receptors in the lower respiratory tract [193]. However, a predominance of α2,6 SA receptors was reported throughout the respiratory tract of ferrets, including the lower respiratory tract [192]. In contrast, the pattern of SA receptors on the respiratory tracts of mice and cynomolgus macaques strongly differs from that in humans.

Despite this, experimental pathogenicity of human viral pneumonia after IAV infection has generally been reproduced in mice, ferrets and non human primates, due to the similarity of lung pathology observed in these species. Even so, all three species have their advantages and disadvantages (Table 3).

Advantages	Disadvantages
Laboratory mice	
Inexpensive to acquire and house	Anatomy and histology of respiratory tract different from that of humans
Well-characterised genetics	Pattern of virus attachment (PVA) for human and avian influenza virus different from that of humans. Seasonal human influenza viruses require adaptation to replicate efficiently and cause disease
Inbred strains result in low host variability	*Mx* gene missing (present in humans)
Availability of Knockout mouse strains	Systematic disease in HPAI H5N1 infection different from humans
Pathobiology of 1918H1N1 and HPAI H5N1 influenza viral pneumonia similar to humans	
Availability of microarrays	
Many reagents available	
Domestic ferret	
Anatomy and histology of respiratory tract moderately similar to that of humans	Genetically outbreed, resulting in variation in host response to virus
PVA for humans and avian influenza virus similar to that of humans	No specific pathogen free (SPF) animals; thus, the need to check each time for influenza and other diseases
Pathology of human and avian influenza viral pneumonia similar to that of humans	Appears more susceptible than humans to developing influenza pneumonia
	Systemic disease in avian influenza different from that of humans
	Many reagents unavailable
Cynomolgus macaque	
Anatomy and histology of respiratory tract similar to that of humans	PVA for human influenza virus not similar to that of humans
PVA for avian influenza virus similar to that of humans	Genetically outbreed, resulting in variation in host response to virus
Host immune response similar to that of humans	No SPF animals; thus, the need to check each time for influenza and other disease
Pathology of human and avian influenza viral pneumonia similar to that of humans	Expensive to acquire and house
Absence of systematic disease in avian influenza similar to that of humans	Strong ethical concerns about use as experimental animal
Many reagents cross-react with those of humans	

Table 3. Advantages and disadvantages of experimental animal species used to model IAVs infection in humans. Adapted from Kuiken *et al.* 2010 [191].

3.1 Mice

The mouse (*Mus musculus)* remains the primary animal model used for studying IAV infections *in vivo*, due to the inexpensiveness of the animals and their caging, and the availability of reagents to study the effects of virus infection on the mouse immune system [197]. However, mice are not infected by IAVs in the wild and so may not fully replicate the interactions occurring between these viruses and their natural hosts [191]. Furthermore, mice are, in general, not susceptible to infection by

human derived IAV because they express avian-like SAs α2,3 on their cell surface proteins, in contrast to human cells which express α2,6 SAs [193].

In general, seasonal influenza viruses require adaptation to mice in order to efficiently replicate and cause disease. The adapted virus can infect mice lung cells, probably as a result of amino acid changes in the viral surface Has, which enable the virus to bind α2,3 SAs [198]. In contrast, mice are generally more susceptible to 1918 H1N1, HPAI H5N1 and H1N1v viruses [191]. Experimental infection of H1N1v in mice resulted in prominent bronchiolitis and alveolitis with viral antigen presence in ciliated bronchiolar epithelial cells, type II pneumocytes, and alveolar macrophages [191]. However, the susceptibility of mice strains to IAVs and associated disease differs greatly, which influences the outcome of infection [158,199]. In addition to the surface receptor, which determines host susceptibility to virus infection, restriction factors contribute to the host's ability to control viral replication. Many studies have been conducted using murine models, to study the relationship between host genetics and IAV pathogenicity. However, the conclusions drawn from these efforts must be interpreted whilst taking into account the identical genetic backgrounds of inbred mouse populations [158].

3.2 Cynomolgus Macaques

Cynomolgus macaques (*Macaca fascicularis*) have seldom been used as a nonhuman primate model to study influenza pathogenicity but are often thought to best imitate human infectious disease, including IAVs infection. The H1N1v virus replicates efficiently in the lungs and other respiratory organs of infected non-human primates, causing morbidity, but not mortality [74,200]. Gross lesions consist of pulmonary consolidation. Microscopically, there is bronchiolitis and diffuse alveolar damage, characterised by necrosis of alveolar epithelial cells, accumulation of neutrophils and alveolar macrophages in the alveolar lumina, and hyaline membrane formation [200]. Virus antigen expression is mostly observed in type I and type II pneumocytes, as occurs in humans, and rarely in epithelial cells of larynx and nasal cavity [74,200].

3.3 Ferrets

In recent years, the ferret (*Mustela putorios furo)* has emerged as a useful animal model to characterise numerous viruses that cause respiratory tract infections, including human and avian influenza viruses [201-206]. Ferrets are an attractive model for pathogenesis studies of human IAVs, due to the fact that they share similar lung physiology with humans [193,207].

Ferrets are one of the most attractive animal models to study human IAVs pathogenesis and virus-host interactions, due to the fact that ferrets are highly susceptible to influenza viruses, transmit virus to healthy animals, and mimic numerous clinical features and pathological lesions, which are associated with human influenza disease [190]. In ferrets experimentally infected with H1N1v virus, elevated body temperatures are detected as early as 1 day post-inoculation, and more virulent viruses generally elicit high fever which can persist for several days [208]. Nasal discharge and sneezing are also frequently observed in influenza infected ferrets up to 1 week post-inoculation, with sneezing detected more frequently following seasonal influenza virus infection as observed in humans [146,206].

In addition, ferrets develop a productive infection after inoculation with human and avian influenza viruses, without prior virus adaptation. Besides this, quantitative differences in severity of lower respiratory tract disease between seasonal, pandemic and HPAI influenza, together with differences related to the tropism of the virus, and the ability of the host to counter infections, are also observed in ferrets [79,84], mimicking human IAV infections. For highly virulent influenza viruses, such as HPAI H5N1 and 1918 H1N1 virus, intranasal inoculation is sufficient to consistently induce pneumonia in the ferret model [191], and for less virulent influenza viruses such as H1N1v, intratracheall inoculation is used to model human influenza pneumonia [209].

Experimental H1N1v infection in ferrets causes mild lesions at 12 hours post infection (hpi), developing into moderate to severe lesions from 1 to 7 days post infection (dpi) [84]. Gross lesions consist of multifocal or coalescing pulmonary

consolidation, affecting from 20 to 70 % of the lung parenchyma. Histological lesions varied from mild bronchointerstitial pneumonia to DAD. In ferrets, high viral titres in the lungs strongly suggest active viral replication in those tissues with subsequently more damage [146]. What is more, virus antigen expression by IHC has been observed in type I and II pneumocytes, alveolar macrophages, glandular bronchial epithelial, and bronchial and bronchiolar epithelial cells [191].

Because ferrets demonstrate a similar disease entity to human influenza infection, their immune response to influenza virus infection may be more relevant than the immune response observed in other animal models. The polygenic nature of influenza virus pathogenesis and transmission underscores the importance of using a mammalian model with the potential to be assessed in terms of both parameters. What is more, reports showing detrimental higher levels of proinflammatory cytokines following IAV virus infection in humans have emphasized the need to study the induction of innate immune responses in severely infected hosts [82,210], also the need for a reliable animal model to study such interactions. However, immunological studies in ferrets are limited by the lack of readily available reagents, such as ferret specific antibodies which recognize immune cell-surface markers [190,211]. Additionally, the access to pathogen-free (IAV seronegative) ferrets is already an issue, and will increasingly become a problem as demand for ferret studies grows.

In vivo assessments of the innate and adaptive immune function following IAV infection have primarily been limited to the mouse model owing to the reasons listed above, also the incomplete genome sequencing of the ferret species. Recently, the regulation of ferret pro-inflammatory mediators has been measured by real-time reverse transcription polymerase chain reaction (RRT-PCR) [71,212-214]. Canine reagents have also been used successfully to assess ferret host responses, and numerous mouse monoclonal antibodies have demonstrated cross-reactivity with proteins expressed by ferret lymphocytes in flow cytometry and immunoassays [214,215] [216]. Continued immunology-based research in the ferret will result in a valuable outbreed mammalian

model for the study of innate and adaptive immune responses, leading to an improved understanding of human infection.

CHAPTER 2

HYPOTHESIS AND OBJECTIVES

Hypothesis

The spectrum of disease after H1N1v infection in humans ranges from mild to severe disease. Severe H1N1v outcomes have been related with high viral replication capacities and exacerbated host inflammatory immune responses. From these observations, we hypothesized that the host innate immune response and its interaction with viral characteristics are responsible for severe outcomes after H1N1v infection.

Objectives

1. To set up techniques for i) the phenotyping of different immune cells in formalin-fixed paraffin-embedded (FFPE) ferret tissues by IHC and ii) the characterisation of ferret immune response through the detection of innate immune molecules by RRT-PCR.
2. To characterise viral-host interactions occurring in the lungs of ferrets experimentally infected with different strains of H1N1v virus.

Ethics statement

These studies were carried out in strict accordance with the recommendation of the *Comissió d'Experimentació Animal de la Generalitat de Catalunya.* The protocols were approved by the *Comissió d'Ètica en l'Experimentació Animal i Humana* of the *Universitat Autònoma de Barcelona.* Every effort was made to minimize suffering.

PART II

STUDIES

CHAPTER 3

STUDY I: *Immune System Cells in Healthy Ferrets. An Immunohistochemical Study*

3.1 Introduction

In recent years, the ferret has emerged as a useful animal model to characterise several physiologic and pathologic conditions, including influenza virus infection [79,168,191,201,217].

Recent studies have expanded the range of methods and reagents suited to the study of immunologic parameters in ferrets [71,214-216,218]. However, few studies have focused attention on the immunohistochemical characterisation of immune system cells in FFPE tissues in this animal model. IHC would be a very useful tool for investigating the pathogenesis of different diseases, through the characterisation of the inflammatory response in ferret tissues. There are still only 2 studies that successfully used human antibodies to differentiate T- and B-cell lymphomas in ferrets, by IHC [219,220].

The aim of this study was to characterise the distribution of different immune system cells in different lymphoid and nonlymphoid organs, of conventional, healthy ferrets to settle a basis for future pathological studies. Therefore, IHC techniques were standardized in FFPE and frozen ferret tissues, using 8 antibodies: CD3, CD79α, HLA-DR, CD20, lysozyme, CD163, SWC3, and Mac387.

3.2 Materials and Methods

Animals and Sampling

Five 3-year-old, male, neutered, healthy ferrets were used in this study. Animals were randomly selected from a stable, purposely bred colony. Animals were housed in standard ferret cages (Biosis Biologic Systems, SL, Spain), with stainless steel grid roofs, in an environmentally controlled room (19°–20°C, 40%–70% humidity, 12 hours (h) light/dark cycle). They received a commercial pellet diet (Totally Ferret Active, Totally Ferret) and tap water ad libitum, until their use in this study. The colony

was vaccinated for rabies (Im rab-3, Rhone Merieux, Inc), and dewormed with selamectine upon arrival at the laboratory, 3 years ago.

Blood samples were taken the day before euthanasia to test for influenza A virus infection and Aleutian disease. Animals were seronegative to influenza A virus (influenza A antibody competition multispecies enzyme-linked immunosorbent assay (ELISA), ID ScreenR, France). They were also negative for Aleutian disease virus, tested for by PCR in plasma (Applus Laboratories, Spain). Ferrets were euthanized by intravenous injection of sodium pentobarbital (100 mg/kg), under sedation with ketamine (5–10 mg/kg; Imalgene 1000, Merial, SA, Spain) and medetomidine (0.05 mg/kg; Domtor Pfizer, SA, Spain).

A complete necropsy was performed on all animals between 1 and 2 h posteuthanasia, and no gross lesions were observed in any animal. The following tissues were collected during necropsy: mesenteric and mediastinal lymph nodes, spleen, thymus, bone marrow, small and large intestine, stomach, pancreas, liver, kidney, heart, lung, trachea, nasal turbinate, brain, skin, skeletal muscle, and eye. Tissue samples were embedded in optimal cutting compound (OCT) (Tissue-Tek, Torrance, CA), fast frozen using isopentane (M32631, Sigma-Aldrich Química, SA, Spain), precooled in liquid nitrogen, and stored at –80°C. Other portions of the same tissues were fixed for 48 h in neutral-buffered 10% formalin. They were then embedded in paraffin wax, sectioned at 3 µm, and stained with haematoxylin and eosin (HE). Stomach sections were stained with Warthin-Starry silver impregnation, for detection of *Helicobacter spp*. Kidney sections were stained with Prussian blue staining, for the detection of haemosiderin deposits in tissues.

IHC in FFPE Tissues

Serial 3-µm-thick sections of all tissues were cut and placed on silane-coated slides (3-trietoxysilyl-propylamine). Eight primary antibodies were used. The polyclonal anti-human antibodies tested were as follows: the anti-CD3 (Polyclonal Rabbit Anti-

Human CD3, nº IS503, Dako), the anti-CD20 (CD20 Rabbit Polyclonal Antibody, nº RB-9013-P, Thermo Scientific), and the anti-lysozyme Polyclonal Rabbit Anti-Human Lysozyme EC 3.2.1.17, nº A-0099, Dako). The monoclonal anti-human antibodies tested were as follows: the anti-CD79α (Monoclonal Mouse Anti-Human CD79αcy Clone HM57, nº M7051, Dako), the anti-HLA-DR (Monoclonal Mouse Anti-Human HLA-DR Antigen, Alpha-Chain Clone TAL.1B5, nº M0746, Dako) and the anti-myeloid/histiocyte antigen (Monoclonal Mouse Anti-Human Myeloid/Histiocyte Antigen Clone MAC 387, nº M0747, Dako). The mouse anti-swine monoclonal antibodies tested were as follows: the anti-CD163 (INIA research institute on-loan antibody against swine antigen 2A10/11, CD163 IgG1) and the anti-SWC3 (INIA research institute on-loan antibody against swine antigen, BA1C11, SWC3/CD172).

Different immunohistochemical protocols, with different antigen retrieval methods and antibody temperature incubations, were carried out. Successful protocols are represented in (Table 4).

Antigen (Ag)	Immunolabelled expected cells	Source	pAb* / mAb†	Dilution	Ag retrieval method
CD3	T cells	Dako	Polyclonal	1:200	Citrate, Tween
Lysozyme	Myeloid mature cells	Dako	Polyclonal	1:1000	Proteainase K, Tween
CD20	B cells	Thermo Fisher	Polyclonal	1:300	Citrate, Tween
CD79α	B cells	Dako	Monoclonal Clone (HM57)	1:50	EDTA, Triton
HLA-DR	Some type of B cells, T cells, macrophages, dendritic cells	Dako	Monoclonal Clone (TAL 1B5)	1:160	Citrate, Tween
MAC387	Monocytes, macrophages, neutrophils	Dako	Monoclonal Clone (Mac387)	-	-
CD163	Monocytes, macrophages	INIA‡	Monoclonal	-	-
SWC3	Monocytes, macrophages	INIA	Monoclonal	-	-

Table 4. Antibodies used in immunohistochemistry. * polyclonal antibody. † monoclonal antibody. ‡ INIA (Instituto Nacional de Investigación y Tecnología Agraria y Alimentaria, Madrid, Spain) (-): Neither dilution, nor treatment, has proved successful in ferret tissues.

Briefly, tissue sections were deparaffinised with xylene and rehydrated throughout with graded alcohols. Endogenous peroxidase activity was blocked by incubation with H_2O_2 3% in methanol for 30 minutes (min). Tissue sections were rinsed in 0.1M phosphate buffered saline (PBS; pH = 7.5). For the antigen retrieval, citrate, retrieval solution (Target Retrieval Solution, 10× concentrate, nº S1699, Dako), and ethylenediaminetetraacetic acid (EDTA), buffers were tested at 98°C for 20 min. For the anti-Mac387, anti-CD163, anti-SWC3, and anti-lysozyme antibodies, an enzymatic digestion with proteinase K was also tested as antigen retrieval treatment. Afterwards, Triton 0.2% for the anti-CD79α antibody and Tween 0.1% for the rest of antibodies, diluted in PBS for 10 min, were used to permeabilize the cell membranes. For the anti-Mac387, anti-CD163, and anti-SWC3 antibodies, both detergents were used in different attempts. Later, slides were blocked with 2% bovine serum albumin (BSA) (85040C, Sigma-Aldrich Química) for 1 hour (h) at room temperature (RT). Next, primary antibodies were applied overnight (∼18 h) at 4°C, except CD79α, which was incubated at RT. A biotinylated goat anti-mouse antibody (E-0433, polyclonal goat anti-mouse immunoglobulin biotinylated antibody, Dako) diluted 1:200, was used as a secondary antibody for the HLA-DR, CD79α, and Mac387 antibodies. Meanwhile a biotinylated goat anti-rabbit antibody (1:200) was used for the anti-CD3 antibody.

An avidin–biotin–peroxidase complex (ABC) (Pierce Biotin Quantisation Kit, Thermo Fisher Scientific), diluted 1:100, was applied at RT for 1 h in CD3 and HLA-DR detection. For CD79α, anti-lysozyme, anti-SWC3, anti-CD163, and anti-CD20, a polymer-based non–avidin–biotin–peroxidase system (Dako EnVision + System, Peroxidase-HRP) was used, and applied directly to the slides, and incubated for 30 min at RT. For Mac387, both methods were tested. Afterwards, sections were incubated in 3,3-diaminobenzidine tetrahydrochloride (DAB) hydrogen peroxide solution, counterstained with Harris haematoxylin, dehydrated, covered with a coverslip, and examined under microscope. Swine lymph node and lung tissue sections, in which the specific primary antibodies were substituted with PBS or an irrelevant antibody, were used as negative controls.

Swine lymph node and lung tissue sections were used as positive control for all the primary antibodies [221-223], except for CD20, in which canine lymph node sections were used as positive controls [224].

Immunofluorescence and IHC in Frozen Tissues

The anti-myeloid/histiocyte (Mac387), anti-CD163, and anti-SWC3 antibodies were also tested for immunofluorescence and IHC in frozen samples from spleen, lymph node, and lung. Briefly, frozen samples were stored at –80°C until they were cut into 7-µm-thick serial tissue sections using a cryostat (Leica Microsystems, Germany) at –25°C. They mounted on SuperFrost Plus glass slides (631-9483, VWR International Eurolab, SL, Spain).

Tissues were thawed for 30 min at RT and fixed using precooled acetone at –20°C for 10 min, then dried at RT for a further 10 min. Later, samples were rinsed 3 times with PBS (pH = 7.5) and blocked with 2% BSA (85040C, Sigma-Aldrich Química) in PBS, containing 0.1% Triton X-100 (T8787, Sigma-Aldrich Química), 1 h at RT. After that, sections were incubated overnight with the nondiluted primary antibody at 4°C. Then, the samples were rinsed with PBS and incubated with a goat anti-mouse (Alexa Fluor 488, Invitrogen, Spain) as a secondary antibody, diluted 1:300 in PBS for 1 h at RT.

Nuclear counterstaining was performed using Hoechst 33258 (Sigma-Aldrich Química), diluted 1:500 in PBS, for 10 min at RT. Samples were rinsed with PBS and sealed with antifade Vectashield mounting medium. Negative controls consisted of the same tissue incubated with blocking buffer instead of the primary antibody. Swine lung and spleen tissues were used as positive controls.[221 225] For the IHC in frozen tissues, the same procedure was carried out using a different secondary antibody, a biotinylated goat anti-mouse antibody (1:200), incubated for 1 h. Afterwards, an ABC (Pierce Biotin Quantisation Kit, Thermo Fisher Scientific) diluted 1:100, was applied at RT for 1 h. Finally, sections were incubated in DAB hydrogen peroxide solution,

counterstained with Harris haematoxylin, dehydrated, and covered with a coverslip, and then, examined under microscope. Tissue sections, in which the specific primary antibodies were substituted with PBS, were used as negative controls. Swine lymph node and lung tissue sections were used as positive controls for all the primary antibodies.[222] [223]

Double Immunohistochemical Staining for Codetection of Antibodies

Double immunohistochemical staining in FFPE tissues was performed for the codetection of the antigens HLA-DR + CD79α, HLA-DR + CD20, and CD79α + lysozyme, in lymphoid tissues (lymph nodes, spleen, thymus, small intestine, including Peyer's patches and bone marrow), to elucidate the nature of several cells with myeloid morphology, and positive staining for anti-CD79α antibody. The protocol used in this experiment was similar to that described in other studies[226] [227] with minor modifications.

Briefly, paraffin-embedded tissue samples were dewaxed, cut to 3 µm in thickness, and blocked to eliminate the endogenous peroxidase activity using 3% H_2O_2 in methanol. Antigen retrieval was carried out with citrate buffer at 98°C for 20 min, and later permeabilised using Triton 2% for the anti-CD79α primary antibody, and Tween 1% for the anti-CD20 primary antibody in PBS, for 15 min. Slides were blocked with 20% normal goat serum diluted in PBS for 1 h at RT. The primary staining corresponded to the incubation with the antibody against CD79α diluted 1:25, and against CD20 diluted 1:300, in blocking buffer. Antibodies were incubated overnight at RT and 4°C, respectively. After incubation of the primary antibody, tissues were rinsed for 15 min with PBS. Later, a secondary goat anti-mouse antibody, conjugated with a polymer-based non–avidin–biotin–peroxidase system (Dako EnVision + System, Peroxidase-HRP), was applied directly to the slides, and incubated for 30 min at RT. Finally, sections were incubated in DAB hydrogen peroxide solution for 10 min. The presence of positive staining was visualized in brown.

For the second staining, samples were rinsed and permeabilised 3 times, with Tween 1% diluted in PBS, and blocked again with normal goat serum, 20% diluted in PBS. After that, tissue sections were incubated with the second primary antibody anti-HLA-DR, diluted in blocking buffer, overnight at 4°C (diluted 1:80 when combined with CD79α, and diluted 1:50 when combined with CD20). Later, the slides were rinsed in PBS for 15 min and incubated in an alkaline phosphatase conjugate goat anti-mouse Ig (H+L) secondary antibody (1010-04, Southern Biotechnology), diluted 1:100 in PBS.

For the second staining using the polyclonal antibody anti-lysozyme, slides were incubated with anti-lysozyme, diluted 1:1000 in blocking buffer overnight at 4°C. Later, the slides were rinsed in PBS for 15 min and incubated in the alkaline phosphatase conjugate goat anti-rabbit secondary antibody (EXPOSE Rabbit Specific AP [red] Detection IHC Kit, ab94738, Abcam, UK) without dilution. The presence of positive staining was visualized in blue using nitroblue tetrazolium chloride 5-bromo-4-chloro-3-indolyl phosphate (NBT-BCIP; 11 681 451 001, Roche). Immunolabelling of HLA-DR and lysozyme positive cells were visualized in blue.

Codetection was visualized as a deep violet colour. Samples were not counterstained. Negative controls consisted of the incubation of a sequential sample, with PBS instead of the primary antibodies. Positive controls, consisting of ferret lymph node sections, were included for each antibody separately. To check the unspecific cross-reactions between antibodies, the whole technique was carried out in each control.

Cell Quantification

A semiquantitative assesment of positive cells in IHC was assessed for every tissue and antibody. Positivity was considered and represented with different numbers, depending on the percentage of positive cells per high-power field. This was measured in 4 areas of each organ of every animal. The mean and standard deviation results for each organ for all 5 animals were recorded. The proportion of positive cells

was scored as follows: (0) nil (fewer than 5 positive cells), (1) scarce (less than 25% of positive cells), (2) slight (25%–50% positive cells), (3) moderate (50%–75% of positive cells), and (4) intense (>75% of positive cells).

3.3 Results

Histopathology

Minor histopathologic lesions were observed in some animals. Four of the 5 ferrets showed mild to moderate lymphocytic infiltration, with few eosinophils in the lamina propria of the stomach, consistent with mild gastritis. These cells were mainly T lymphocytes and HLA-DR-positive cells, with low numbers of B cells. A small number of bacillary bacteria were detected with Warthin-Starry special stain in the lumen of the stomach. However, no spiral-shaped bacteria consistent with *Helicobacter spp.* were observed in any animal.

In the kidneys of all animals, a mild accumulation of a brown, finely granular pigment in the cytoplasm of tubular epithelial cells was observed. This pigment was negative following Prussian blue staining. No relevant microscopic lesions were observed in the remaining tissues.

Relevant results for lymphoid and non-lymphoid tissues are shown in (Tables 5 and 6), respectively.

	Lymph Node					Spleen		Peyer's Patch		Thymus	
	Cortex			Medulla		PALS	Follicles	GC	Mantle	Medulla	Cortex
	GC	Mantle	Paracortex	Cords	Sinus						
CD3	0.9	0.9	3.4	1.2	0.7	3.6	1	0.9	1.33	3.5	1.5
	0.2	0.4	0.4	0.2	0.2	0.5	0.3	0.5	0.5	0	0
CD79α	2.9	4	0.9	3.1	1.1	0.8	3.9	2.1	4	1.5	0
	0.2	0	0.2	0.1	0.2	0.4	0.4	0.5	0	0.2	0
CD20	3.8	4	1.1	2.8	0.9	1.2	3.9	3.1	4	2.3	0.2
	0.2	0	0.4	0.5	0.2	0.4	0.2	0.2	0	0.2	0.2
HLA-DR	2,1	2	1,7	1.7	1.3	1.4	2.8	2.5	2	3.5	0.8
	0.5	0.7	0.4	0.4	0.4	0.5	0.7	0.5	0	0.5	0.2
Lysozyme	1.3	0	1.3	0.8	0	1	1.4	1	1	0.6	0.3
	0.2	8	0.2	0.2	0	0	0.4	0.5	0	0.2	0.5

Table 5. Comparative immunohistochemical staining distribution in different lymphoid areas. The average and the standard deviation (below) are shown for different areas of every organ. GC: germinal centre. PALS: periarteriolar lymphoid sheaths. 4: >75% positive cells per high power field (x400). 3: 50-75% positive cells per high power field (x400). 2: 25-50 % positive cells per high power field (x400). 1: <25% positive cells per high power field (x400). 0: 0 or <5 positive cells per high power field (x400).

	Intestine		Lung		Liver		Nasal turbinate
	IE	LP	BALT	Alveoli	Periportal	Sinusoids	
CD3	2.1	1.2	0.8	0-3	2.1	0.3	0.8
	0.2	0.4	0.2	0.4	0.2	0.4	0.2
CD79α	0.2	1.2	2	1.6	0.9	0	1
	0.2	0.4	0	0.5	0.7	0	0
CD20	0.6	1	1.1	1.4	1.75	1.25	0.8
	0.4	0.7	0.4	0.2	0.9	0.5	0.2
HLA-DR	2.3	1.8	1.7	1.1	2.1	0	1.3
	0.7	0.4	0.2	0.2	0.2	0	0.5
Lysozyme	0.3	0.4	ND	ND	1.2	4	0.1
	0.4	0.5			1.6	0	0.2

Table 6. Comparative immunohistochemical staining distribution in different non-lymphoid organs. The average and the standard deviation are shown for different areas of every organ. IE: Intraepithelial. LP: Lamina propria. BALT: Bronchus associated lymphoid tissue. ND: Not determined. 4: >75% positive cells per high power field (x400). 3: 50-75% positive cells per high power field (x400). 2: 25-50 % positive cells per high power field (x400). 1: <25% positive cells per high power field (x400). 0: 0 or <5 positive cells per high power field (x400).

IHC

CD3

The anti-CD3 antibody labelled the surface and cytoplasm of round cells, consistent with lymphocytes in FFPE (Figure 7a). These cells were located in T-cell areas of the lymph nodes (Figure 8a), Peyer's patches (Figure 8d), spleen (Figure 8g), and thymus (Figure 8j). In the lymph node, these areas corresponded to interfollicular and paracortical areas and to periarteriolar lymphoid sheaths (PALS) in the spleen. Moderate to abundant numbers of positive cells were found in cortical and medullary areas, of the thymus, with higher concentration of CD3-positive-labelled cells in the medulla. A small number of positive cells were observed, forming a marginal layer of CD3-positive-labelled cells around Peyer's patches. A very small number of CD3-positive-labelled cells were located, scattered in the follicular germinal centres of lymph nodes, spleen, Peyer's patches, bone marrow, and medullary areas of lymph nodes. In nonlymphoid tissues, moderate numbers of CD3-positive cells were observed in periportal areas of the liver, and the lamina propria and intraepithelial compartment of the intestine. A small number of CD3-positive-labelled cells were located in the bronchus associated lymphoid tissue (BALT) of the lung, and multifocally distributed in the interstitium of pancreas. A very small number of CD3-positive-labelled cells were observed in the lamina propria of trachea, and nasal turbinates.

None or a very limited number of CD3-positive-labelled cells were observed in the heart, skin, muscle, eye, subarachnoid space, and the choroid plexus of the brain. Variable numbers of CD3-positive-labelled circulating cells were detected in the blood vessels of all tissues studied.

CD79α

The anti-CD79α antibody positively labelled the cell membrane and cytoplasm of small round cells in FFPE tissues. These cells presented a centrally located nucleus and a

narrow rim of cytoplasm, consistent with lymphocytes (Figure 7b). These cells were localized in B-cell areas, mainly in the lymphoid follicles of the lymph nodes (Figure 8b), Peyer's patches (Figure 8e), and spleen (Figure 8 h). There was a denser concentration of positive labelling in the mantle of lymph nodes and Peyer's patches. Smaller numbers of CD79α-positive-labelled small cells were located in the thymic medulla (Figure 8k) and the dome region of Peyer's patches. High numbers of CD79α-positive small cells were also located in the bone marrow, and medullar cords of the lymph nodes.

In nonlymphoid tissues, moderate numbers of immunolabelled small cells were observed in the lungs, and intestinal lamina propria. Cells were located within the bronchiolar epithelium, mucous glands, BALT, peribronchiolar connective tissue, and alveolar septa. Low numbers of positive small cells were observed in the periportal areas of liver, tracheal lamina propria, meninges, and choroid plexus of the brain. In the pancreas, kidney, skeletal muscle, and eye, very few positive cells were detected in the interstitial connective tissue. Variable numbers of CD79α-positive-labelled circulating cells were detected in the blood vessels of all studied tissues.

Interestingly, a subpopulation of CD79α positive cells which were characterised as showing irregular cell borders, abundant cytoplasm, and eccentric and round-to-oval nucleus, was detected in the follicular germinal centres (Figure 7b) of the spleen, lymph nodes, and Peyer's patches. In the thymus, a moderate amount of these cells were also observed in the thymic medulla.

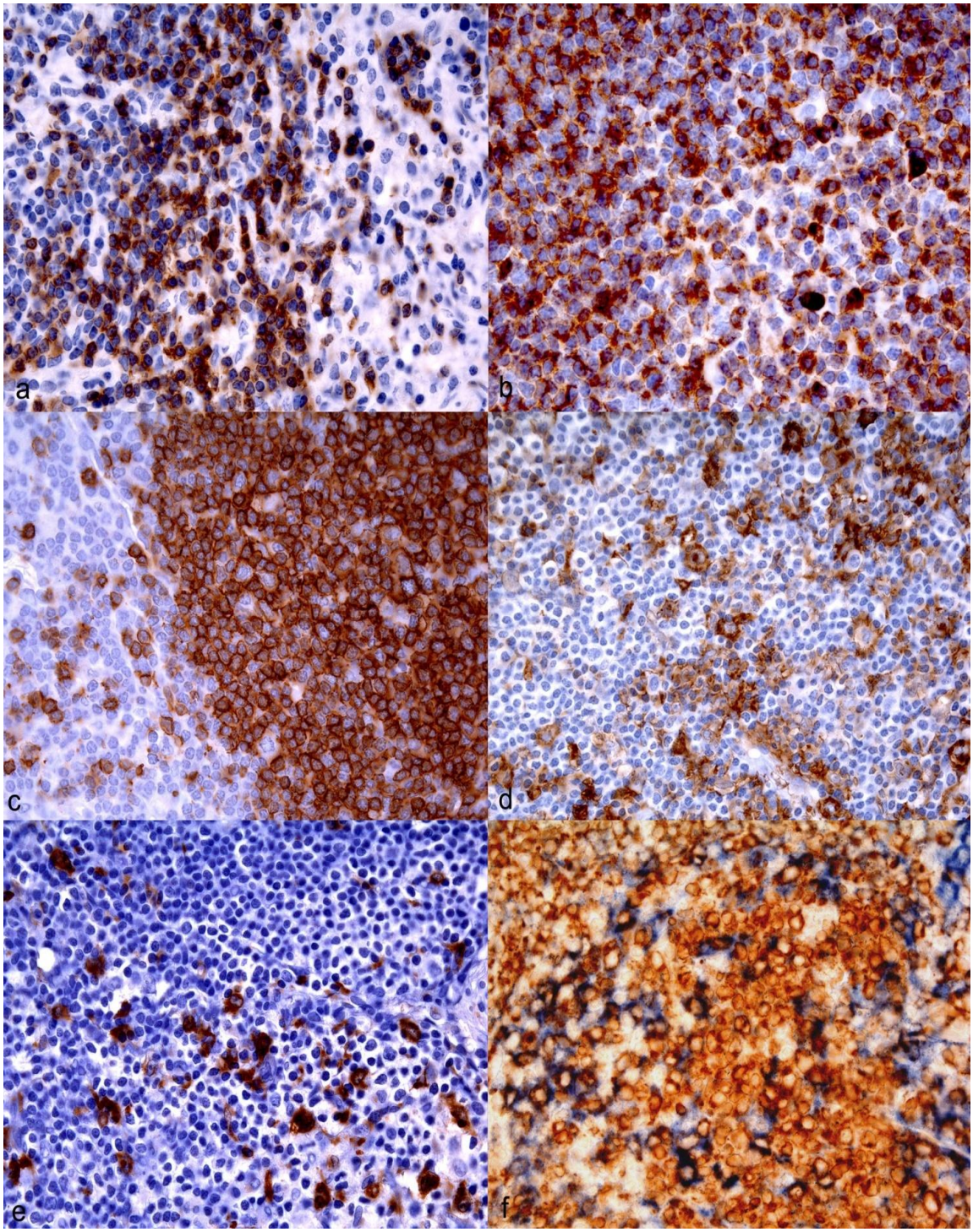

Figure 7. Lymph node, ferret. (a) T cells immunolabelled with anti-CD3 antibody. (b) B cells immunolabelled with anti-CD79α antibody. (c) B cells immunolabelled with anti-CD20 antibody. (d) Follicular dendritic cells and macrophages in follicular germinal centres immunolabelled with the anti-HLA-DR antibody. (e) Macrophages in follicular germinal centres immunolabelled with the anti-Lysozyme antibody. DAB staining, haematoxylin counterstain. (f) Double immunostained cells with the anti-CD79α and the anti-HLA-DR antibodies in germinal centres of lymphoid follicles. Anti-HLA-DR antibody immunostained in blue NBT-BCIP and anti-CD79α antibody immunostained in brown DAB without counterstaining.

HLA-DR

The HLA-DR antibody labelled different cell types in FFPE tissues. Some HLA-DR-positive cells were small and round with a centrally located nuclei and a narrow rim of cytoplasm consistent with lymphocytes. Besides these, medium-sized cells with a moderate amount of cytoplasm, and oval-to-round nuclei consistent with cells of the macrophage/dendritic lineage, were also detected by using this cell marker (Figure 7d).

Moderate numbers of HLA-DR-positive lymphocyte-like cells were observed in the mantle of lymphoid follicles in lymph nodes, Peyer's patches, and spleen. Moderate numbers of HLA-DR-positive macrophage/dendrite-like cells were also observed in the follicular germinal centres in the lymph nodes (Figure 8c), Peyer's patches (Figure 8f), and spleen (Figure 8i). These cells were considered as follicular dendritic cells, and tingible body macrophages. Low numbers of positive macrophage/dendrite-like cells were detected in medullar and paracortical areas of the lymph nodes. They were considered interfollicular dendritic cells and tingible body macrophages. In the thymus, a small number of positive cells were located in the cortex and were also considered to be tingible body macrophages. A moderate to high number of positive cells were observed in the thymic medulla (Figure 8l). These cells were considered to be epithelial reticular cells, or interdigitating cells of the thymus.

In nonlymphoid tissues, moderate numbers of HLA-DR lymphocyte–positive cells were present in the periportal areas of the liver, and lamina propria of the intestine. In the lung, positive labelling was present in lymphocyte-like cells located in the bronchiolar lamina propria. In the liver, the anti-HLA-DR antibody labelled Kupffer cells located in the sinusoids. In the lung, macrophage/dendrite-like cells were located in the alveolar lumen and wall, and were considered to be pulmonary alveolar macrophages. A moderate number of positive cells, consistent with macrophage/dendrite-like cells, were also observed in the intraepithelial compartment and lamina propria of the intestine, nasal turbinate, and trachea.

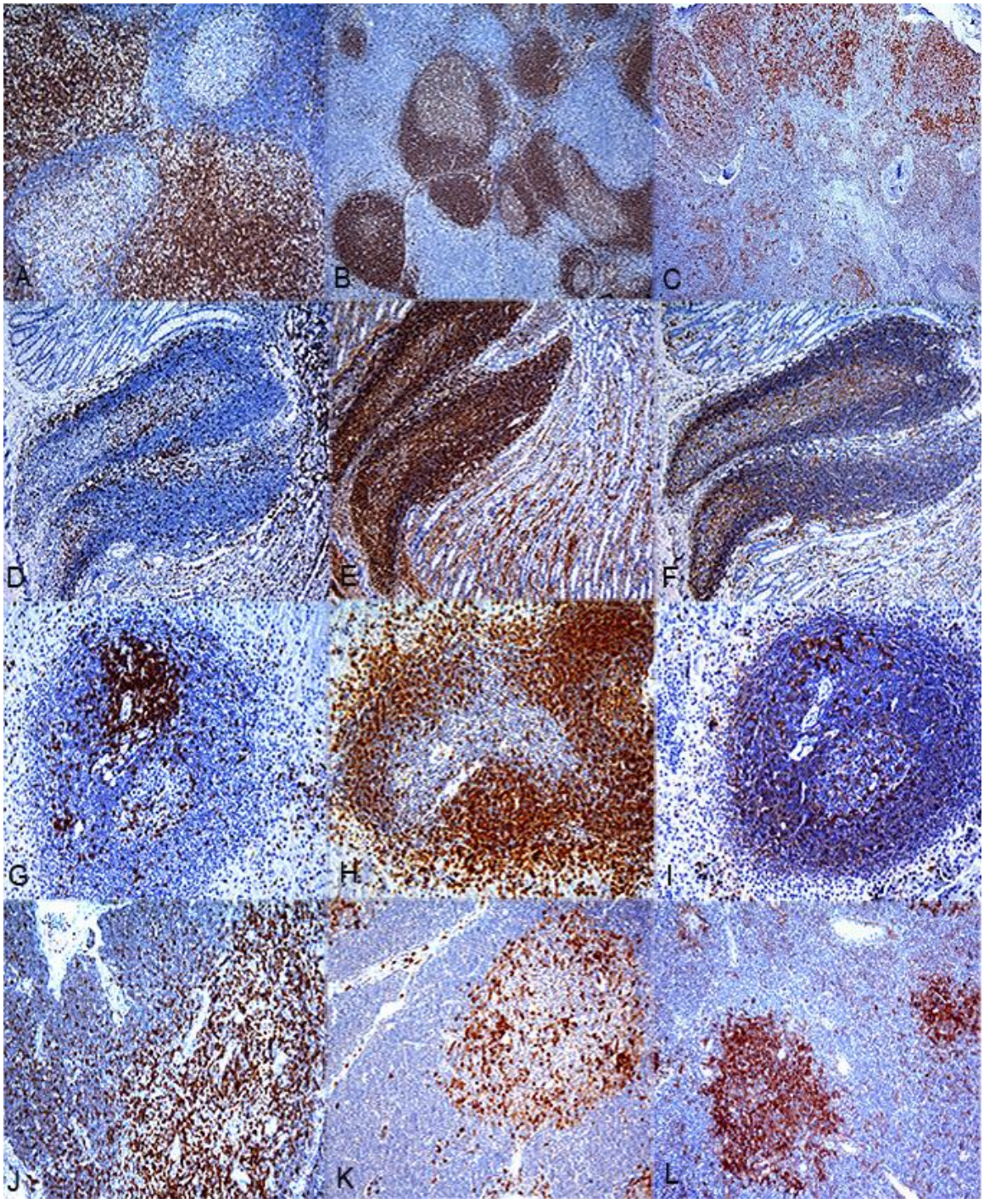

Figure 8. Lymphoid tissues, ferret. Lymph node cortex: Immunostained T cells with the anti-CD3 antibody. (b) Immunostained B cells with the anti-CD79α antibody. (c) Immunostained immune cells with the anti-HLA-DR antibody.
Peyer's Patches: (d) Immunostained T cells with the anti-CD3 antibody. (e) B cells immunostained with the anti-CD79α antibody. (f) Immunostained cells with the anti-HLA-DR antibody.
Spleen, white pulp: (g) Immmunstained T cells with the anti-CD3 antibody. (h) Immunostained B cells with the anti-CD79α antibody (i) Immunostained cells with the anti-HLA-DR antibody.
Thymus: (j) Immunostained T cells with the anti-CD3 antibody (k) B lymphocytes and large irregular cells, immunostained with the anti-CD79α antibody (l) Immunostained cells with the anti-HLA-DR antibody.
DAB staining, haematoxylin counterstain.

In the interstitium of the kidney, bone marrow, pancreas, heart, meningeal and choroid plexus of the brain, muscle, skin, and eye, HLA-DR labelled a very low number of macrophage/dendrite-like cells. Variable numbers of HLA-DR-positive-labelled circulating cells were detected in the blood vessels of all tissues studied.

CD20

The anti-CD20 antibody immunolabelled the membrane of small round cells, with scarce cytoplasm and a central round nucleus, consistent with lymphocytes in FFPE tissues (Figure 7c). These cells were located forming primary and secondary follicles in lymph nodes immunolabelled mantle and germinal centre with equal intensity (Figure 9a), Peyer's patches (Figure 9c), and white pulp of the spleen (Figure 9e). In the follicular germinal centres, the anti-CD20 antibody also slightly immunolabelled larger round cells with large amounts of cytoplasm, and a bigger central round nucleus, consistent with immunoblasts. Moderate numbers of CD20-immunolabelled small cells were located in the thymic medulla (Figure 9g).

Interestingly, the CD20 antibody also immunolabelled a subpopulation of large macrophage/dendritic positive cells characterised as showing irregular cell borders and abundant cytoplasm, with an eccentric and a round-to-oval nucleus. These cells were detected in the follicular germinal centres of the spleen, lymph nodes, and Peyer's patches. In the thymus, a moderate amount of these cells were also observed in the thymic medulla. High numbers of CD20 positive-labelled small cells were also located in the bone marrow and in the medullary cords of the lymph nodes.

In nonlymphoid tissues, the anti-CD20 antibody immunostained the membrane of small round cells, consistent with lymphocytes. Low numbers of positive cells were observed in the lung (alveolar septa and BALT) and in the liver (periportal areas and sinusoids). The anti-CD20 antibody also labelled low numbers of cells in the lamina propria of the intestine, trachea, meninges, and choroid plexus of brain.

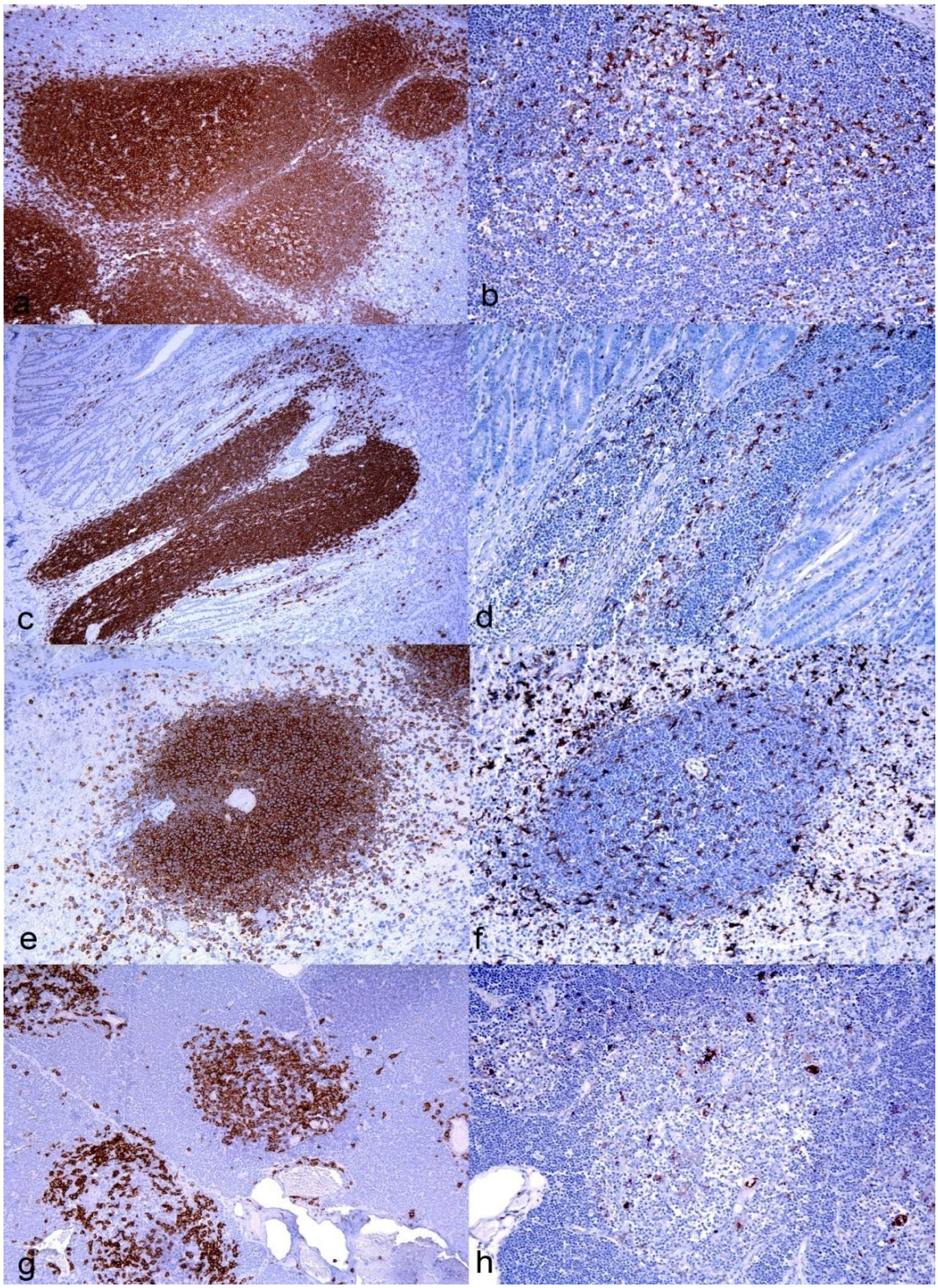

Figure. 9. Lymphoid tissues, ferret.
Immunostained B cells with the anti-CD20 antibody. (a) Lymph node, (c) Peyer's Patches, (e) Spleen. white pulp, (g) Thymic medulla. Immunostained macrophages and tingible body macrophages with the anti-Lysozyme antibody. (b) Lymph node follicle, (d) Peyer's Patches, (f) Spleen, (h) Thymic medulla. DAB staining, haematoxylin counterstain.

In the pancreas, kidney, heart, skeletal muscle, and eye, very few positive cells were detected in the interstitial connective tissue. Variable numbers of CD20-positive-labelled circulating cells were detected in the blood vessels of all studied tissues.

Lysozyme

In formalin-fixed paraffin-embedded tissues: the anti-lysozyme antibody immunolabelled the cytoplasm and membrane of round-to-polyhedral, medium-size cells with abundant and irregular cytoplasm and round to “bean-shape” exocentric nucleus consistent with macrophages (Figure 7e). High numbers of positive polyhedral cells were located in the red pulp of the spleen. Low numbers of positive cells were located in the germinal centres of lymphoid follicles in the lymph nodes (Figure 9b), Peyer’s patches (Figure 9d), spleen (Figure 9f), and paracortical areas and cords of lymph node and thymus (Figure 9h). In the bone marrow, moderate to large numbers of positive cells were also observed and were interpreted as myeloid leukocytes.

In nonlymphoid tissues, large numbers of positive cells were observed between hepatic sinusoids of the liver. Low numbers of positive cells were located in the tracheal lamina propria, meninges, and choroid plexus of the brain. In the pancreas, skeletal and heart muscle, kidney, stomach, and eye, very few positive cells were detected in the interstitial connective tissue.

The anti-lysozyme antibody also immunolabelled the cytoplasm of different nonlymphoid cell types, namely ciliated epithelial cells of the trachea, glandular cells in the bronchus, trachea, and stomach, plus high endothelial venules of lymph nodes and renal proximal tubules. Variable numbers of lysozyme-positive circulating cells were detected in the blood vessels of the different tissues studied.

Mac387, CD163, and SWC3

No positive labelling was detected in any ferret tissue using the anti-Mac387, anti-CD163, or anti-SWC3 antibodies in frozen or FFPE tissues.

Double Immunohistochemical Staining

To clarify the origin of the CD79α- and CD20-positive cells with nonlymphocytic morphology, a double IHC was carried out using different combinations of antibodies. The intention was to find out if these cells could belong to the macrophage/dendritic lineage. Low to moderate numbers of cells were labelled with both anti-CD79α and anti-HLA-DR (Figure 7f). Double immunolabelled cells were located in germinal centres of lymphoid follicles, spleen, and Peyer's patches (Figure 10). A smaller number of cells were also labelled with both anti-CD20 and anti-HLA-DR antibodies, in the germinal centres of lymphoid follicles. No co-expression of anti-CD79 + anti-lysozyme antibodies was observed in follicular germinal centres of lymphoid follicles in lymph nodes, spleen, nor Peyer's patches and in medullar areas of the thymus.

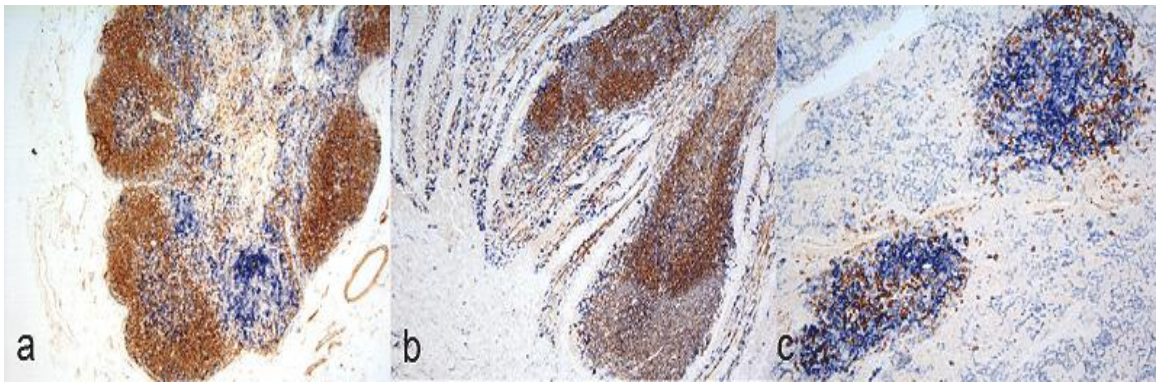

Figure 10. Double immunohistochemistry with anti-HLA-DR antibody immunostained in blue and anti-CD79α antibody immunostained in brown. (a) Lymph node, ferret. Germinal centre of lymphoid follicles showed double labelling of CD79α and HLA-DR antibodies, in follicular dendritic like cells. (b) Peyer's patches, ferret. Germinal centre of Peyer's patches follicles showed double labelling of CD79 and HLA-DR antibodies, in follicular dendritic like cells. (c) *Thymus*, ferret. Thymic medulla showed double labelling of CD79α and HLA-DR antibodies in interdigitating like type cells. Anti-CD79α antibody immunostained with DAB and anti-HLA-DR antibody immunstained with *NBT-BCIP, without counterstain.*

3.4 Discussion

A detailed knowledge of normal immune system cell distribution is required to better understand the pathologic changes of many infectious and non-infectious diseases. In recent years, the ferret has become a reliable animal model for infectious and degenerative diseases [190,228]. However, there are still no detailed descriptions of the main ferret immune system cells. In this study, both standard and double IHC techniques were performed towards that end. Furthermore, a histological description was made of the previously uncharacterised antibodies CD20, lysozyme, and HLA-DR.

Animals from this study were clinically healthy, although 4 presented a mild to moderate lymphocytic infiltration in the stomach, mainly formed by CD3- and HLA-DR-positive cells. The cause of this infiltration is currently unknown because animals tested negative to Aleutian disease by PCR in plasma and no spiral-shaped bacteria compatible with *Helicobacter spp*. were detected in Warthin-Starry stain.

The anti-CD3 and anti-CD79α antibodies were formerly used to characterise ferret lymphomas [219,220]. In our study, the distribution of T and B cells in lymphoid tissues of healthy ferrets correlated with that described in other mammal species and humans [221,229-232].

The anti-CD20 antibody has been described as a B-cell marker in other species, such as dogs and mice [224,233]. In humans, dogs, and mice, the anti-CD20 antibody is expressed in pre–B cells and in mature B cells [224,225,233]. In ferret tissues, CD20 immunolabelled the membrane of B cells located in B-cell areas. In addition, CD20 intensely immunostained the germinal centre of lymphoid follicles, impeding the differentiation between the germinal centre and the mantle zone. The strong immunostaining found in follicular germinal centres made it difficult to differentiate between the different shapes and structures of the cells within the germinal centre, as described in other species [224].

The intense expression of CD20 in germinal centres clearly stands out when compared with the CD79α immunolabelling. This could be the result of different expression between the CD79α and CD20 molecules, which is dependent on the stage of B-cell maturation. Resting naïve B lymphocytes in the mantle express a higher number of CD79α molecules, and the activation of germinal centre B cells into mature B cells downregulates CD79α expression [234]. In contrast, the CD20 antigen expression increases on B cells located in lymphoid germinal centres, as they mature [224,225].

The primary purpose of MHC-II molecules is to allow antigen-presenting cells and B cells to display the epitopes of the invading pathogen to T cells. In humans, histocompatibility class II antigens are expressed in a limited number of cell types: macrophages, monocytes, B cells, and a variable number of T cells [235], dendritic cells [236], and in some types of epithelial cells, such as thymic epithelial cells and pneumocytes type II [237]. In this study, it was possible to identify these cells for the first time in ferret tissues and to study their distribution using the anti-HLA-DR antibody. This antibody strongly labelled cells which presented different characteristics. Some had round central nuclei and a small rim of cytoplasm. These were considered B or T lymphocytes [238], depending on their expression of CD20, CD79α, or CD3 molecules, as well as their location and morphology. It is worth mentioning that in our study, not all CD79α- and CD20-positive B cells were immunolabelled with the anti-HLA-DR antibody, even though the expression of MHC-II molecules in all B cells has been reported in different mammal species and humans [230,238]. The other sub-population of HLA-DR-positive cells was large and irregular, and was recognized as macrophages or dendritic cells, depending on their shape and distribution in the lymphoid and nonlymphoid organs [239,240].

The anti-human lysozyme antibody has been described as a useful marker to immunostain cells of the myeloid series in different mammal species and humans [221,241,242]. In ferret tissues, the anti-lysozyme antibody immunolabelled mature peripheric myeloid cells and different types of resident macrophages. However, the

anti-lysozyme antibody failed to immunolabel resident macrophages in the lungs as described in other species [221,234], which could be a consequence of incomplete formalin penetration during tissue fixation.

In addition to B cells, the CD79α and the CD20 antibodies immunolabelled atypical B cells with a macrophage/dendritic morphology, located in nontypical B cell areas. The expression of B-cell markers in large cells with an atypical morphology has been described in humans at follicular germinal centres, and scattered in the thymic medulla [243-245]. Furthermore, a subpopulation of large interfollicular B cells showing a dendritic morphology has been described in humans [246]. These cells were positive to the B-cell markers CD79α and CD20, yet negative to dendritic and macrophagic markers. In the present study, double IHC techniques combining different B-cell markers with the HLA-DR antibody (expressed in follicular dendritic cells [247], interdigitating cells, and macrophages [235]) and the macrophagic marker lysozyme, have been used to elucidate the origin of these atypical B cells. Results showed that these cells did not coexpress the lysozyme and the CD79α antigens, but did coexpress both B-cell markers (CD20 and CD79α) with the HLA-DR antibody, suggesting that these cells did not have a macrophagic origin, and that they do have a B-cell origin, despite their morphology.

The results obtained in this work led us to hypothesize that these atypical large B cells found in lymphoid germinal centres and thymic medulla might be a subpopulation of B cells similar to those described before in humans and mice [243,245,246] or, less likely, follicular dendritic cells. The lack of reliable dendritic markers that cross-react with ferret tissues impeded us from further testing this hypothesis. Hence, further investigation into the immunophenotyping of ferret cells should be undertaken to further elucidate the origin of these cells.

The monoclonal swine antibodies CD163 and anti-SWC3 were described as useful markers for immunostaining cells of the monocyte/macrophage lineage in swine tissues [222,223]. The monoclonal human anti-L1 (Mac387) antibody has been described as

a useful marker for immunostaining macrophages or polymorphonuclear cells in different mammal species [221,230,232,248]. Different protocols for the standardization of the IHC technique with these antibodies (in frozen and FFPE ferret tissues) were implemented in the present study. However, despite the positive results obtained in swine tissue controls, the Mac387, CD163, and SWC3 antibodies did not cross-react with ferret tissues in this study.

The current study investigated the normal distribution of immune cells in lymphoid and non-lymphoid FFPE tissues of conventional healthy ferrets, using immunohistochemical techniques with different antibodies. This study represents a preliminary histological investigation of the distribution into certain immune system cells in conventional healthy ferrets. This will help to establish a basis for future research, which could lead to a better understanding of immune responses in ferrets. Moreover, it contributes to the standardization of several immunohistochemical markers in this species, which may help in the diagnosis, and research into different infectious and non-infectious ferret diseases.

CHAPTER 4

STUDY II: *Experimental Infection of Ferrets with Two H1N1v Viral Isolates from Patients Presenting Different Pathological Outcomes of Disease*

4.1 Introduction

The physiopathology of H1N1v infection in humans differs between individuals. Whilst most patients developed mild upper respiratory-tract infection, some patients progressed to develop severe lower respiratory-tract complications, with fatal consequences [163,249]. The cause of death in the severe cases was identified as a consequence of DAD, which is also termed acute interstitial pneumonia [154].

The striking heterogeneity of the clinicopathological outcomes observed after H1N1v infection in humans led to numerous studies initially focused on the impact of viral evolution and mutation on the virulence of the infection. The viral strains used in this study have been sequenced, and several mutations have been found in each of the viral strains[250]. However, the importance of these mutations in the pathogenicity of H1N1v still needs to be clarified [250]. In addition, a variety of studies have suggested that host characteristics associated with appropriate immune responses, play important roles in determining the outcome of infection after H1N1v infection [157,171-176,251,252].

This study attempted to clarify whether the diversity in virulence of H1N1v isolates in humans significantly correlates with the clinicopathological outcome in ferrets. The aim of this study was accomplished by experimentally infecting ferrets with two H1N1v isolates, from two human patients, who had developed different clinical outcomes. The viral dynamics and host immune responses of the lungs of the infected ferrets were thoroughly investigated. Assessments of the pathologic patterns of the lungs and measurements of immune cell, cytokine responses, and apoptotic cell induction, were performed to identify the factors involved in the outcome of disease.

4.2 Material and methods

Viruses

Two strains of human H1N1v virus which had been isolated from geographically similar locations were used in the present study. The viruses were isolated at the National Influenza Centre, *Centro Nacional de Microbiología, Insituto de Salud Carlos III* (CNM, ISCIII) from respiratory samples sent by the Spanish Influenza Surveillance System for virological characterisation.

The H1N1v subtype isolates A/CastillaLaMancha/RR5661/2009 and A/CastillaLaMancha/RR5911/2009 were isolated from respiratory samples of two patients who were both Caucasian, and free of previous co-morbid conditions at the time of infection. Hereafter, the following designations will be used: virus R61 for the A/CastillaLaMancha/RR5661/2009 virus, which was isolated from a 23-year old man exhibiting mild respiratory disease, and virus R11 for the A/CastillaLaMancha/RR5911/2009 virus, which was isolated from a 35-year old woman who developed a severe disease, which resulted in fatality. Both viruses were isolated via bronchoalveolar lavage as described by Rodríguez *et al.* [250], and were passaged three times in Madin-Darby Canine kidney (MDCK) cells. The R61 virus had a titre of $10^{8.3}$ 50% Tissue Culture Infective Dose ($TCID_{50}$) per mL, and the R11 virus had a titre of $10^{8.2}$ $TCID_{50}$/mL, as determined in the Reed and Muench method [253].

Ferrets

Ten ferrets between the ages of twelve and twenty-four months that were seronegative for IAV (influenza A antibody competition multi-species ELISA, ID Screen®, France), and Aleutian disease virus were randomly selected from a stable, purposely bred colony (Isoquimen, Spain). Upon arrival at the *Centre de Recerca en Sanitat Animal* (CReSA), the animals were placed in biosafety level 3 (BSL-3) facilities. The ferrets were randomly assigned to different experimental groups, separated into experimental isolation rooms, and then maintained for one week for acclimation. The

animals were maintained in standard housing cages, and provided with commercial food pellets and tap water *ad libitum,* throughout the experiment. All experiments were performed under a protocol (n° 1976) that was reviewed and approved by the Animal and Human Experimentation Ethics Commission of the *Universitat Autònoma de Barcelona* (UAB).

All ferrets were monitored daily for clinical signs, and any animal which was determined to be in a moribund state, was ethically euthanized. Any animal losing 25% of its original body weight or presenting severe respiratory signs such as severe tachypnea, nasal and conjunctival exudates, and/or, severe apathy (irresponsiveness to external stimulus), were considered to be in a moribund state and were humanely euthanized. Anorexia was measured daily by observing the amount of faeces and the amount of food that needed to be replaced and the attitude of the animals towards food. Depression was evaluated with reference to the activity of the animals and their response to external stimulus (such as sound or human presence). Tachypnea was considered when respiratory rate was higher than 70 breaths per minute, accompanied by abdominal breathing.

The animals were divided into three groups. The control group included two ferrets that were inoculated intratracheally with 0.1 M PBS (pH = 7.5). The R61 group included 4 ferrets that were infected with the R61 virus, and the R11 group included 4 ferrets that were infected with the R11 virus. The ferrets were intratracheally inoculated with 10^6 $TCID_{50}$/mL of the appropriate virus, and necropsies were performed on days 4 and 7 postinfection. The animals were euthanized by intravenous injection of sodium pentobarbital (100 mg/kg), under anaesthesia with ketamine (5-10 mg/kg) (Imalgene 1000® Merial, S.A., Spain) and medetomidine (0.05 mg/kg) (Domtor® Pfiser, S.A., Spain). They were then necropsied according to a standard protocol.

Histopathology

Right lung lobe sections (cranial, medial and caudal), nasal turbinate, and trachea, were taken for histological examination according to standard protocols. The tissues were fixed for 48 h in neutral-buffered 10% formalin, then embedded in paraffin wax, sectioned at 3 µm, and stained with HE for examination by light microscopy.

Cross sections of the cranial, middle and caudal pulmonary lobes of each animal were separately evaluated, and semiquantitative assessments of IAV-associated microscopic lesions in the lungs were performed. The lesional scoring was graded on the basis of lesion severity as follows: grade 0 (no histopathological lesions observed), grade 1 (mild to moderate necrotising bronchiolitis), grade 2 (bronchointerstitial pneumonia characterised by necrotising bronchiolitis and alveolar damage in adjacent alveoli), and grade 3 (necrotising bronchiolitis and diffuse alveolar damage in the majority of the pulmonary parenchyma).

Microscopic lesional scores were assigned for each lobe, and the means of the three lobes were used for the final histopathological score for each animal. Animals with lung lesion scores over 2 which presented diffuse alveolar damage in at least 2 of the examined lung lobes were considered to have presented with severe lung lesions, and animals with scores below 2 were considered to have developed mild lung lesions.

Viral Detection and Quantification

For detection of IAV antigen by IHC, the tissues were stained with a primary antibody against the influenza A NP, as previously described [254]. Briefly, an antigen retrieval step was performed using protease XIV (Sigma-Aldrich, UDA) for 10 min at 37 °C, and then blocked for 1 h with 2% BSA (85040C, Sigma-Aldrich Química, S.A., Spain) at RT. Samples were then incubated with a commercially available mouse-derived monoclonal antibody (ATCC, HB-65, H16L-10-4R5) concentration (343 mg/mL),

as a primary antibody, at a dilution of 1:100 at 4 °C overnight, followed by 1 h incubation with biotinylated goat antimouse IgG secondary antibody (Dako, immunoglobulins As, Denmark). Finally, an ABC system (thermo Fisher Scientific, Rockjord, IL, USA) was used and the antigen–antibody reaction was visualized with DAB as chromogen. Sections were counterstained with Mayer's Haematoxylin. Positive control consisted of FFPE chicken heart, experimentally infected with influenza. The same sections in which the specific primary antibodies were substituted with PBS were used as negative controls. Semiquantitative assessments of influenza virus antigen expression in the lungs were performed, and the results were correlated with the lesional patterns. The positive cells in 6 arbitrarily chosen 20x objective fields in alveolar areas, and 5 arbitrarily chosen 20x objective fields in bronchial or bronchiolar areas, were quantified separately in each lung lobe (cranial, medial and caudal), for every animal. The mean of the total cell counts per field, across the three lobes, was calculated for each animal. The viral loads in the lung tissues were assessed by quantitative RRT-PCR, following a Taq-Man one-step RRT-PCR, performed with Fast 7500 equipment (Applied Biosystems, Foster city, CA, USA), as previously described [255].

Viral RNA was extracted with QIAamp viral mini kit (Qiagen, Valencia, CA, USA), obtaining 60 µL of eluted viral RNA. The M gene fragment amplification was carried out using the primers showed in the annex (Table 1), ,and One-Step RRT-PCR Master Mix Reagents (Applied Biosystems) following the manufacturer's instructions using 5 µL of eluted RNA in a total volume of 25 µL. The amplification conditions were as follows: reverse transcription at 48 °C for 30 min; initial denaturation reaction at 95 °C for 15 min and 40 PCR-cycles of 95 °C 15 s, and 60 °C 1 min. Standard curves and quantification were achieved through prior amplification of a 99 bp fragment of the M gene, using One Step RRT-PCR reagents (Qiagen), following manufacturer's instructions. The M gene fragment amplicon obtained was cloned into pGEMT vector (Promega, Madison, WI, USA), and transformed by heat shock in *Escherichia coli* competent cells (Invitrogen, Paisley, UK). The recombinant plasmid was purified using the QIA prep Spin kit (Qiagen) and spectrophotometrically quantified (Qubit,

Invitrogen) as previously described [256]. Serial 10-fold dilutions of both plasmids of known concentration were made and the standard curves were generated. The genome equivalent copies (GEC) of plasmid from the collected samples were determined based on these standard curves, and by taking their volumes into account.

Immunophenotyping and Quantification of Lung Inflammatory Cells

Phenotyping of the different inflammatory cell lineages following IHC were performed on the lungs of the infected and control animals to determine which inflammatory cell types were associated with the different lung lesional patterns. Neutrophils and macrophages were detected by IHC, using anti-lysozyme polyclonal antibodies (Dako, Polyclonal Rabbit Anti-Human Lysozyme EC 3.2.1.17, ref A0099), T and B cells were detected using anti-CD3 (Dako, Polyclonal Rabbit Anti-Human CD3, n° IS503) and anti-CD20 (Thermo Scientific, CD20 Rabbit Polyclonal Antibody, ref RB-9013-P) polyclonal antibodies, using the techniques described in the previous study.

CTLs and NK cells were detected using the anti-CD8α (Sino Biological, Polyclonal Rabbit anti-ferret CD8a Antibody, ref 60001-RPO2, China) polyclonal antibody. Briefly, tissue sections were deparaffinised with xylene and rehydrated through graded concentrations of alcohol. Endogenous peroxidase activity was blocked by incubation with 3% H_2O_2 in methanol for 30 min. Tissue sections were rinsed in PBS and immersed in Retrieval Solution (Dako, Target Retrieval solution 10x concentrate, n°S1699) for antigen retrieval. Later, the slides were blocked with 2% BSA (85040C, Sigma-Aldrich Química, S.A., Spain) for one h at RT, and incubated with the primary antibody overnight, at 4 °C at a dilution of 0.5 µg/mL. Next, a polymer-based non-avidin-biotin peroxidase system (Dako EnVision® + System, Peroxidase-HRP, Dako, Denmark) was applied directly to the slides and incubated for 30 min at RT. The reaction was developed with DAB (Sigma-Aldrich, Madrid, Spain) at RT, followed by counterstaining with Mayer's haematoxylin. Ferret lymph node sections were used as positive controls. The same sections in which the specific primary antibodies were substituted with PBS were used as negative controls.

Semiquantitative assessments of the inflammatory cells detected in the lungs were also performed. The cells that were positive in the IHC for the anti-lysozyme (macrophages and neutrophils), anti-CD3 (T cells), anti-CD8α (CTLs and NK cells), and anti-CD20 (B cells) antibodies, were quantified for every animal and antibody. Positive cells in 6 arbitrarily chosen 40x objective fields in alveolar areas, and 5 arbitrarily chosen 40x objective fields in bronchi or bronchiolar areas, were counted separately for each lobe (cranial, medial and caudal) of every animal. The means of the total cell counts per field, across the three lung lobes, were then calculated for each animal and antibody.

Gene Expression Profiles

The gene expressions of IFNα, IFNγ, TNFα, IL- 6, IL-1α, IL-8, CCL5, CXCL10, CCL3, CCL2, and TLR3, were detected by RRT-PCR. Briefly, RNA extraction was performed on the ferret lung tissue samples with an RNeasy Mini Kit (Qiagen), using the RNA stabilisation and on-column DNase digestion protocols (Qiagen). Reverse transcription was performed using an ImProm-II reverse transcription system (Promega), at 0.5 µg RNA. PCR was performed using a Power SYBR green kit (Applied Biosystems), and Fast 7500 equipment (Applied Biosystems). PCR reactions were performed in 10 µL reaction volumes using the Power SYBR green kit (Applied Biosystems); 40 amplification cycles were used, and the annealing temperature was 60°C. The expression levels were normalised using the house-keeping gene β-actin, and the results are expressed as arbitrary units. The primer sequences and their publication sources are presented in the annex (Table 1). Primer sequences for the β-actin, IL-1α and CCL3 genes were designed as described previously [213]. The ferret-specific genes are available in the NCBI nucleotide database [257]. The designed primer sequences and the GenBank accession numbers are presented in the annex (Table 1). The amplification products were detected by electrophoresis to validate the sizes of the product, in accordance with the primer design, and the products were purified using a QIAquick PCR Purification Kit (Qiagen). Sequencing reactions were performed with ABI Prism BigDye Terminator

Cycle Sequencing v.3.1 Ready Reaction (Applied Biosystems), and analysed using an ABI PRISM model 3730 automated sequencer (Applied Biosystems). The amplified sequences correlated with the ferret specific target sequences.

Apoptotic Cell Detection and Quantification

The expressions of the proapoptotic genes caspase 8 (CASP8) and BCL2-associated X protein (BAX) were quantified by RRT-PCR. The designed primer sequences and the GenBank accession numbers are presented in the annex (Table 1). The RRT-PCR techniques and the primer sequence designs were performed as described in the above section. The expression levels were normalised using the house-keeping gene β-actin, and the results are expressed as arbitrary units. Primer validation was performed, as described in the above section.

Apoptotic cells in the lungs were also detected by IHC, using the anti-caspase 3 polyclonal antibody (Cell Signalling, Cleaved Caspase-3 (Asp175) Antibody, ref 9661), diluted 1:100 in PBS, using EDTA as the antigen retrieval method. The IHC technique was performed as described above, for inflammatory cell immunophenotyping. Swine and ferret lymph node sections were used as positive controls, and the sections in which the specific primary antibodies were substituted with PBS, were used as negative controls.

Statistical Analyses

Histopathological scores and positive cell quantification data were expressed as the means ± the standard errors of the mean (SEMs). The correlations between the IAV antigen quantifications, and the histopathological scores of each animal, were calculated by linear regression. Comparisons between the immunophenotypes and the IAV antigen quantifications of animals infected with the R11 and the R61 viruses, and between animals with severe and mild lung lesions, were performed using a non-parametric one-way analysis of variance (Kruskal-Wallis), followed when necessary by a Mann-Whitney U test. A robust analysis (one iteration) was used to obtain the means

± the SEMs for the RRT-PCR data. RRT-PCR comparisons between animals infected with the R11 and the R61 viruses, and comparison between animals with severe and mild lung lesions, were performed using Student's *t*-tests. In all cases, the results were considered statistically significant when the *P* value was < 0.05. All statistical analysis and data visualisation were performed with GraphPad Prism 6 (GraphPad Software, La Jolla, CA, USA).

4.3 Results

Clinical Signs

Two animals infected with the R61 virus, and two animals infected with the R11 virus, began to present anorexia, depression, and tachypnea at 2 dpi. Of these four animals, one animal infected with the R11 virus died between 3 and 4 dpi, and one animal infected with the R61 virus had to be sacrificed at 4 dpi for ethical reasons. Animals showing more severe clinical signs also presented higher body weight loss, which also correlated with more severe pathological findings in the lungs. Temperature was not affected by viral group, or by disease severity.

Gross Lesions and Histopathology

Gross pathological changes were mainly observed in the lungs of the infected animals which were necropsied at 4 dpi. One and two ferrets infected with the R11 and R61 viruses respectively, presented macroscopic lung lesions. The macroscopic lesions were characterised by heavy, firm, red and oedematous lungs. The animals in the control group did not exhibit any gross or histopathological changes.

In general, the three lung lobes of any given animal were equally affected. No major differences in terms of histopathological scores were observed between the viral groups. Two animals infected with the R11 viral strain and two animals infected with R61 viral strain, presented severe lung lesions that were characterised by severe and diffuse alveolar damage. In general, the three lung lobes were equally affected,

alveolar epithelial necrosis was observed, and the alveoli were distended and contained dense proteinaceous debris, desquamated cells, and high numbers of macrophages and neutrophils. In some cases, alveolar haemorrhage and hyaline membranes were also observed (Figure 11).

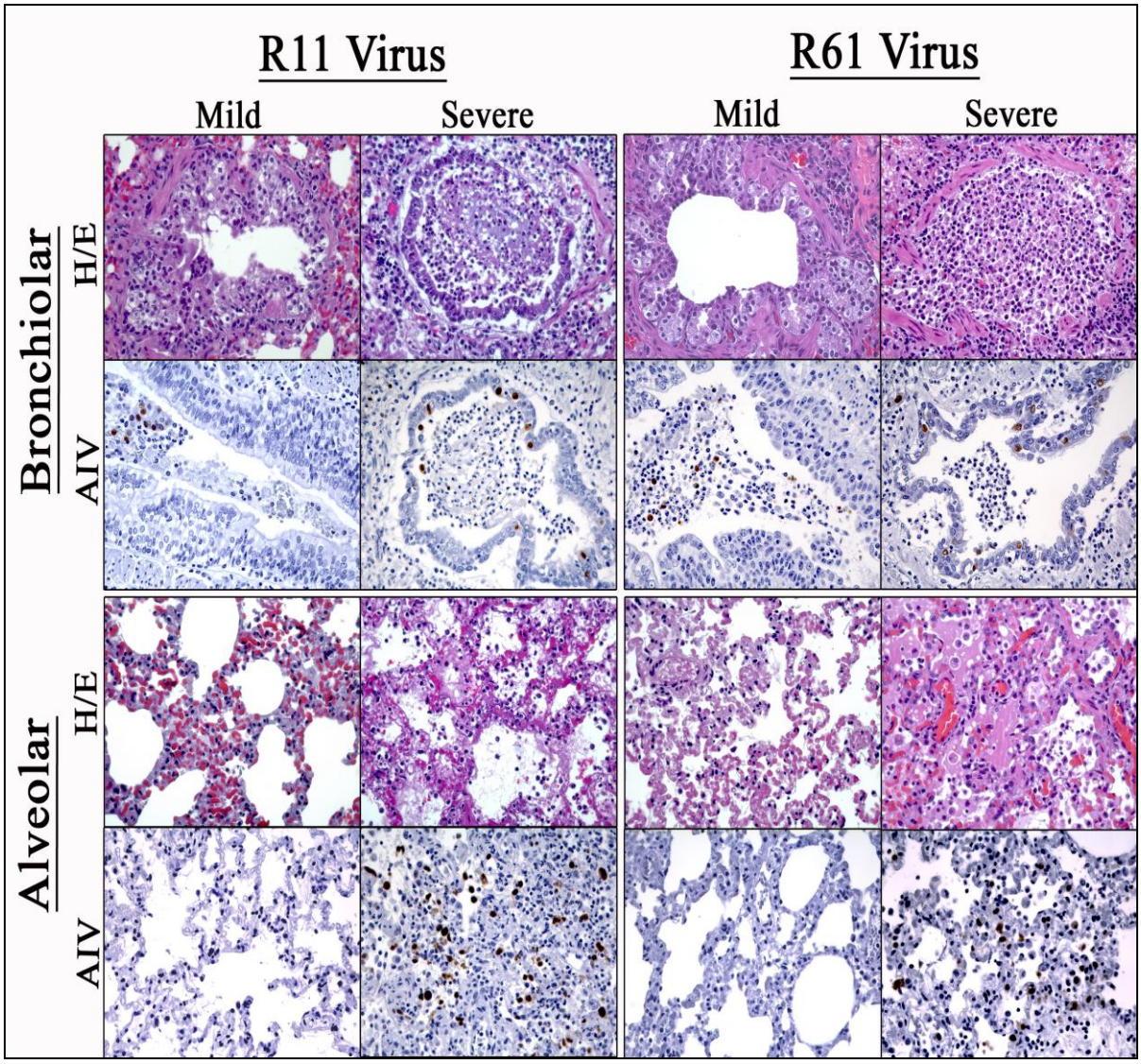

Figure 11. Pulmonary histopathological lesions in H1N1v-infected ferrets at 4 dpi. Pictures show different severity of lesions in alveolar and bronchiolar areas for R11 and R61 viruses. HE and immunohistochemical staining for IAV antigen (40x objective field).

The remaining infected animals (two infected with the R11 virus and two infected with the R61 virus) presented mild lung lesions that consisted of moderate to severe bronchial, bronchiolar, and glandular necrosis, with lymphoplasmacytic

inflammation (Figure 11). The histopathological lesions observed at 7 dpi were similar to those described at 4 dpi, but also included bronchiolar epithelial regeneration.

The trachea and nasal turbinates were also microscopically examined. In general, the ferrets which presented severe lung lesions also presented necrotising rhinitis, with mucous and tracheitis, and with a lymphoplasmacytic infiltration. The ferrets which presented mild lesions also presented lesions in the trachea and nasal turbinates, which were characterised by a catarrhal rhinitis with mucous secretion, and tracheal glandular necrosis.

Viral Detection and Quantification

IAV antigen expression was only detected in the lungs of the infected animals at 4 dpi, and no differences in IAV expression, as quantified by IHC or RRT-PCR, were observed between animals in the R11, or R61 viral groups.

Interestingly, IAV antigen quantifications in the lungs were significantly correlated with the histopathological scores of the infected animals (Figure 12A). Higher viral antigen quantifications and higher viral loads (Figure 12B and 12C) were observed in the lungs of the animals which presented severe lung lesions, than in those which presented mild lung lesions at 4 dpi.

The animals which developed severe lung lesions exhibited viral antigen expression in bronchi/bronchiole epithelial cells, and scattered expression in the alveolar parenchyma. Positive labelling was observed in the nuclei of type II pneumocytes and, to a lesser extent, in the type I pneumocyte nuclei, and the nuclei and cytoplasm of macrophages and interstitial lymphocytic cells (Figure 11).

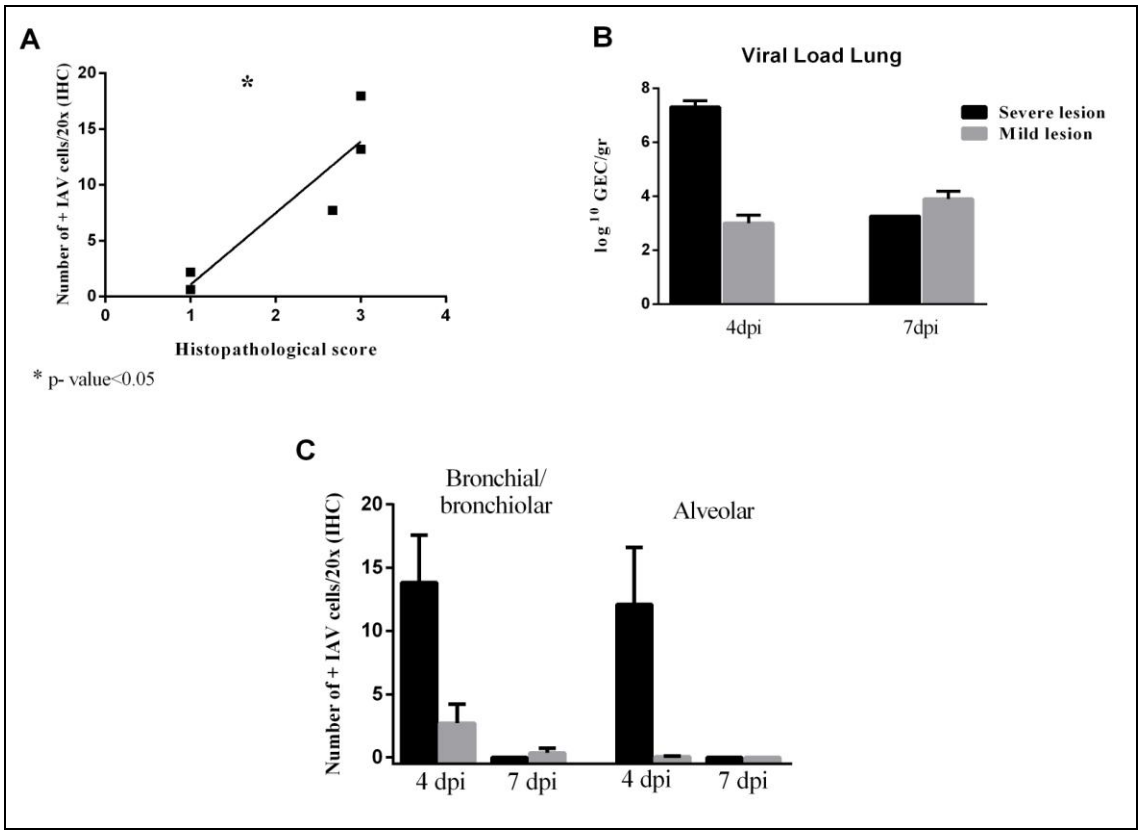

Figure 12. Relation between histopathological score and quantification of viral antigen in H1N1v-infected ferrets. (A) Linear regression shows the correlation between IAV antigen quantification and histopathological scores of infected animals at 4 dpi, independently of viral strains (*p value < 0.05). (B) Relation between viral load measured by RRT-PCR and histopathological score; GEC of plasmid per gram of lung tissue. (C) Immunohistochemical cell quantification of IAV-positive cells in ferret lungs segregated by histopathological score; Results express the mean cell counts with SEM (20x objective field).

In contrast, IAV antigen expression in the animals which developed mild lung lesions was restricted to the bronchi and bronchiolar areas (Figure 11), in which IAV antigens were mainly detected in the nuclei of the bronchi, or bronchiolar epithelial, and glandular cells.

Immunophenotyping and Quantification of Lung Inflammatory Cells

Quantifications of the different inflammatory cell populations for the animals grouped by histopathological score are illustrated in Figure 13.

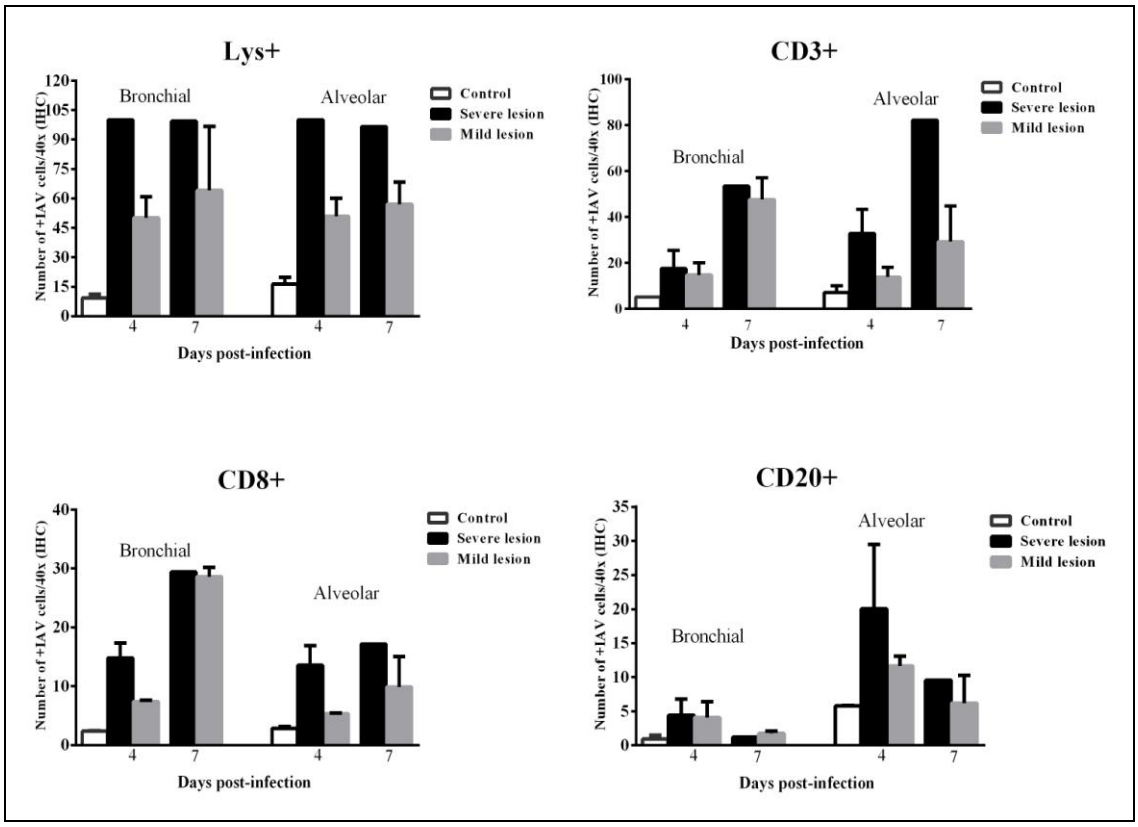

Figure 13: Immunohistochemical quantification of inflammatory cells in ferret lungs infected with H1N1v IAV. Results express the mean cell counts with SEM (40x objective field) for lysozyme, CD3, CD8, and CD20-positive cells. Animals are segregated by histopathological score.

Inflammatory cell averages were higher in the lungs of infected animals than in those of the control group. In general, lysozyme positive cells were the most abundantly observed cells in the lungs of the infected animals, and the maximum cell counts were observed at 4 dpi. The lungs of the ferrets which presented with severe lung lesions, exhibited elevations in lysozyme+ cell averages, in both the alveolar and the bronchi-bronchiolar compartments, when compared to the animals with mild lung lesions (Figure 13), particularly in the alveolar areas (Figure 14).

The CD3+ and CD8+ cell averages of the infected animals were higher at 7 dpi than at 4 dpi. More importantly, the CD3+ and CD8+ cell counts were higher in the ferrets which developed severe lung lesions (Figure 13), particularly for alveolar CD3+ cell averages (Figure 14). The CD8+ bronchial cell averages were similar in the animals which exhibited severe and mild lung lesions, at 7 dpi.

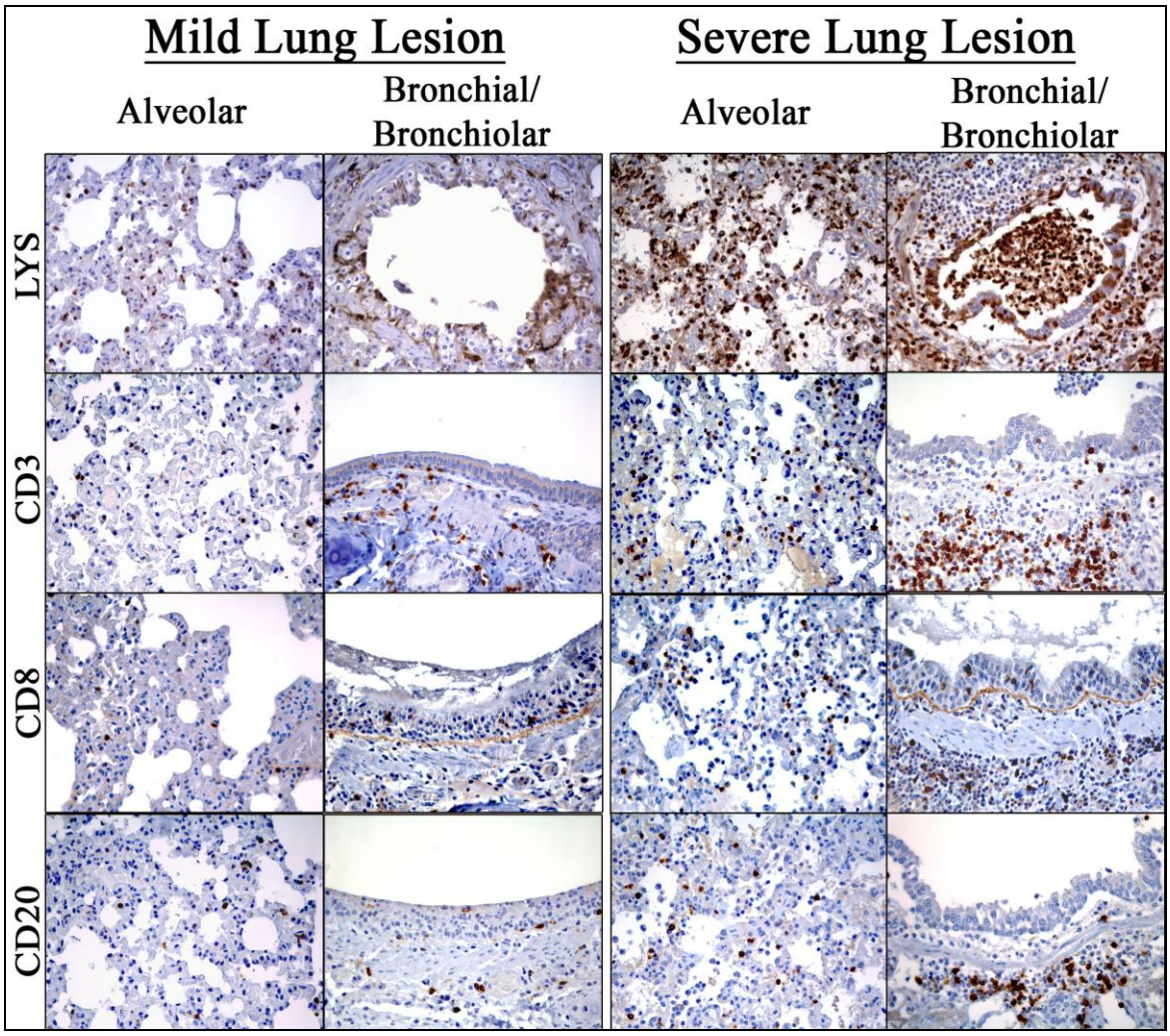

Figure 14. Immunohistochemical caracterisation of inflammatory cell populations in ferret lungs infected with H1N1v IAV at 4 dpi. IHC stain for Lysozyme-, CD3-, CD8α-, and CD20-positive cells. Haematoxylin counterstain (40x objective field).

In contrast to the observations regarding CD3+ and CD8+ cell quantifications, the CD20+ cell averages decreased in both histopathological groups, at 7 dpi (Figure 13). In general, the CD20+ cell averages were lower than CD3+, CD8α and Lysozyme+ cells (Figure 14). The animals which presented severe lung lesions exhibited slightly higher bronchial CD20+ cell counts, at 4 dpi, but not at 7 dpi (Figure 13).

Gene Expression Profiles

To determine the relationships between the observed immunophenotypes, the different pathological outcomes and the cytokine, chemokine and TLR3 gene expressions, RRT-PCR was performed. Both infected groups exhibited elevated gene expression of pro-inflammatory markers and TLR3, when compared to the control group at both 4 and 7 dpi. The gene expression profiles of the lungs of the animals which presented severe lung lesions, exhibited increased expressions of IL-8, CCL3, IFNγ, CXCL10, IL-1α, CCL5, IL-6, and TLR3, when compared to those of the animals which presented mild lung lesions at both 4 dpi (Figure 15), and 7 dpi.

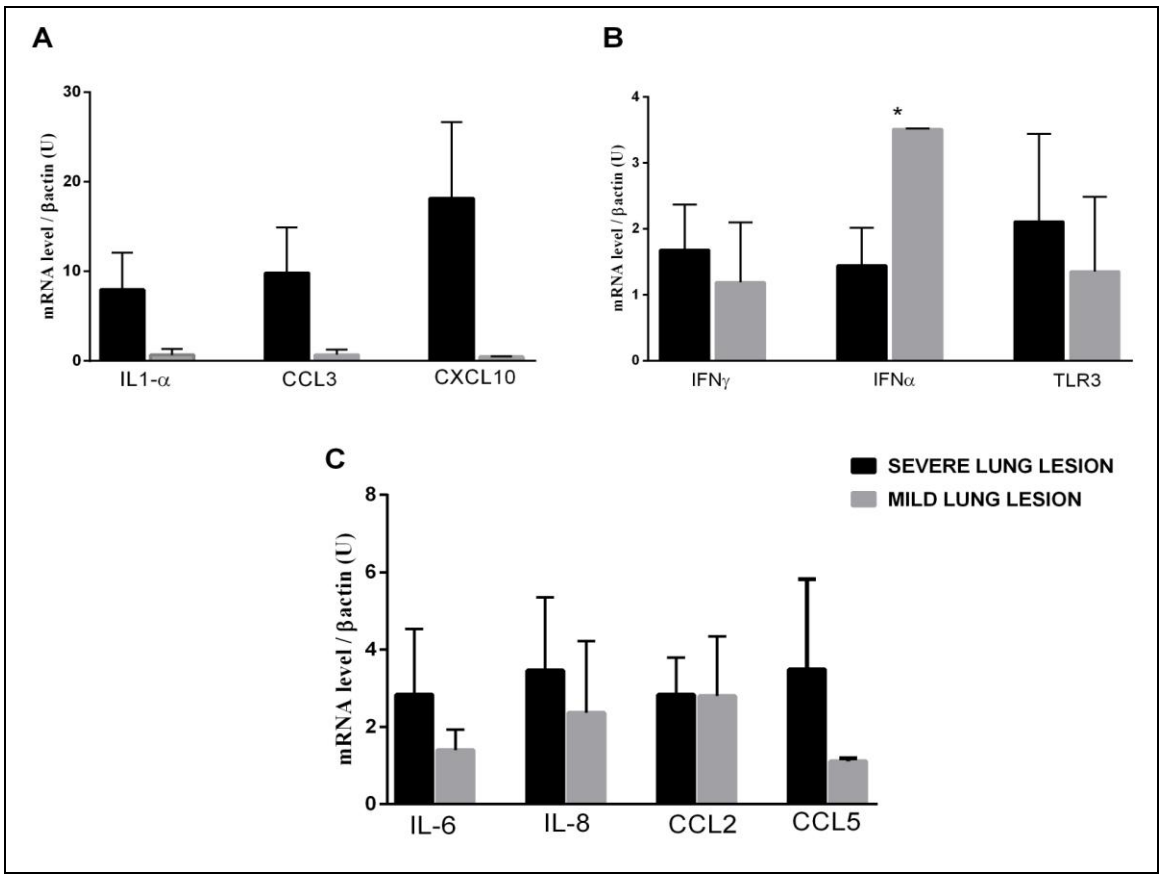

Figure 15. RRT-PCR quantification of the genes expressed in H1N1v-infected ferrets with severe and mild lung lesions. Comparisons of the cytokine, chemokine and TLR3 gene expression levels in lungs at 4 dpi. Gene expression of IL-1α, CCL3, and CXCL10 (A); IL-8, IL-6, CCL2, and CCL5 (B) and IFN-α, IFN-γ, and TLR3 (C). The data is presented as the means and the SEMs, (*p value < 0.05).

Interestingly, at 4 dpi, a statistically significant elevation in the induction of IFNα was observed in the lungs of the animals which presented mild lung lesions (Figure 15B). No differences in CCL2 expression were observed between the pathological groups (Figure 15C). The expressions of all cytokines decreased in both pathological groups at 7 dpi, with the exceptions of CCL2 and TLR3 in the animals with severe lung lesions.

Apoptotic Cell Detection and Quantification

The apoptotic genes BAX and CASP8 in the lungs of infected animals were analysed with RRT-PCR. The gene expressions of BAX and CASP8 were elevated in both infected groups compared to the control group. Comparison of the apoptotic induction in the lungs of the animals that presented with different grades of lung pathology revealed that the animals with severe lung lesions exhibited elevations in the inductions of both apoptotic markers, when compared to the animals with mild lung lesions, at both 4 and 7 dpi (Figure 16A).

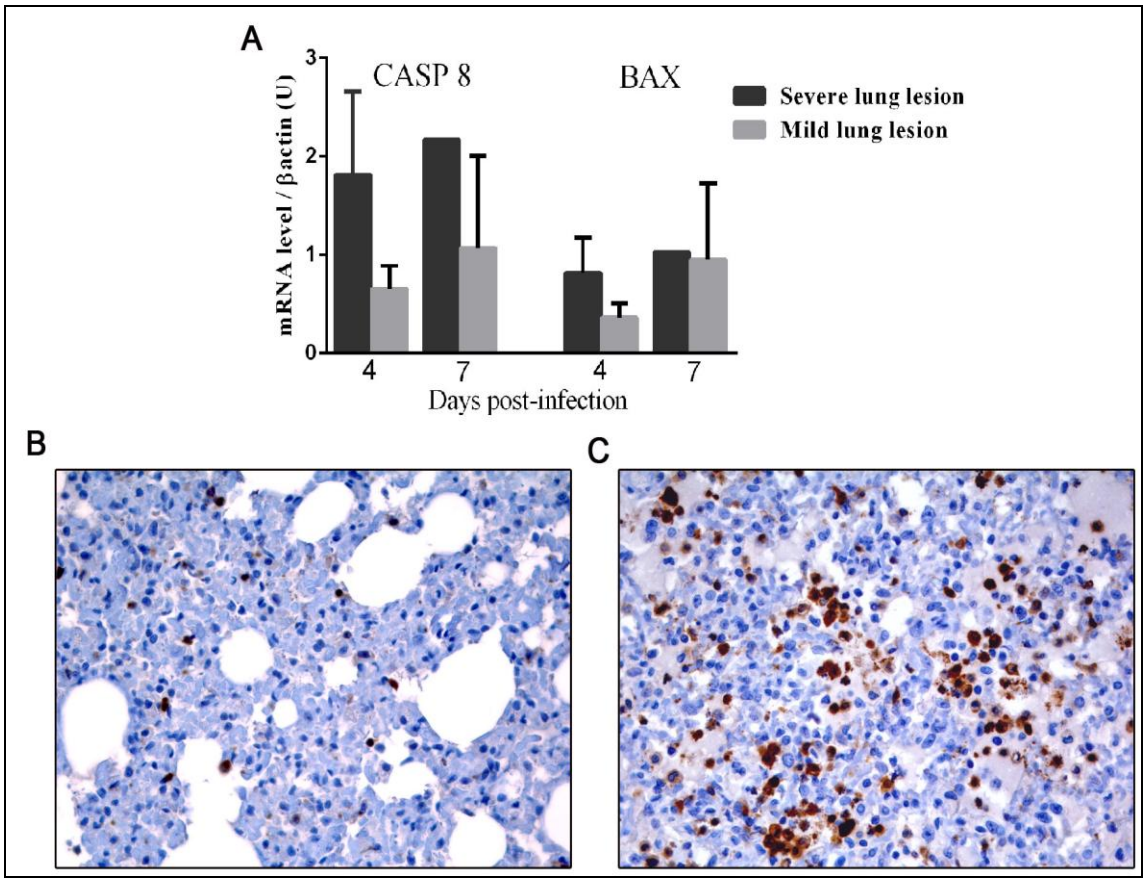

Figure 16. Gene expressions of proapoptotic genes and IHC of apoptotic cells in lungs of H1N1v-infected ferrets at 4 and 7 dpi. (A) Comparison of BAX and CASP8 gene expression levels in lungs with both severe and mild lesions as measured by RRT-PCR. The data expresses the means with SEMs. (B) and (C) IHC staining for caspase 3 in the lungs of the ferrets with mild (B) and severe (C) lesions; haematoxylin counterstain (40x objective field).

4.4 Discussion

Pathogenesis of H1N1v infection results from various processes involving the host immune system, and their response to virus-induced changes. Understanding both virus and host response characteristics in individuals who develop mild or severe disease, is important for the future development of therapeutic strategies for cases of severe influenza infection.

In this study, ferrets were infected with two H1N1v isolates, from two patients who had developed significantly different clinical outcomes. Although the number of animals used in each infectious group is limited, our results demonstrated that the virulences of the H1N1v strains in ferrets were not associated with the clinical phenotypes of the corresponding human patients. Similar findings have been

described by other studies in animal models infected with H1N1v isolates, from patients who exhibited diverse degrees of disease severity [160,258]. Indeed, the severity of infection in ferrets can range from a sublethal infection with mild symptoms to lethality rates of 30-50% [74,167,201]. This variability suggests the strong influence of differences in viral strains and individual host variability on the severity of infection.

A previous study which employed the viral isolates used in this trial, showed differences in the in vitro and in vivo characteristics of the two strains. In that study, the R11 strain exhibited higher replication rates in mice at 2 dpi, and this difference was accompanied by more severe pathological lesions, relative to those induced by the R61 strain [250]. As previously stated, in this study, the virulence of the R11 isolate was not consistently observed in ferrets, and more surprisingly, the R61 strain induced unexpectedly high viral titres in the lungs, which were associated with severe pathological lesions in two animals. These contradictory results may be attributable to the following explanations: i) the mouse model may not be the most suitable model for assessing influenza virus pathogenicity [158,190,199], and ii) ferrets, as an outbreed animal, may exhibit differential individual susceptibilities to viral infection.

In humans, the genetic factors of the host are increasingly being linked to disease courses [82,259]. Host-specific characteristics, such as the presence of homozygous CCR5 deleterious alleles (*$CCR5_D32$)*, have been found to be associated with poor outcomes of H1N1v infection [157,171,172,252]. Interestingly, the patient from which the R11 virus was isolated was recently discovered to have this genotype [250].

Our results revealed a significant correlation between lung lesional scores and virus quantification in the lungs, which was independent of the viral strain that was inoculated. This finding led us to further investigate the immune responses and viral kinetic patterns, by grouping the animals according to lung lesion severity, rather than only considering the infecting viral strain.

Viral quantification and localisation of the viral antigen in the lung compartments differed between individuals that were infected with the same virus,

yet correlated with the severity of the lung lesions. Interestingly, in the animals which developed severe lung lesions, the viral antigen was observed in alveolar areas. This observation, suggests that sustained viral replication in the alveolar parenchyma was critical for the establishment of severe pathology, as observed previously [191]. In contrast, the animals which developed mild lung lesions did not present IAV antigens in alveolar areas, and their viral quantifications were significantly lower.

Although viral replication is fundamental in determining the severity of the disease, the inflammatory response to the presence of the virus also plays important roles in tissue damage and pathological outcomes [260]. The induction of proinflammatory cytokines and chemokines after influenza infection, is known to promote respiratory tract inflammation by recruiting inflammatory cells to the site of infection [162]. In this study, we found that the ferrets which developed severe lung lesions exhibited elevated expressions of proinflammatory cytokines (IL-1α, IL-6 and IFNγ) and chemoattractants (IL-8, CXCL10, CCL3 and CCL5), which correlated with increased levels of phagocytic and T cell infiltrates in the lungs. The most abundant cell populations were the Lysozyme+ phagocytic cells (neutrophils and macrophages), followed by the CD3+, and CD8+ T cell populations.

The exacerbated recruitment of neutrophils and macrophages into the lung parenchyma and alveolar spaces, has been recognised as contributing to the detrimental effects of influenza immunopathology, via the production of pro-inflammatory molecules, and the release of reactive oxygen species, and nitric oxide [73,78,84,162].

In the present study, CD3+ and CD8+ cells were found more abundantly in the ferrets which exhibited severe lesional patterns. In correlation with these findings, animals presenting severe lung lesions showed a higher expression of IFNγ, CCL5 and CCL3. Several studies have shown that NK and CD8 T cell concentration increased in mouse and human lungs, following severe influenza infection, both in the early stages of influenza infection, and in the later viral clearance stage [94,153,162,261-263]. Moreover,

the suppression of the early innate cell infiltration of NK and CD8 T cells has been shown to significantly increase mouse survival rates, without altering the kinetics of viral clearance. This suggests that the infiltration of these cells has a negative inflammatory role, which is independent of viral kinetics [95,264].

Several studies have identified common cytokine gene expression profiles involved in neutrophil recruitment, stimulation of T cell proliferation, and CD8+ cell-mediated inflammation in influenza associated pathology [59,81,93]. Gene expression profiles which promote T helper (Th) 1 cell responses have also been shown to be closely related to poor outcomes in severe cases of H1N1v infection [81,164,168]. Here, the animals which developed severe lung lesions, also presented elevated expressions of Th1 response-inducers (CCL5, CCL3, CXCL10 and IFNγ), whilst no differences in the expression of the Th2 response-inducer CCL2 were observed between animals with severe and mild lesions.

IFNα gene expression in the animals which developed mild lung lesions was significantly elevated compared to that of the animals with severe lung lesions at 4 dpi. This finding suggests that IFNα has a protective role in the early stages of infection. Supporting this supposition, Svitek and colleagues found that ferrets which develop mild seasonal influenza also exhibit increases in the expression of IFNα [71]. Moreover, some studies of mice and macaques have shown that the exogenous administration of IFNα protects animals against influenza A and severe acute respiratory syndrome (SARS) coronavirus infections [265,266].

To determine the differences in viral sense signalling between the animals with different pathological outcomes, TLR3 gene expression was measured. TLR3 is an innate immune recognition receptor that has key roles in dsRNA detection, the initiation of innate immune responses, and the linking of innate and adaptive immunity to limit virus production [267]. It is known that aberrant TLR3 signalling plays a key role in mediating lung pathology, and contributes to detrimental host inflammatory responses through the induction of proinflammatory molecules and the recruitment of

CD8+ and phagocytic cells, during IAV virus infection [65,78,153,267-269]. Polymorphisms which alter the function of TLR3 have been shown to be related to severe cases of H1N1v and H5N1 influenza infection [172,268,270]. In the present study, the animals which developed severe lung lesions exhibited elevated TLR3 gene expression in the lungs that correlated with increased viral quantifications, and increased recruitment of CD8+, and Lysozyme+ cells, in these animals. However, severely ill animals exhibited significantly lower expressions of IFNα, which should be up-regulated by TLR3 induction. Nevertheless, this striking phenomenon may be indicative of inappropriate functioning of either the TLR3, or the Interferon receptor (IFNR)1, or impairments of the TLR3-IFNR1 pathway.

Yang and colleagues [271] have recently demonstrated that H1N1v can induce caspase-3-dependent apoptosis in alveolar epithelial cells. In our study, the animals with severe lung lesions presented increased expression of both the BAX and CASP8 proapoptotic genes in the lungs. However, immunohistochemical analyses revealed that apoptotic cells at 4 and 7 dpi were mainly identified as macrophages and neutrophils. This finding may elucidate another mechanism of lung tissue damage, which is mediated by a delayed clearance of inflammatory cells from infected lungs. The occurrence of complete resolution of inflammation requires apoptotic neutrophils to be cleared by local tissue macrophages. However, if either neutrophil apoptosis or the clearance of apoptotic neutrophils by macrophages is delayed, inflammation-related tissue damage occurs and leads to the exacerbation of inflammation [272,273]. These observations, correlate with the results observed in this study, as increased numbers of apoptotic inflammatory cells were observed in the ferrets presenting severe lung lesions. Moreover, these findings are likely to be related to the delayed viral clearance, and the positive feedback loop,, of proinflammatory cytokines.

This study represents an exhaustive characterisation of the inflammatory cell populations and proinflammatory gene expression profiles in the lungs of H1N1v-infected ferrets. Additionally, despite the limited number of animals used, we provided further evidence regarding the implications of viral replication efficiency, inflammatory

cytokine induction, and phagocytic and cytotoxic cell infiltration, in influenza-infected lungs which are associated with pathology at the time of the switch from the innate to the adaptive immune response. More importantly, our results support the notion that viral replication and the correct orchestration of the early inflammatory response are key factors in the development of severe influenza.

CHAPTER 5

STUDY III: *Experimental Infection of Ferrets Infected with a Wild Type and an Oseltamivir Resistant H1N1v Isolates from Patients Presenting Fatal Pathological Outcomes*

5.1 Introduction

Since the emergence of the 2009 pandemic, the H1N1v has been established worldwide and it has now replaced the previous seasonal H1N1 virus [113,274]. As H1N1v strains are resistant to adamantine antiviral therapeutics [275], the pharmacological therapy against H1N1v infection depends completely on NIs antivirals, namely Oseltamivir and Zanamivir [113,275]. Among the NA viral substitutions which enable the virus to resist NIs, a histidine-to-tyrosine substitution at position 275 (H275Y) is one of the best characterised, and most commonly found OR mutations [132,276].

It had previously been thought that any resistant mutation in the NA enzymatic site would compromise viral fitness [131,274], as NAIs resistant viruses have generally been associated with poorer viral replication and transmission in seasonal H1N1 and H3N2 strains [277,278]. However, seasonal H1N1 with the H275Y mutation emerged and spread globally in the absence of Oseltamivir selection pressure [279], demonstrating that viral fitness was no longer compromised by the resistance mutation. Various investigations have revealed the presence of several "permissive" mutations (R222Q and V234M) in seasonal, and H1N1v viruses, which enabled the acquisition of H275Y, without compromising viral fitness [280].

In general, OR H1N1v viral infections have mainly been detected in immunocompromised patients who had been treated with antivirals [129,276]. Nonetheless, two major community clusters of OR H1N1v viruses have recently been reported. One in Newcastle, Australia, where 23.5% of pH1N1 viruses contained the H275Y mutation during the peak month of the epidemic [281], and another one in Sapporo, Japan, where a cluster of cases occurred sporadically in patients who had no epidemiological link, and had not received NIs [282].

The transmissibility and pathogenicity of several strains of OR H1N1v virus have been studied *in vitro* and *in vivo* in different mammal species, showing inconsistent results according to the isolates tested [130-132,283,284]. In general, *in vitro* studies showed that OR viruses exhibited slower initial growth [130,131,275]. However, some *in vivo* studies

have observed that OR strains retained, or, even that they were superior in replicative fitness, transmissibility, and virulence, in the ferret and the mouse model [130,132,285]. On the contrary, other studies have observed that OR H1N1v strains presented lower fitness and transmissibility in ferrets [128,131,283].

The main objective in this study is to compare the virulence of an OR H1N1v virus and its wild type (Wt) counterpart, in the ferret model, and to study the immunological parameters in local tissues which could correlate with virulence. Thus, identification of differences in the viral-host interaction, associated with viral genetic characteristics and the host innate immune response, will be analyzed.

5.2 Material and Methods

Viruses

Two strains of human H1N1v were used in the present study. The viruses were isolated at the National Influenza Centre (CNM, ISCIII) from respiratory samples sent by the Spanish Influenza Surveillance System for virological characterisation. The virus A/Baleares/RR6121/2009 bears the H275Y mutation which makes it OR; this virus is here referred to as R6. It was isolated from a leukemic patient who died after infection. The virus A/CastillaLaMancha/RR5911/2009 is here referred to as F. It was isolated from a 35-years old woman, without co-morbidities, who developed a severe disease and died.

Viral Aminoacidic Sequence Comparison of the Proteome

Aminoacidic differences in the F and R6 strains' predicted proteins were identified. The frequency of the aminoacid in the mutated positions was calculated for each viral protein, over an alignment of more than 1800 sequences of IAV. Those last belonged to the H1N1v lineage, and were retrieved from Global Initiative on Sharing Avian Influenza Data (GISAID) database.

Ferrets

Nineteen neutered male ferrets, between eight and nine months of age, and seronegative for IAV (influenza A antibody competition multi-species ELISA, ID Screen®, France) and Aleutian disease virus, were randomly selected from a stable, purposely bred colony *(Euroferret,* Denmark*)*. Upon arrival at the CReSA, the animals were placed in BSL-3 facilities. Ferrets were randomly assigned to different experimental groups, separated into experimental isolation rooms and then acclimated for one week. The animals were placed in standard housing cages, and they were provided with commercial food pellets and tap water *ad libitum,* throughout the experiment. All experiments were performed under a protocol (nº 1976) which was reviewed and approved by the Animal and Human Experimentation Ethics Commission of the UAB.

Animals were divided into three groups. Control group included three ferrets. The R6 group included eight ferrets infected with the R6 virus, and the F group included eight ferrets infected with the F virus. Control animals were euthanized at 0 dpi, in order to minimize the number of animals used in the study, and the housing space. We made this decision whilst taking into account the observations made during the acclimatization of the animals, and the data of the precedent study, in which control animals did not show differences in the experimental data, throughout the experiments.

Infected ferrets were intratracheally inoculated with 10^5 $TCID_{50}$/ml of the appropriate virus, and necropsies were performed on days 1, 3 (three ferrets) and 10 (two ferrets) postinfection. Animals were euthanized with an intravenous injection of sodium pentobarbital (100 mg/kg) under anaesthesia with ketamine (5-10 mg/kg) (Imalgene 1000® Merial, S.A., Spain) and medetomidine (0.05 mg/kg) (Domtor® Pfiser, S.A., Spain). They were then necropsied according to a standard protocol.

Clinical Signs

Ferrets were monitored daily for various clinical signs such as changes in temperature and body weight, general activity, sneezing, coughing and nasal or ocular discharge, following a clinical score modified from Martinez-Orellana *et al.* (unpublished results), and described in (Table 7). Clinical signs in control animals were monitored during the acclimation period, and at 0 dpi.

CLINICAL SCORE	**0**	**0.5**	**1**	**2**
Activity	Normal	Mild Apathy	Apathetic	Lethargic
Lost weight	No lost weight		(5-10%)	(>10%)
Temperature	No		>0.5ºC	> 1ºC
Conjunctival secretion	No		Yes	
Nasal secretion	No		Yes	
Coughing	No		Yes	
Sneezing	No		Yes	
Diarrhoea	No		Yes	
Neurological signs	No		Yes	

Table 7. Clinical score punctuation.

Acute Phase Proteins

The Acute phase proteins (APP) Haptoglobin (Hp) and Serum Amyloid A (SAA), were quantified in sera by the ELISAs Haptoglobin Assay, and Multispecies Serum Amyloid A Immunoassay, (Tridelta Development Ltd, County Kildare, Ireland). Blood samples were collected at 0 dpi in control animals, and at 0, 1, 3, 6 and 10 dpi, in infected animals.

Histopathology

Right lung lobe sections (cranial and caudal), were taken for histological examination according to standard protocols. The tissues were fixed for 48 h in 10% neutral-buffered formalin, then embedded in paraffin wax, sectioned at 3 µm, and stained with HE for examination under light microscopy.

Cross sections of the cranial and caudal pulmonary lobes of each animal were separately evaluated, and semiquantitative assessments of IAV-associated microscopic lesions in the lungs were performed. The histopathological scoring system was graded as follows: 0 (no histopathological lesions observed), 1 (mild to moderate necrotizing bronchiolitis), 2 (bronchointerstitial pneumonia characterised by necrotizing bronchiolitis and inflammation of surrounding alveoli), and 3 (necrotising bronchiolitis and diffuse alveolar damage, i.e. severe inflammation of large areas of alveolar septa). Microscopic lesion scores were assigned for each lobe, and the means of the two lobes were used for the final histopathological score for each animal.

Viral Detection and Quantification

Viral RNA in the lung was extracted with NucleoSpin® RNA Virus Kit (Macherey-Nagel, Düren, Germany) following the manufacturer's instructions. IAV M gene was then quantified on the RNA extracted by the Taq-Man one-step quantitative RRT-PCR using the primers, probe, and the amplification conditions described in study II, and reviewed in the annex (Table 1). Reactions were performed in a Fast7500 equipment (Applied Biosystems, Foster City, CA, USA). Samples with a threshold cycle (Ct) value ≤40 were considered positive for IAV infection.

IAV was also quantified in the lung by IHC. Fixed FFPE tissues were stained with a primary antibody against the influenza A NP, as previously described [254]. Sections were counterstained with Mayer's Haematoxylin. The positive control consisted of a FFPE heart chicken, experimentally infected with influenza. The same section, in which the specific primary antibody was substituted with PBS, was used as negative control.

Viral secretion shedding in nasal swabs, collected on 0, 1, 3, 6 and 10 dpi, was determined by plaque forming units (PFU), determination as described by Martínez-Orellana *et al.* (unpublished results).

Gene Expression Profiles

Gene expressions of IFNα, IFNβ, IFNγ, TNFα, IL6, IL8, CXCL10, and RIG-I, were detected by Two-step RRT-PCR, and RIG-I and IFNβ were designed as described in the previous study. Primers sequences are illustrated in the annex (Table 1). Briefly, RNA extraction was performed on ferret lung tissue samples with an RNeasy Mini Kit, using the RNA stabilization and on-column DNase digestion protocols (Qiagen, Valencia, CA). Reverse transcription was performed using an ImProm-II reverse transcription system (Promega, Madison, WI) at 0.5 µg RNA. PCR was performed using a Power SYBR green kit (Applied Biosystems, Foster City, CA) and Fast 7500 equipment (Applied Biosystems, Foster City, CA, USA). The expression levels were normalized using the house-keeping gene β-actin (ACTB), and the results are expressed as arbitrary units.

Hemagglutination Inhibition (HI) Assay

Antibodies against IAV were measured using a HI assay using chicken red blood cells (RBC). Before the assay, sera were treated overnight with four volumes of Receptor Destroying Enzyme (RDE) (Sigma-Aldrich SA, Madrid, Spain) solution (100 U/ml) at 37 ºC, to remove non-specific inhibitors of hemagglutination. The next day, serum samples were incubated for 30 min at 56ºC, after the addition of five volumes 1.5% sodium citrate. Treated sera were tested by 1:2 titrations in PBS. Finally, 4 hemagglutination units of H1N1v, and one volume of a 50% suspension of RBC, was added, and incubated for 1 h at 4ºC. Known positive and negative sera were used as controls. HI titres >40 were considered positive.

Statistical analyses

Data visualization was performed with GraphPad Prism 6 (GraphPad Software, La Jolla, CA, USA). All statistical analysis was performed using SPSS 15.0 software (SPSS Inc., Chicago, IL, USA). For all analysis, ferret was used as the experimental unit. The significance level (α) was set at 0.05. The Shapiro Wilk´s and the Levene test were used to evaluate the normality of the distribution of the examined quantitative variables and the homogeneity of variances, respectively. No variable which had a normal distribution was detected. Thus, a non-parametric test (Wilcoxon test) using the U

Mann-Whitney test to compare each pair of values, was used to compare the different values obtained for all the parameters (weight loss, clinical signs, acute phase proteins, histopathology, viral load and genetic expression profiles), between groups (control, F and R6 influenza virus), at all sampling times.

5.3 Results

R6 and F Viruses' Analysis

The virus R6 bears the H275Y mutation which makes it OR. Firstly, a comparison between the predicted proteome of F and R6 viruses was performed and the identified mutations were screened in the GISAID database to determinate their frequency in the H1N1v viruses (Table 8).

Differences in aminoacidic signatures were identified in the PB2, PB1, PA, NP, HA, NA and NS1 proteins. The majority of the mutations were falling into the viral polymerase complex proteins, particularly into the PB2 and PA. Moreover, those in the F virus were mostly rare in the H1N1v viruses (minimum less than 2.5%). The R6 virus, however, also showed some rare mutations with a frequency of 0.5%. The other mutations were distributed among the rest of the proteins and most of them were uncommon in the R6 virus. Noteworthy, one mutation in the HA protein of the R6 virus is extremely rare (0.1%, just one sequence). Unfortunately, only the domains in which they fall have been roughly identified, and the functional implication of the identified mutations has not been identified before (apart of the Oseltamivir resistance).

Protein	Portion compared	Mutated position	F	R6	Frequency	Domain	Ref.
PB2	1-757	127	Y	H	127H 98.8% (1837)	N-terminal-PB1,NP interaction	286
		191	K	E	191E 97.5% (1812)		
		221	T	A	221A 99.7% (1854)		
		660	K	R	660R 2.5% (47)	627Domain – host range	287
PB1	1-757	257	T	A	257A 0.5% (10)	Nucleotide binding site	288
PB1-F2	1-11 TRUNCATED	-					
PA	1-716	328	R	K	328K 99.8% (1855)	PB1 interaction	
		529	N	D	529D 99.8% (1855)		289
		716	K	E	716E 0.5% (9)		
NP	2-497	400	R	K	400K 98.8% (1836)	Body	290
HA	34-349	38	E	K	38K 0.1% (1)	Fusion HA1 chain	291
		127	L	S	127S 99.8% (1860)	Receptor binding HA1 chain	
NA	188-420	275	H	Y	275Y 0.8% (14)	Head domain	292
M1	1-252	-					
M2	1-97	-					
NS1	1-219	93	M	I	93I 2.2% (40)	N/A	
NS2	1-121	-					

Table 8. **Aminoacidic sequence comparison of the F and R6 strains.** Aminoacidic differences between the two strains. Mutation frequency and the domain in which they fall were also annotated.

Clinical Signs

After comparing both viruses for their predicted proteomic sequence, the clinico-pathological characteristics of F and R6 viruses were compared via an experimental infection in ferrets. In terms of clinical signs, IAV infected animals presented higher temperature, weight loss, and clinical scores, than control animals.

The increased weight loss and clinical scores were statistically significant than control animals at 3 dpi ($p<0.05$) (Figure 17).

Infected animals presented the first temperature elevation from 1 dpi to 3dpi, from which, temperatures came back to basal and no differences in temperature variation between infected groups was observed. At 4 dpi, both F and R6 viral groups showed a second temperature augmentation until 6 dpi, which was more notable in F-infected ferrets (Figure 17C).

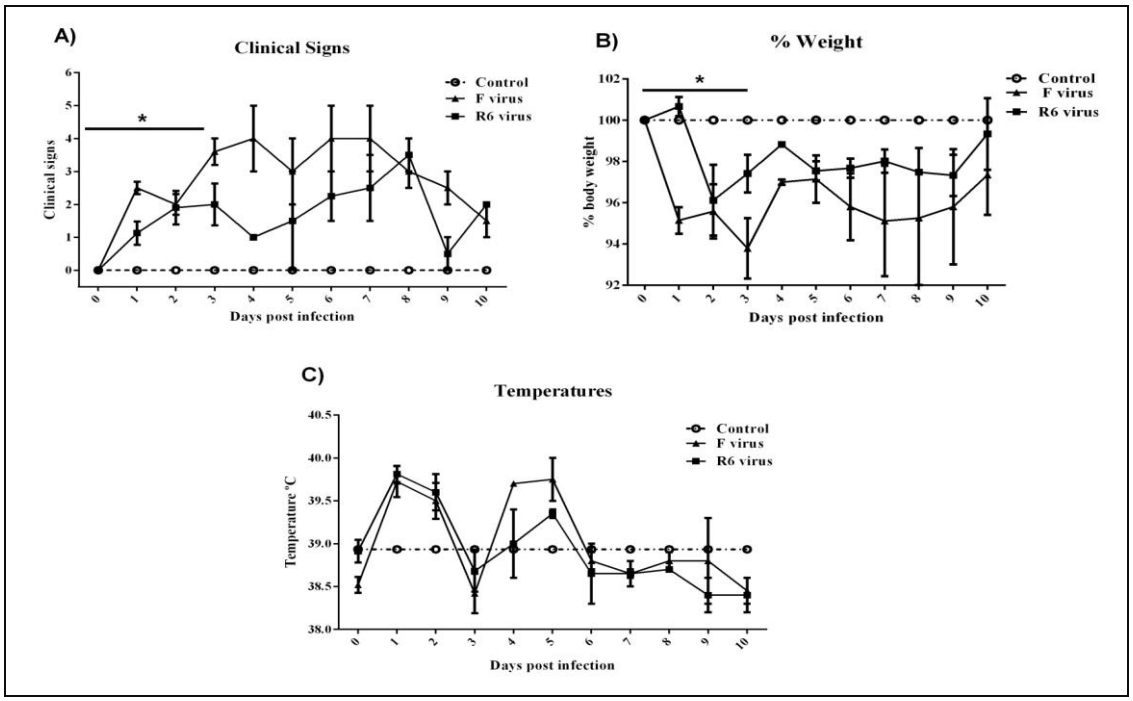

Figure 17. Clinical signs. A) Clinical score B) Percentage of weight compared with weight at 0 dpi (100%) B) body temperature and C) Clinical scores in ferrets during experimental infection. Values for control animals at 0 dpi are assumed not to have varied throughout the experiment, and are represented in a discontinuous line. All values are represented with the mean and SEM ±. Statistically significant differences represented by * (p value < 0.05).

In general, F-infected ferrets presented a higher percentage of weight loss and clinical scores than the R6-infected ferrets ($p<0.05$) at 1dpi, whilst no major differences were observed in temperature, between the infected groups (Figure 17). At 2 and 3 dpi, both infected groups started to gain weight until 5 dpi, and then animals presented another peak of weight loss, which was more notable in animals infected with the F virus (Figure 17B). F-infected ferrets presented higher clinical scores from 3 to 7 dpi, than R6 infected animals (Figure 17A).

APP

Two major APP, Hp and SAA were analyzed in infected and control ferrets (Figure 18). Infected animals showed statistically significant higher Hp levels at 3dpi in comparison with the control group ($p<0.05$). F-infected animals generally showed higher Hp levels in comparison to R6 infected ferrets, with statistically significant differences observed at 1 dpi ($p<0.05$) (Figure 18A). Hp levels increased in both F- and R6- infected groups after 1 and 3 dpi respectively, with no major differences being observed between both groups at 3 dpi. Hp serum levels returned to basal at 6 dpi, for animals infected with the R6 virus. However, the Hp levels of F virus infected ferrets continued to increase until 10 dpi.

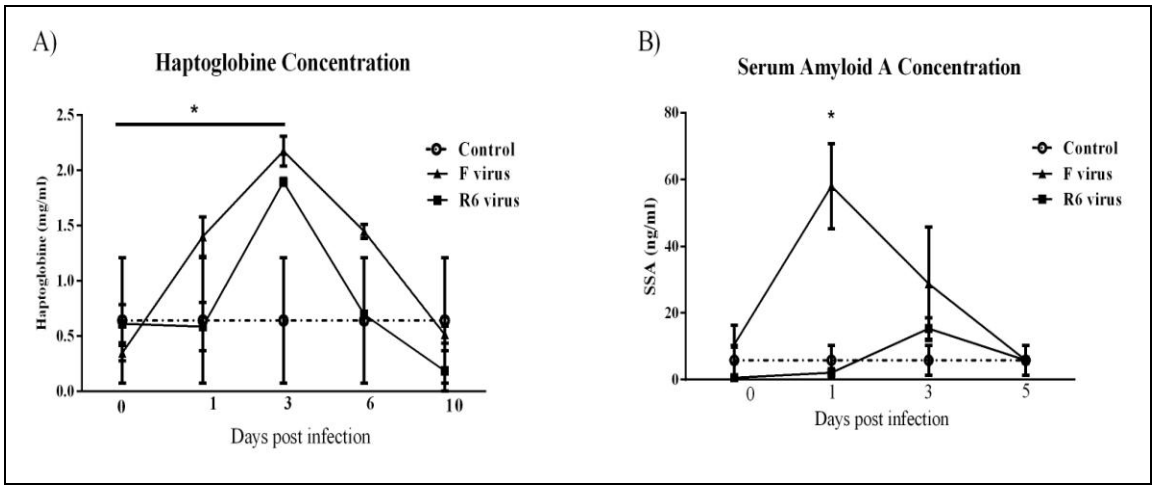

Figure 18. Sera levels of APPs. (A) Hp and B) SAA. All values are represented with the mean and SEM ±. Values for control animals at 0 dpi are assumed not to have varied throughout the experiment, and are represented in a discontinuous line. Statistically significant differences represented by * (p value < 0.05).

F-infected animals presented increased SAA levels from 1dpi to 3dpi, whereas, SAA levels of animals infected with R6 virus only slightly increased at 3 dpi (Figure 18B). F-infected ferrets statistically showed significantly higher SAA levels, than R6 infected and control group, at 1 dpi ($p<0.05$).

Gross Lesions and Histopathology

Gross lesions were only observed in infected animals. At 1 dpi, one animal infected with the F virus presented mild consolidation of the right cranial and caudal

lung lobes, while no gross lesions were observed in R6 infected animals. At 3 dpi, two R6 infected animals presented mild consolidation of the caudal lobes, and (one and two F infected ferrets) presented generalized emphysema and consolidation of the caudal lung lobes, respectively. Pulmonary histopathological scores are represented in (Figure 19A). All infected ferrets presented lung histopathological lesions at all-time points which were significantly higher than the control group ($p<0.05$). Animals infected with the F virus presented higher histopathological scores than R6 infected animals throughout the trial, but without observing statistically significant differences between them (Figure 19A). In general, the histopathological lesions observed in animals infected with the F virus were characterised by bronchointerstitial pneumonia, with different grades of extension at 1 and 3 dpi. Diffuse alveolar damage, with high neutrophilic and macrophagic infiltration, was also observed in the caudal lobes of two animals infected with the F virus at 1 dpi (Figure 19B). Histopathological lesions observed in the lungs of R6 infected ferrets were mainly characterised by different grades of necrotizing bronchiolitis, characterised by bronchiolar and glandular necrosis with lymphoplasmacytic inflammation (Figure 19C). Two animals infected with the R6 virus also presented mild bronchointerstitial pneumonia in the cranial lobes (one at 1 and the other at 3 dpi).

Viral Detection and Quantification

Infected animals showed nasal shedding of the virus at 3 dpi PFU assay (data not shown). The presence of the virus was checked in lung tissues by RRT-PCR; once more, all infected animals were positive at 1 and 3 dpi, whilst the control animals were negative. One animal infected with the R6 virus also showed positivity at 10 dpi. At 1dpi, F infected ferrets showed higher viral titters, in comparison with R6 infected animals, but without observing statistically significant differences between them (Figure 19D). Conversely, viral titres were similar in the lungs of R6 and F infected animals at 3 dpi.

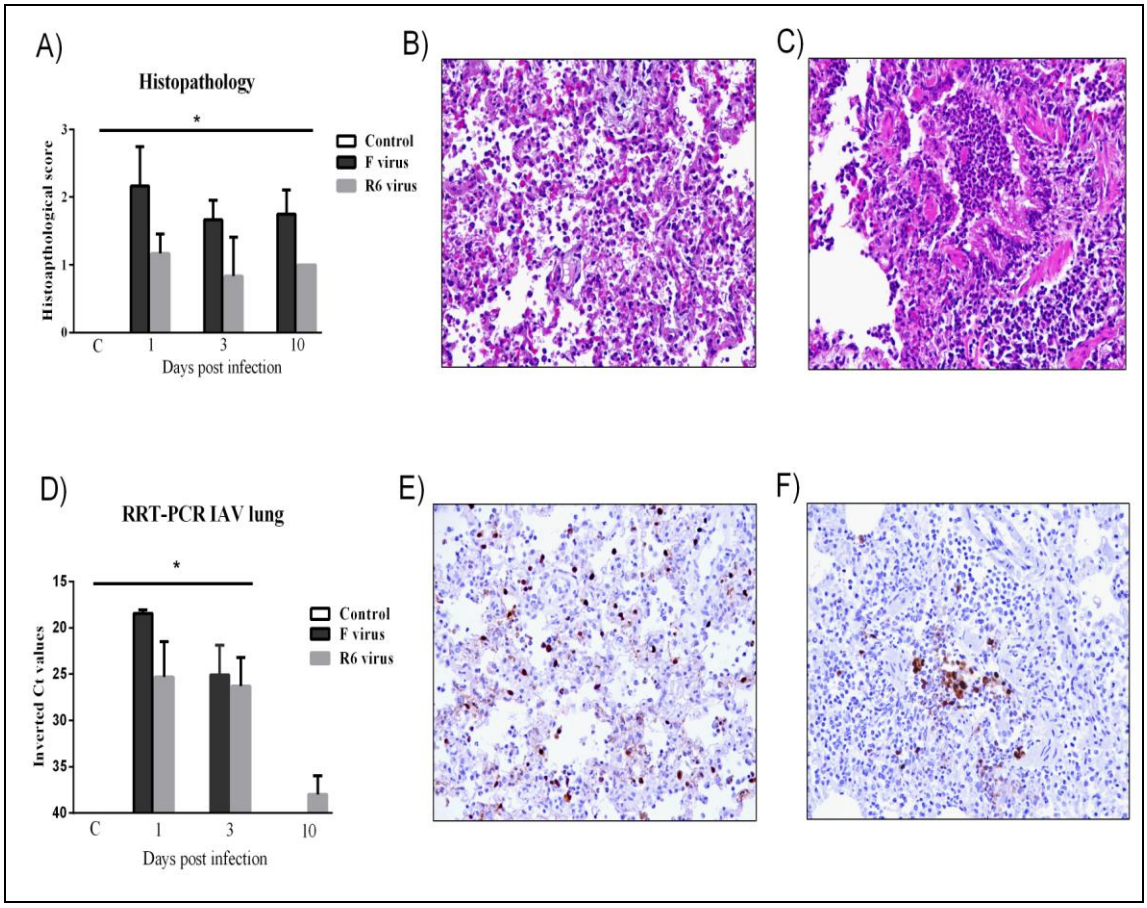

Figure 19. Histopathology and viral quantification. (A) Histopathological scores representing lung lesion severity (B) diffuse alveolar damage in one animal infected with the F virus and (C) necrotizing bronchiolitis in one ferret infected with the R6 virus. HE staining (40x objective field). (D) IAV RRT-PCR in the lungs. Values represented as inverted Ct values (E) IAV positive cells by IHC located in the alveolar septa in one ferret infected with the F virus (F) IAV positive cells located in the bronchiolar epithelium in one animal infected with the R6 virus (20x objective field). The data expresses the means with SEMs. Images correspond to HE and immunohistochemical staining for IAV antigen (20x objective field). Statistically significant differences between histopathological scores and viral load represented by * (p value < 0.05).

IHC was performed to detect and check the distribution pattern of the viral antigen, in the lungs of infected animals (Figure 19E-F) .No IAV positive cells were observed in the lungs of control animals. Positive cells were observed in both infected groups at 1 and 3 dpi, but not at 10 dpi. In general, at 1 dpi higher amounts of IAV positive cells were observed in infected groups in comparison with 3 dpi. Viral antigen was mainly observed in epithelial and glandular bronchiolar cells, pneumocytes and alveolar macrophages (Figure 19E). Lungs of F virus infected ferrets presented more IAV positive cells than R6 virus infected animals, particularly in alveolar areas (Figure 19F).

Gene Expression Profiles

The clinicopathological outcome of infection with the two different H1N1v strains was analyzed for correlation with the host immune response in lungs from infected animals. Therefore, some cytokines, chemokines and the PRR RIG-I, already known to be related with IAV infection, were quantified by RRT-PCR at 1 and 3 dpi.

Control animals presented depreciable levels of all studied molecules. Samples of F-infected ferrets presented higher expression of IL-6 and IFNγ at both time points, without any statistically significant differences (Figure 20 and 21).

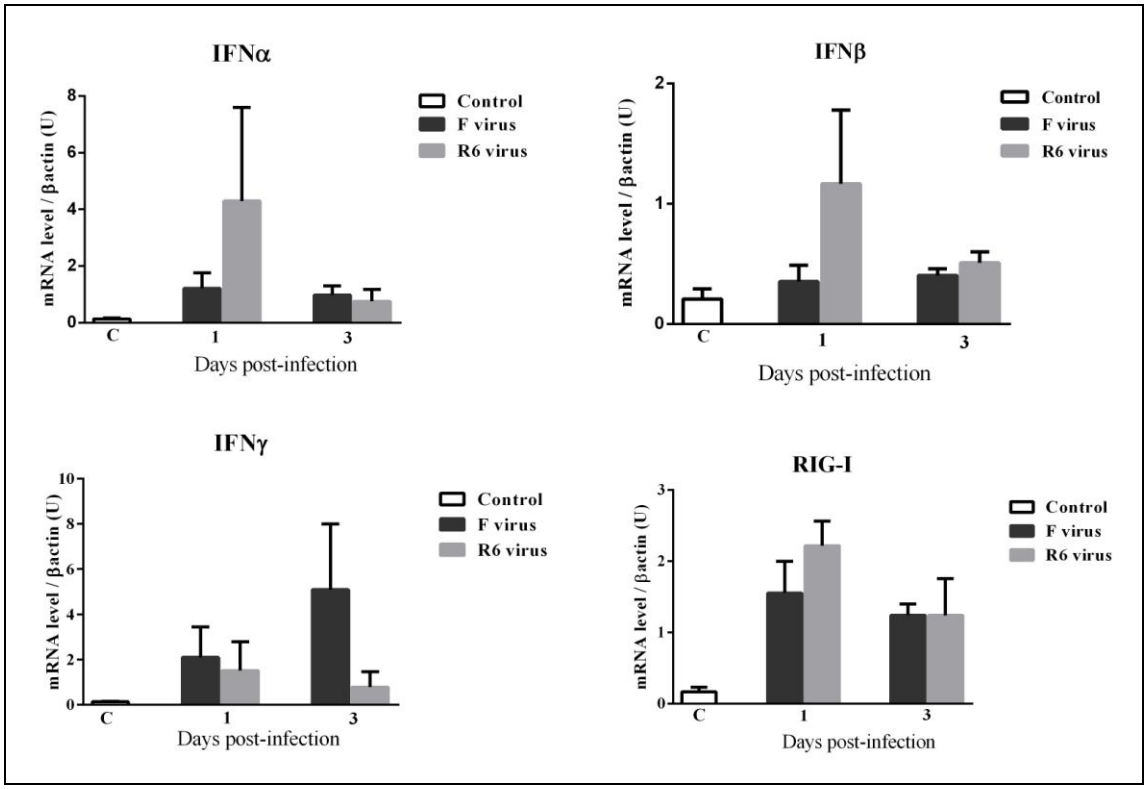

Figure 20. Cytokines and RIG-I gene expression in the lungs. Comparisons of the gene expression levels in the lungs at 1 and 3 dpi, by RRT-PCR. Gene expressions of IFNα, IFNβ, IFNγ, and RIG-I. The data expresses the mean with SEMs. No statistically significant differences were observed between groups.

However, samples from R6 infected ferrets exhibited higher induction of RIG-I, IFNα, IFNβ, IL-8, CXCL10 and TNFα at 1 dpi, whereas, F-infected animals presented higher induction of CXCL10 and IL-8 at 3 dpi. However, no statistically significant differences were observed between infected groups (Figure 20 and 21).

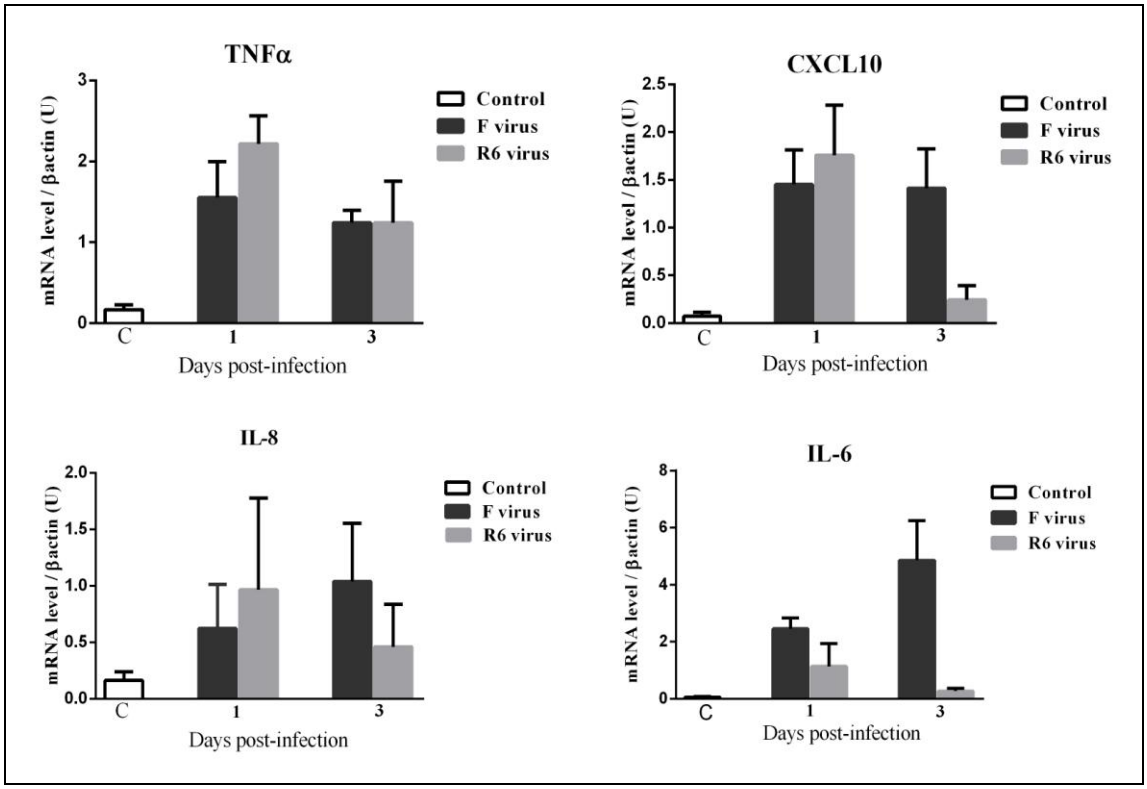

Figure 21. Cytokine gene expression in the lungs. Comparisons of the gene expression levels in lungs at 1 and 3 dpi by RRT-PCR. Gene expressions of TNFα, CXCL10, IL-6 and IL8. The data expresses the mean with the SEMs. No statistically significant differences were observed between groups.

Antibody Response

Antibody response to R6 and F viruses was determined by HI assay in sera at 0 and 10 dpi (Table 9).

GROUP	A/CastillaLaMancha/RR5911/2009 (F)		A/Baleares/RR6121/2009 (R6)	
	0 dpi	10 dpi	0 dpi	10 dpi
CONTROL	-	No sample	-	No sample
	-	No sample	-	No sample
R6	-	< 5,120	-	<10,240
	-	< 2,560	-	< 2,560
F	-	< 20,480	-	<640
	-	< 20,480	-	<640

Table 9. **Antibody response by HI.**

All ferrets were seronegative prior infection, and control ferrets remained negative up to culling. A strong HI antibody response to both viruses was observed in the serum from infected animals at 10 dpi (Table 9).

Samples from F-infected ferrets showed higher HI titres in sera samples, when compared with samples from R6 infected animals. Cross-reactivity was observed in serum, from both F and R6 infected animals.

5.4 Discussion

It is believed that OR H1N1v viral strains with H275Y NA mutation are less virulent than WT viruses [293,294]. However, several *in vivo* experiments have found conflicting results regarding their virulence in the mouse and the ferret models [128,130-132,281,283,285]. The results presented in this work showed that Wt (F virus) was more virulent in terms of clinical signs, gross and microscopic lesions, and early viral pulmonary replication, than the OR (R6 virus) in the ferret model.

Aminoacidic sequences of the viruses used in this study were compared, which showed that F and R6 viruses exhibited differences in amino acidic signatures in PB2, PB1, PA, NP, HA, NA, and NS1 proteins. It is noteworthy that most of the signatures of the F virus are rare in the H1N1v linage, and therefore, it cannot be excluded that they are related with F virus higher pathogenicity, in comparison with R6 virus. The high number of mutations observed in the F virus polymerase complex suggests that it has been under strong selection pressure, even higher than the surface glycoprotein, and this might be related with the selected patient [250]. Nevertheless, none of the changes observed in the aminoacidic sequences have been characterised, nor have they been described as playing a role in the domains in which they fall [295].

It has been suggested that seasonal and H1N1v OR virus variants with the same NA mutation differ in replication or transmission fitness, depending on other viral components [128]. Several studies have shown that a specific combination of residues in seasonal and H1N1v viruses, such as V234M or R222Q, which were not present in

earlier H1N1 viruses, resulted in a greater affinity of the NA cleavage balance, and were significantly beneficial in compensating for the deleterious effect of the OR mutation [280,296]. Interestingly, viruses from both the Newcastle and Sapporo clusters contained the permissive NA mutations V241I and N369K, which have recently been shown to improve the replication and transmission fitness of viruses containing the H275Y mutation [297]. In our study, no compensating mutation was found in the R6 virus, which might explain the slower viral replication observed in this group compared with the F group at early stages of infection. Supporting this observation, an *in vitro* study with the F and the R6 virus, showed a slower replication of the R6 virus at 6 hpi (Martínez-Orellana *et al.* unpublished results).

Animals infected with the F virus presented higher lung viral titres at 1 dpi. In addition, more severe histopathologic lesions were apparent throughout the infection in ferrets belonging to this group. This was combined with a higher local release of pro-inflammatory cytokines in the lungs, and higher levels of acute phase proteins in the serum. In correlation with these results, F-infected animals exhibited significantly higher clinical scores when compared with their OR counterparts. Several studies have already concluded that high viral replication rates in the lungs, and increased levels of APP, are related with severe influenza virus infection in ferrets, and other mammals [84,191,298].

The lung immune response in F-infected animals was characterised by a higher induction of the pro-inflammatory cytokines IL-6, IL-8, CXCL10, and IFNγ, at 3 dpi. The presence of viral antigen in alveolar areas, together with the up-regulation of pro-inflammatory cytokines, has previously been described as a marker of severe H1N1v infection in humans and animal models [79,83,153,157,191,299]. From these observations, it is conceivable that lung lesions and clinical signs observed in F-infected animals might be, in part, a consequence of the lung pro-inflammatory response, resulting from the spread of the virus to alveolar areas.

Duan and colleagues (2010) hypothesized that OR delayed virus growth *in vitro* may be a consequence of a delay in release of progeny virions from the host cell surface, due to reduced NA enzyme efficiency. This delay would not affect the final virus exert, but would allow the host's first line innate immune defence to neutralize the virus in *in vivo* experiments [131]. In addition, several studies have pointed to the correct regulation of the innate immune response, particularly the up-regulation of IFN type I genes, as protective factors in the pathological outcome, after H1N1v infection [71,83,157,299,300]. In our study, the R6-infected ferrets presented a higher expression of Type I IFN and RIG-I genes, in correlation with lower viral titres at 1 dpi. These observations led us to conclude that R6 virus might be better recognized by the host innate immune response, due to the slower viral growth at early stages of infection. This slower viral growth would allow the host to restrict the viral infection to bronchiolar areas, avoiding the spread of the virus to alveolar areas, the release of detrimental pro-inflammatory cytokines, and the resulting severe alveolar damage.

All in all, this study provides more evidence for the influence of interactions between viral capacities and the host innate immune response, on the outcome of disease after IAV infection. Thus, understanding the interaction between both viral genetic characteristics within the host immune genetic context is of great importance to the development of future therapies against IAV infection.

CHAPTER 6

STUDY IV: *Involvement of the Different Lung Compartments in the Pathogenesis of H1Nv1 Influenza Virus Infection in Ferrets*

6.1 Introduction

The physiopathology of H1N1v infection in humans differs across individuals. Whilst most patients developed mild upper respiratory-tract infection, some patients progressed to develop severe lower respiratory-tract complications, with fatal consequences. Severe cases after H1N1v infection are consequence of DAD, also termed interstitial pneumonia. In these cases, alveolar epithelial damage caused by the infection, together with a detrimental inflammatory response, triggered by an exacerbated host immune response, have been suggested culprits [153,301].

Lung function is largely dysregulated by the damaging effects of leukocytes on epithelial and endothelial cells [79,83,302,303]. The income of leukocytes into the lungs is mediated through the signalling effects of innate immune molecules, like cytokines and chemokines, induced by different cell types in the lungs. Although cytokines have specific functions and are released in a cell-type-dependent manner, all of them are produced/activated via common mechanism, involving the activation of PRRs [63,75]. Activation of these receptors results in the release of cytokines and chemokines, which promote a local antiviral state, and the recruitment of immune cells to the site of infection [181]. Although innate immunity is indispensable for limiting viral spread and the protection of the host against IAV infection, an exacerbated proinflammatory response can harm rather than protect the host. Several hypotheses have been made about the mechanisms involved in the dysregulation of the host inflammatory response. However, all of them involve the up-regulation of pro-inflammatory cytokines form different lung cell types [83,263,303].

During IAV infection, cytokines are produced by epithelial infected cells, endothelial cells, and leukocytes. However, cytokine and chemokine regulation mechanisms and the dynamics of their release have not been entirely elucidated. In order to identify the main producers of pro-inflammatory cytokines, and the temporal dynamics of the innate immune response against H1N1v infection, we studied the induction of different innate immune molecules in different lung anatomic

compartments (bronchiolar, alveolar and vascular), in response to H1N1v infection in the ferret model, by means of a Laser Capture Microdissection (LCM) technique.

6.2 Material and Methods

Virus

The human H1N1v isolate A/CastillaLaMancha/RR5911/2009 was used in the present study. The virus was isolated at the National Influenza Centre (CNM, ISCIII), from a respiratory sample sent by the Spanish Influenza Surveillance System for virological characterisation.

Ferrets

Eleven neutered male ferrets between eight and nine months of age, and seronegative for IAV (influenza A antibody competition multi-species ELISA, ID Screen®, France), were randomly selected from a stable, purposely bred colony *(Euroferret,* Denmark*)*. Upon arrival at CReSA, the animals were placed in BSL-3 facilities. Ferrets were placed in experimental isolation rooms, and then maintained for one week for acclimation. The animals inhabited standard housing cages, and were provided with commercial food pellets and tap water *ad libitum* throughout the experiment. All experiments were performed under a protocol (nº 1976) which was reviewed and approved by the Animal and Human Experimentation Ethics Commission of the UAB.

Animals were divided into two groups. The control group included two ferrets and the infected group included nine ferrets which were intratracheally inoculated with 10^5 $TCID_{50}$/ml of the A/CastillaLaMancha/RR5911/2009 virus. Control animals were euthanized at 0 dpi, prior to the inoculation of the virus to infected animals. Necropsies were performed at 0 dpi in control animals, and at 12, 24 and 72 hpi, in infected animals. Animals were euthanized by an intravenous injection of sodium pentobarbital (100 mg/kg), under anaesthesia with ketamine (5-10 mg/kg) (Imalgene

1000® Merial, S.A., Spain) and medetomidine (0.05 mg/kg) (Domtor® Pfiser, S.A., Spain). Necropsies were performed according to a standard protocol.

Histopathology

Right lung lobe sections (cranial and caudal lobes), were taken for histological examination. The tissues were fixed for 24 to 48 h in neutral-buffered 10% formalin, and then embedded in paraffin wax in two different blocs containing one portion of the cranial and the caudal right lung lobes. One of the paraffin blocks was sectioned at 3 µm, and stained with HE for examination under light microscopy; the second paraffin block was used for microdissection studies.

Cross sections of the cranial and caudal pulmonary lobes for each animal were histopathologically and separately evaluated. Semiquantitative assessment of IAV-associated microscopic lesions in the lungs was performed. The lesional scoring was graded on the basis of lesion severity as follows: grade 0 (no histopathological lesions observed), grade 1 (mild to moderate necrotizing bronchiolitis), grade 2 (bronchointerstitial pneumonia characterised by necrotizing bronchiolitis and alveolar damage in adjacent alveoli), and grade 3 (necrotizing bronchiolitis and diffuse alveolar damage in the majority of the pulmonary parenchyma). Microscopic lesional scores were assigned for each lobe, and the means of the two lobes were used for the final histopathological score for each animal.

Laser Capture Microdissection

Lung samples from infected and control animals were used for the microdissection study. For each animal, 20 µm sections were cut from FFPE lung tissue and mounted in PEN-membrane slides (two sections per slide). Prior to deparaffinization, slides were placed into an oven at 60ºC for 25 min. For each lung sample, sections were cut, deparaffinised, and rehydrated using standard protocols with RNase-free reagents, and stained with 1 % cresyl violet acetate (SIGMA, C5042), and alcoholic 1 % eosin (Alvarez, 10-3051). Stained slides were then dehydrated

through a series of graded ethanol steps prepared with DEPC treated water (Ambion, P/N AM9915G) to 100% ethanol. The slides were then air-dried for 10 min, and individually frozen at -80ºC in 50ml parafilm sealed falcons, before being transferred to the LCM microscope (LMD6500; Leica Microsystems) for simple microdissection.

Bronchiolar, vascular, and alveolar areas were separately selected for analysis using the Leica LMD6500 (Leica) system (x20 magnification, Laser Microdissection 6000 software version 6.7.0.3754). Selected areas were chosen by a pathologist as observed in (Figure 22). In infected animals, areas which exhibited pathological lesions were preferably selected. The total dissected area per selected lung compartment and animal rose approximately 1,5 mm^2. One cap was used per anatomic dissected compartment and animal.

The different dissected areas were then collected separately into RNAse-free 1.5 ml PCR tubes, per lung compartment.

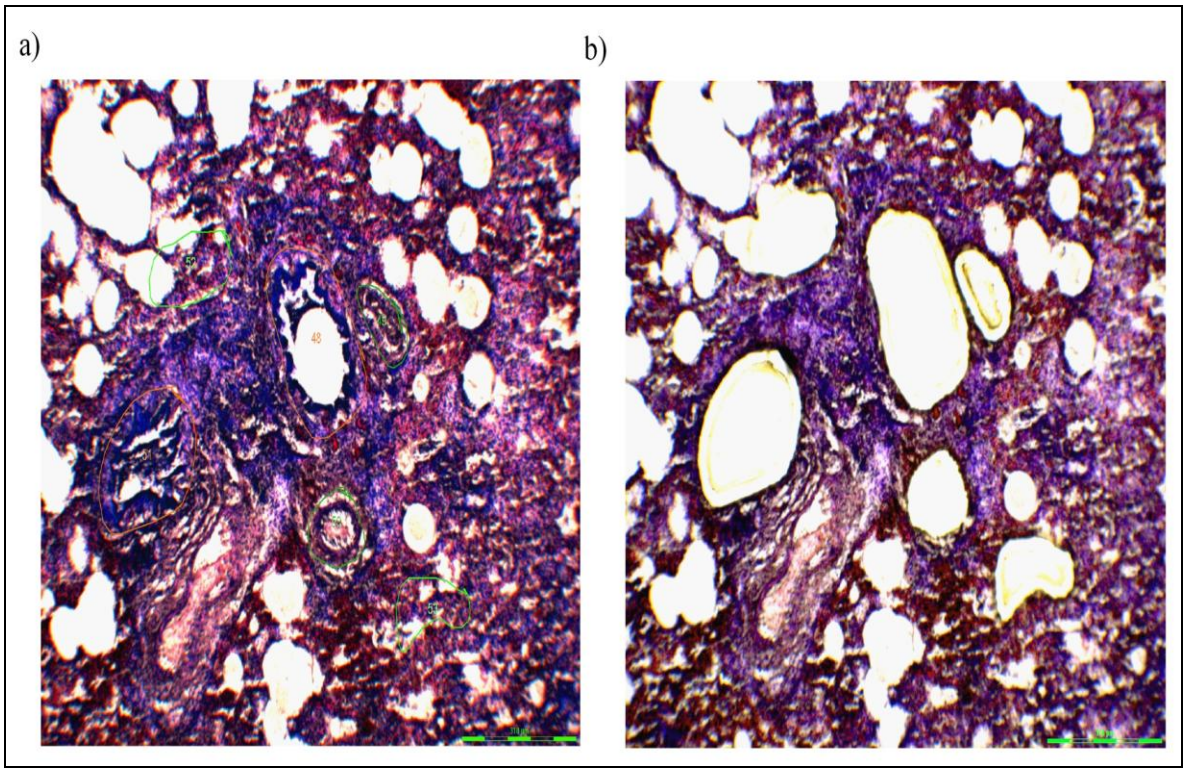

Figure 22. Lung laser microdissected areas. a) Before laser microdissection; b) after laser microdissection.

Viral Detection and Quantification

For the detection of IAV antigen by IHC, paraffin sections were stained with a primary antibody against the influenza A NP, as previously described [254]. Sections were then counterstained with Mayer's Haematoxylin. The positive control consisted of a FFPE heart from a chicken, experimentally infected with influenza. The same section in which the specific primary antibody was substituted with PBS was used as negative control. Semiquantitative assessments of IAV antigen expression in the lungs were performed. The positive cells in 6 arbitrarily chosen 20x objective fields in alveolar areas, and 5 arbitrarily chosen 20x objective fields in bronchial or bronchiolar areas, were quantified separately in each lung lobe (cranial and caudal) for every animal. The mean of the total cell counts per field across two lobes was calculated for each animal.

Viral RNA from total lung samples was extracted with NucleoSpin® RNA Virus Kit (Macherey-Nagel, Düren, Germany), following the manufacturer's instructions. IAV M gene was then quantified from the RNA extracted by the Taq-Man one-step quantitative RRT-PCR using the primers and probe described in the annex (Table 1), and the amplification conditions described n the study III. Reaction was performed using Fast7500 equipment (Applied Biosystems, Foster City, CA, USA). Samples with a Ct value ≤40 were considered positive for influenza viral RNA detection.

Viral RNA detection from different lung anatomic compartments was extracted using the miRNeasy FFPE Kit (nº217504, Qiagen, Valencia, CA) and the RNA stabilisation and on-column DNase digestion protocols (Qiagen, Valencia, CA), following the manufacturer's instructions. Briefly, the transfer film with the attached dissected material, per animal and lung compartment, was placed in deparaffinization melting buffer at 72ºC for 10 min, and then treated with Proteinase K at 60ºC for 45 min. Isolated RNA was concentrated using ethanol precipitation method and membrane column attachment. RNA was eluted twice in 14ul total DEPC water, yielding between approximately 5 and 9 ng/µl of RNA, per sample. RNA extracts were stored at -80°C until required. Reverse transcription was performed using an ImProm-II

reverse transcription system, with random primers (Promega, Madison, WI), using 10 µl of the eluted RNA. IAV M gene was then quantified on the RNA, extracted by Two-step RRT-PCR using the forward and reverse primers for detection of the M gene, described in the annex (Table 1). Briefly, RRT-PCR was performed using a Power SYBR green kit, (Applied Biosystems, Foster City, CA) and Fast 7500 equipment (Applied Biosystems, Foster City, CA, USA). PCR reactions were performed in 10 µl reaction volumes, in quadruplicates; 45 amplification cycles were used, and the annealing temperature was 60º C. Results are expressed as inverted Ct values. Samples with a Ct value ≤45 were considered positive for influenza viral RNA detection.

Gene Expression Profiles

Total RNA was isolated from LCM tissues, using the miRNeasy FFPE Kit (nº217504, Qiagen, Valencia, CA), as described in the above section.

Relative mRNA expression levels of IFNα, IL-6, TLR-3, BAX, IFNγ, TNFα, CCL2, and the housekeeping gene β-actin with amplicon range between 90 and 120 base pairs at each different lung compartment, were assessed by Two-step RRT-PCR, as described in the second and third studies of this thesis. Primer sequences are illustrated in the annex (Table 1). Briefly, RRT-PCR was performed using a Power SYBR green kit (Applied Biosystems, Foster City, CA) and Fast 7500 equipment (Applied Biosystems, Foster City, CA, USA). PCR reactions were performed in 10 µl reaction volumes in quadruplicates; 45 amplification cycles were used, and the annealing temperature was 60º C. The expression levels were normalized using the house-keeping gene β-actin, and the results are expressed as arbitrary units.

Vascular Gene Expression

Relative mRNA expression levels of selectine P-ligand (SELPLG), and the housekeeping gene β-actin in the vascular compartment, were assessed by Two-step RRT-PCR, as described in the above section. Primer sequences design was performed as described in study II. Briefly, RRT-PCR was performed using a Power SYBR green kit

(Applied Biosystems, Foster City, CA) and Fast 7500 equipment (Applied Biosystems, Foster City, CA, USA). PCR reactions were performed as described in the above section and primer sequences are illustrated in the annex (Table 1). The expression levels were normalized using the house-keeping gene β-actin, and the results are expressed as arbitrary units.

Statistical Analysis

Data visualization was performed with GraphPad Prism 6 (GraphPad Software, La Jolla, CA, USA). All statistical analysis was performed using SPSS 15.0 software (SPSS Inc., Chicago, IL, USA). For all analysis, ferret was used as the experimental unit. The significance level (α) was set at 0.05. The Shapiro Wilk´s and the Levene test were used to evaluate the normality of the distribution of the examined quantitative variables, and the homogeneity of variances, respectively. No continuous variable that had a normal distribution was detected. Thus, a non-parametric test (Wilcoxon test) using the U Mann-Whitney test was used to compare the different values obtained for all the parameters (histopathology and viral load), between groups (control versus infected), and between different compartments of the infected group (alveolar, bronchiolar and vascular), for viral load and gene expression profiles, at all sampling times.

6.3 Results

Histopathology

Histopathological evaluation identified lesions mainly localized in bronchial/bronchiolar and alveolar areas (Figure 23). At 12 hpi, histopathological lesions were characterised by mild bronchiolitis, consisting of bronchial/bronchiolar epithelium necrosis, and the presence of a mild macrophagic infiltrate in the bronchial/bronchiolar lumen. Lesions were similar in both cranial and caudal lobes at this stage (Figure 23). At 24 hpi, lesions were consistent with bronchointerstital pneumonia, or, interstitial pneumonia in the caudal lobes. Bronchointerstitial

pneumonia was characterised by bronchial/bronchiolar necrosis and alveolar epithelial necrosis, lymphoplasmacytic infiltration, and mucus and cell debris, filling the bronchi and the adjacent alveoli. In addition, two of the three animals presented interstitial pneumonia (DAD) in caudal lobes, at this time point.

DAD was characterised by a moderate to severe bronchiolar necrosis with lymphoplasmacytic infiltration in the lamina propria, and a variable number of macrophages and neutrophils in the lumen (Figure 23). The alveolar septa was also congested, and presented necrosis of epithelial cells accompanied by interstitial inflammatory infiltrates in the septa and lumen, mainly characterised by macrophages and neutrophils (Figure 23). At 72 hpi, lesions were milder than at 24 hpi (Figure 23), and lesions consisted of mild bronchointerstitial pneumonia.

Higher histopathological scores were observed in the infected group in comparison with the control group. Of infected animals, lower histopathological scores were observed at 12 hpi, while higher histopathoglogical scores were observed at 24 hpi. At 72 hpi, histopathological scores slightly decreased in comparison with histopathological scores, at 24 hpi (Figure 24).

Viral Detection and Quantification

Viral detection and quantification by IHC was performed in lung tissues. Control animals did not show positivity at any time point (Figure 24). In general, viral antigen was observed in the nucleus of bronchial and bronchiolar epithelial and glandular cells of infected animals at 12 hpi (Figure 23).

At 24 hpi, IAV positive cells were observed in the nucleus of the respiratory epithelium (bronchial, bronchiolar and alveolar), and in the nuclei and cytoplasm of macrophages. In the alveolar epithelium, positive cells were mainly observed in type II pneumocytes, but also in type I pneumocytes (Figure 23).

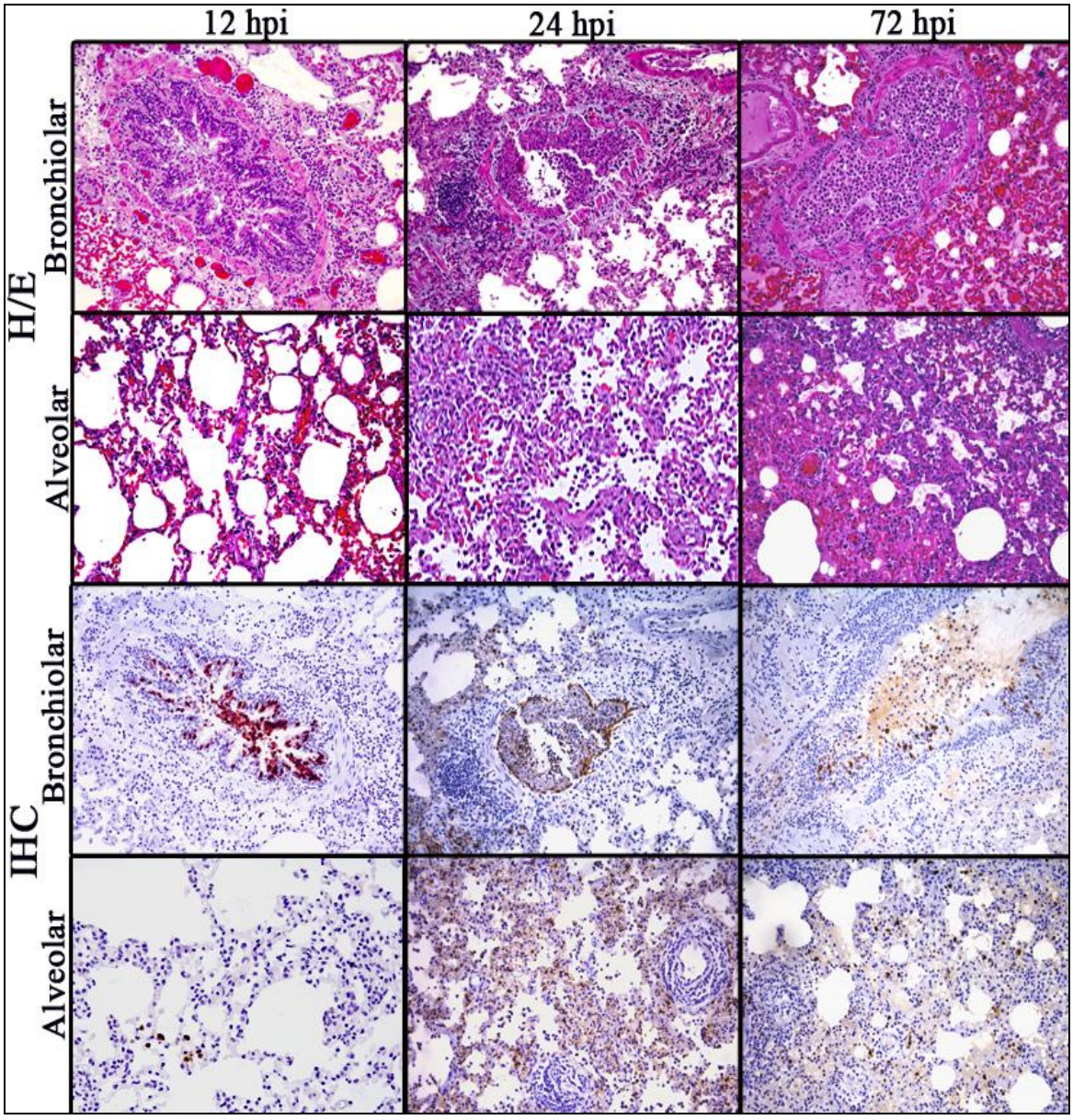

Figure 23. Histopathological pulmonary lesions of H1N1v infected ferrets at different times post infection. Pictures show different severity of lesions in alveolar and bronchiolar areas, and the distribution of viral antigen in the respective areas. HE and immunohistochemical staining for IAV NP antigen (20x objective field).

Quantification of IAV positive cells in the lungs of infected animals revealed that higher numbers of positive cells were observed in bronchiolar areas at 12 hpi. Statistically, significant higher numbers of positive cells in bronchial areas were observed in comparison with alveolar areas at 12 and 72 hpi (Figure 24).

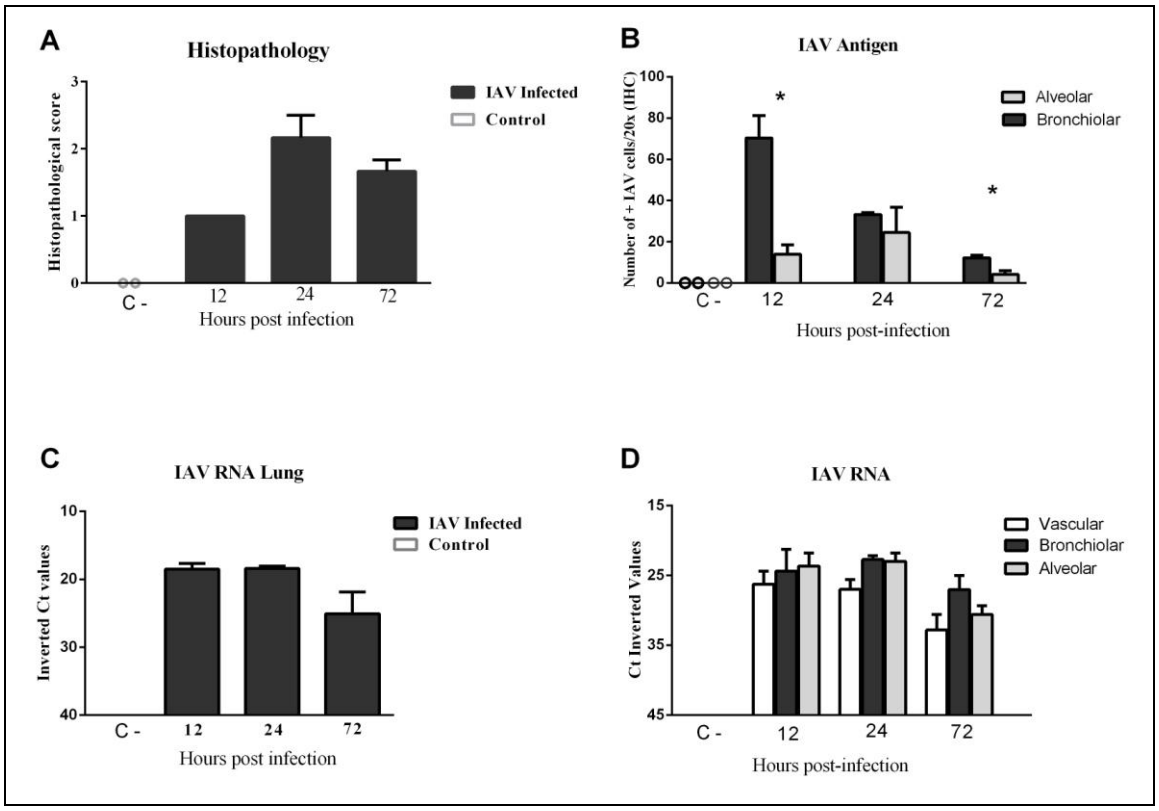

Figure 24. Histopathological scores, IAV antigen quantification by IHC and viral RNA detection by RRT-PCR in the lungs. (A) Histopathological scores representing lung lesion severity in infected and control animals (C-). (B) Immunohistochemical cell quantification of IAV-positive cells in infected and control (C-) ferret lungs; results express the mean cell counts with SEM (20x objective field). (C) IAV RRT-PCR in the total lung of infected and control animals and (D) in different lung compartments of infected and control animals. Values represented as inverted Ct values. The data expresses the means with SEMS. Statistically significant differences are represented by * (p value < 0.05).

Viral RNA detection by RRT-PCR, in the total lung, and in the different lung compartments, was performed. Control animals were negative to viral RNA detection in the total lung, and in the different lung compartments (Figure 24). In the total lung, higher viral RNA detection was observed at 12 and 24 hpi, and then levels decreased at 72 hpi (Figure 24). Viral RNA detection in the different anatomic compartments of infected animals, showed higher viral RNA levels in bronchiolar and alveolar areas at 24 hpi, followed by 12 hpi (Figure 24). At all time points, vascular areas showed higher levels of viral RNA with comparison to control animals. Viral RNA levels were higher at 12 hpi, then decreased gradually until 72 hpi (Figure 24).

Gene Expression Profiles

Innate immune gene expression levels observed in the different anatomic lung compartments are represented in (Figures 25 and 26).

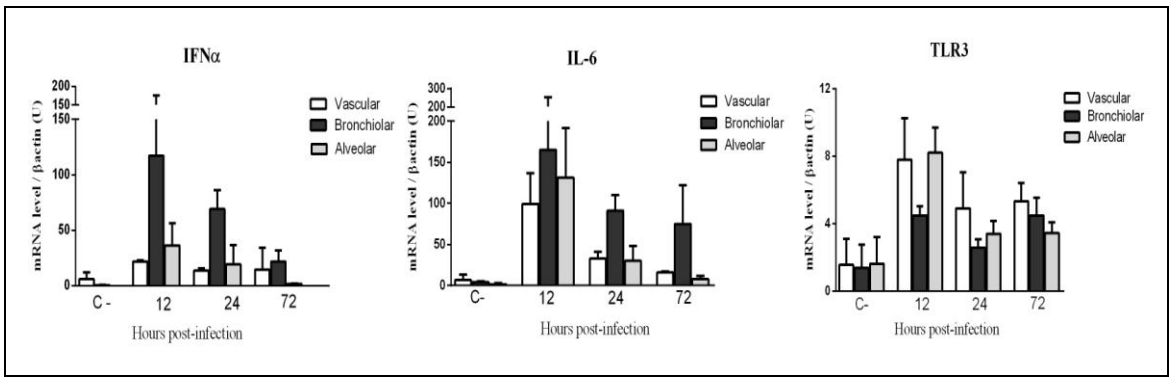

Figure 25. Innate immune gene detection by RRT-PCR in vascular, bronchiolar, and alveolar areas in the lungs. Comparisons of the gene expression levels of IFNα, IL-6, and TLR3, in different anatomic lung compartments of control (C-) and infected ferrets at 12, 24, and 72 hpi. The data expresses the mean with the SEMs. No statistically significant differences were observed between groups.

Innate immune gene expression levels were higher in all anatomical compartments, in comparison with control animals. In general, significantly higher levels of IFNα were observed in bronchiolar areas, in comparison with alveolar and vascular areas.

Higher expression of IFNα was observed at 12 hpi, diminishing gradually at 24 hpi, and later at 72 hpi. IL-6 expression levels were higher in bronchiolar areas than in alveolar and vascular areas at all times post infection, with peak levels observed at 12 hpi. Alveolar and vascular areas expressed higher levels at 12 hpi, diminishing gradually at 24 hpi and later at 72 hpi.

TLR3 expression was higher in alveolar and vascular areas than in bronchiolar areas at 12 and 24 hpi. At 72 hpi, TLR3 levels were higher in vascular areas, followed by bronchiolar and alveolar areas (Figure 25).

TNFα was more expressed in bronchiolar areas, with higher levels observed at 24 hpi, followed by 12 and 72 hpi, and in comparison with alveolar and vascular

compartments. In alveolar areas and vascular areas, TNFα was only slightly upregulated at 24 hpi (Figure 26). IFNγ was more expressed in bronchiolar areas, followed by vascular areas. Higher levels of IFNγ were observed at 24 hpi in all compartments and to a lesser extent at 72 hpi.

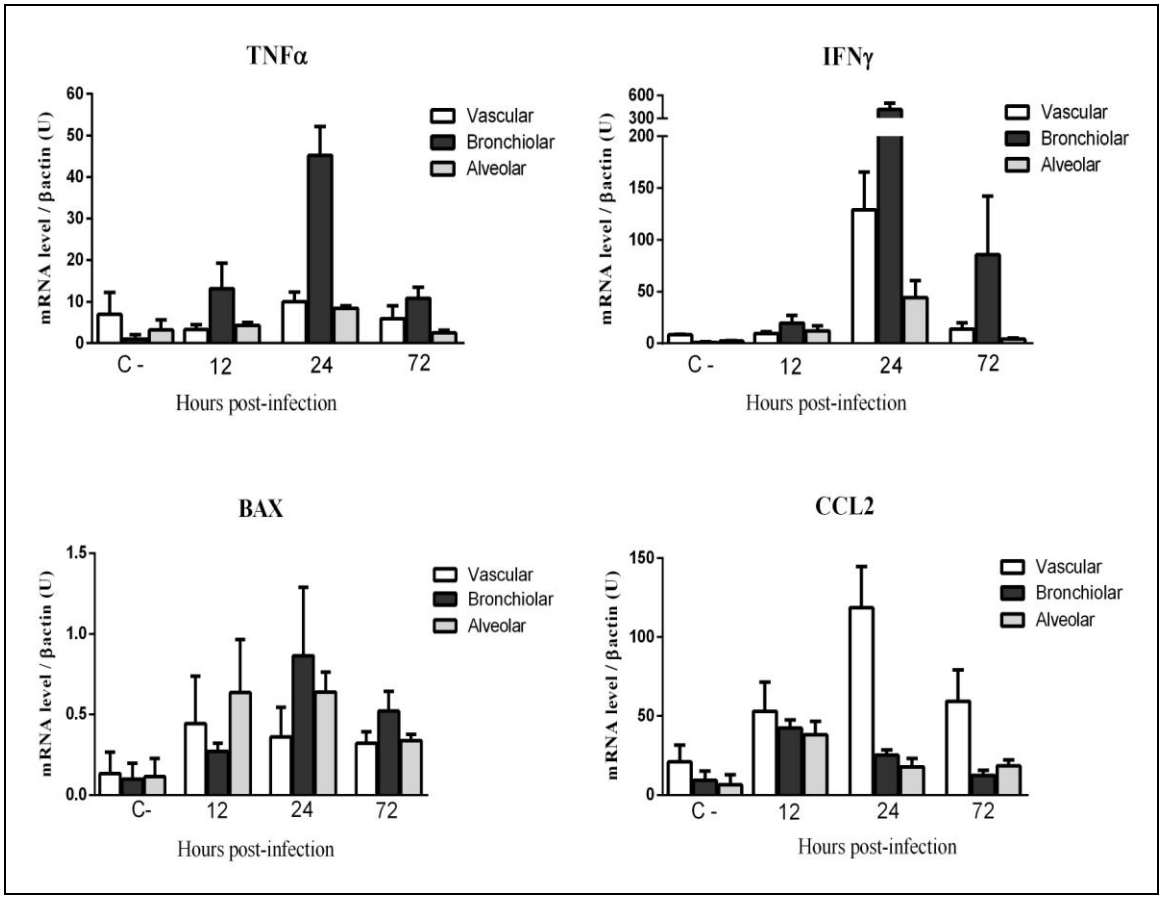

Figure 26. Innate immune gene detection by RRT-PCR in vascular, bronchiolar, and alveolar areas in the lungs. Comparisons of the gene expression levels of TNFα, IFNγ, BAX, and CCL2, in different anatomic lung compartments of control and infected ferrets at 12, 24, and 72 hpi. The data expresses the mean with the SEMs. No statistically significant differences were observed between groups.

Higher levels of BAX were observed in bronchiolar areas at 24 hpi, and 72 hpi, compared to alveolar and vascular compartments. At 12 hpi, BAX levels were higher in alveolar and vascular areas, in comparison with bronchiolar areas. CCL2 was more expressed in vascular areas, followed by bronchiolar and alveolar areas. Higher levels of CCL2 were observed at 24 hpi in vascular areas, followed by 72 and 12 hpi.

Vascular Gene Expression

Vascular adhesion was evaluated by the expression of SELPLG in vascular areas. Infected animals showed higher levels of SELPLG when compared to control animals. SELPLG expression was upregulated throughout the infection, and higher levels were observed at 72 hpi (Figure 27).

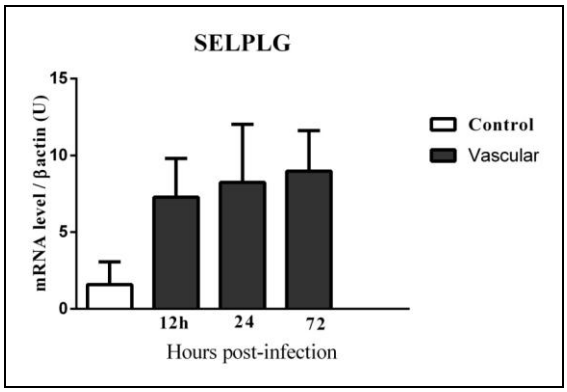

Figure 27. SELPLG gene expression by RRT-PCR in vascular areas of the lungs. Comparisons of the gene expression levels of SELPLG in vascular areas of infected and control animals at 12, 24, and 72 hpi. The data expresses the mean with the SEMs. No statistically significant differences were observed between groups.

6.3 Discussion

Severe cases after H1N1v infection are a consequence of interstitial pneumonia, triggered by alveolar viral replication, and an exacerbated inflammatory immune response. In such cases, H1N1v spreads from the upper to the lower respiratory tract, infecting the alveolar epithelium. Three main mechanisms are suggested to be involved in H1N1v pathogenicity: i) alveolar epithelium necrosis, caused by viral cytopathogenicity, and the release of cytokines by infected cells; ii) activation of lung vasculature, which increases endothelial permeability, releases cytokines, and triggers leukocyte migration; and iii) damage triggered by the inflammatory infiltrates, mainly formed by neutrophils and macrophages, plus the release of cytokines from these cells [303]. These mechanisms work in a feed forward manner, eventually increasing the inflammatory damage produced.

In our study, inflammation was firstly observed in bronchiolar compartments, in correlation with viral replication in bronchiolar epithelial cells, at 12 hpi. In addition,

the bronchiolar compartment expressed the highest levels of IFNα and IL-6 at this time point, as has already been described [304]. Although viral replication was also extensive in the alveolar compartment at 24 hpi, the IFNα response was not as relevant as in the bronchiolar compartment. This differential IFNα expression observed in the lung compartments might reflect diverse intracellular signalling pathways in different cell types, with distinct physiological functions (bronchiolar epithelial cell *versus* pneumocyte).

The upregulation of TNFα, IL-6, and IFNγ, has been related with the lung recruitment of inflammatory cells, such as NK, CTLs, macrophages, and neutrophils, through activation of endothelial cells. Activation of endothelial cells has been related to the expression of cytokines such as CCL2, IFNα, I-L6, and IFNγ, and the upregulation of adhesion molecules for leukocyte extravasation [303]. At 24 hpi, bronchiolar and alveolar areas showed the higher expression of TNFα and IFNγ, which correlates with a higher presence of leukocytes, and higher histopathological scores in these areas. Our data points to bronchial, and later alveolar epithelial cells, as responsible for the initial signalling to local endothelial cells, and subsequent recruitment of leukocytes into the lung. In addition, CCL2, IL-6, and IFNγ upregulation, which has been related to macrophage, NK and CTL cell recruitment into the lungs [79,82,87,88,95,168,181,303,305,306], was evident in the vascular compartment at 12 and 24 hpi in our study. This data confirms the contribution of the vascular compartment in the early induction of proinflammatory molecules, and the income of proinflammatory cells into the lungs after H1N1v infection.

Alveolar and vascular areas also presented a higher induction of TLR3 at 12 hpi, and afterwards, throughout infection, which correlates with the higher induction of pro-inflammatory molecules. TLR3 is expressed in the endosomal compartments of various cellular types, whose activation is mediated by the recognition of dsRNA, entered into the cell by endocytosis [63,75,268,307]. Since dsRNA is a universal pathogen-associated molecular pattern (PAMP), it has been assumed that TLR3 would play a key role in antiviral immunity. However, it has been demonstrated that TLR3 is related with

increased pathology after IAV infection [65,172,268,270,306,308]. In addition, it is known that TLR3 signalling is not required for the initial cell-autonomous recognition of viral infection or the induction of IFNα, which is induced via viral recognition by RIG-I, but not TLR3 [309]. This suggests that RNA viruses actively replicating in the cytoplasm, are recognized by RIG-I, but not TLR3, irrespective of their route of entry [309]. Besides this, it has recently been assumed that influenza virus-infected cells do not generate dsRNA [310], due to the activity of the cellular RNA helicase UAP56 [311]. This suggests that TLR3 recognizes currently unidentified RNA structures, from dying influenza virus-infected cells, or viral components from non-replicative virus.

Upon tissue damage, cell-derived extracellular RNA (eRNA) was shown to be associated with microparticles or exosomes, which are capable of delivering their RNA content to target cells, and induce the release of proinflammatory cytokines from recipient cells. This promotes vascular adhesion and transmigration of leukocytes *in vitro,* as well as, *in vivo*[312]. From these observations, one reasonable hypothesis is that cell-derived eRNA may interact with other cells such as the endothelium, influencing cellular responses, relevant for inflammatory processes.

Besides, a second hypothesis that would explain the up-regulation of innate immune responses at early stages of infection, in alveolar and vascular areas, is that TLR3 and/or other PRRs recognize virus derived RNA structures, in turn inducing the expression of innate immune molecules. Certainly, our results showed higher levels of viral RNA detection in all lung anatomic compartments at 12 and 24 hpi, which correlates with the RNA levels observed in total lung by RRT-PCR, but not with the detection of viral antigen (and thus viral active replication), in vascular areas throughout infection, nor in alveolar areas at 12 hpi. While the respiratory epithelium is the primary target of IAV, the proximity of the lung microvascular endothelium, combined with the damage that the virus causes to the epithelium, provide a plausible route through which the virus would be able to come into contact with the endothelium.

Although epithelial cells are the main targets of human influenza, endothelial cells are known to express α2,6 SA receptors [313,314], the expression of which increases when endothelial cells are stimulated with cytokines [315]. Even though endothelial cell IAV infection has been observed *in vitro,* causing cell death and cytokine production [316-320], the infection of endothelial cells by replicative H1N1v *in vivo* is unlikely. This is due to the fact that infection of endothelial cells has only rarely been reported in H1N1v human cases [154,155], and no IAV IHC positivity has been observed in vascular areas, in this or other studies[84,191,209,305]. Nonetheless, as endothelial cells posses α2,6 SA receptors, abortive infections, in which the virus enters the host-cell, but cannot successfully complete replication (as a result of a non-permissive host-cell), may be a reasonable explanation for the innate immune responses, and the higher expression of TLR3 observed in vascular areas. Supporting this hypothesis, it has been shown that replication-deficient IAV, and defective interfering particles (DIPS), arisen from internal deletions of IAVs, significantly activate endothelial lung cells, inducing a strong host cell response, without causing endothelial apoptosis or necrosis [315-317,321].

In summary, our data points to the role of the respiratory epithelium in bronchial and alveolar areas, as the first source of pro-inflammatory cytokines and the income of phagocytic cells into the lungs, early after IAV infection. In addition, our data indicates that vascular areas contribute to the induction of the proinflamamtory innate immune response, through the activation of TLR3, independently of active viral replication. Following these observations, we hypothesize that the innate immune response induced by vascular areas, may be consequence of signals triggered by the detection of viral RNA, or, through a complex crosstalk mechanism with the infected lung epithelium. However, the mechanisms involved in the detrimental innate immune response observed in severe IAV cases, and the relative contribution of the different lung compartments in the pathogenesis of severe IAV, still need to be further elucidated.

PART III

GENERAL DISCUSSION AND CONCLUSIONS

CHAPTER 7: GENERAL DISCUSSION

The pathogenic features of severe IAV infection result from complex and dynamic processes which involve various components of the host immune system, and their responses to virus-induced changes. Severe H1N1v infection in humans has been related with high viral replication in alveolar areas, and a robust host immune response [79,191,301]. High viral titres reflect properties that are intrinsic to the virus strain, including replication potential, receptor usage, and cytopathic effects on pulmonary epithelial cells [322,323]. Besides this, several reports have revealed that severe disease caused by IAV infection was characterised by the presence of high systemic levels of cytokines, chemokines, and other immune mediators, from the early stages of disease [55,79,162 73,111,210]. In addition, inflammatory infiltrates have been widely related with severe processes [301], suggesting a possible contribution of the host immune response in the development of severe cases, after IAV infection. It is now recognized that interactions between host and viruses play a crucial role in determining the relative magnitude of disease [302]. One example of this is the fact that certain people seem particularly susceptible to developing cytokine-driven clinical symptoms, suggesting a potentially genetic basis for the immune dysregulation, which is thought to be a major factor in severe human influenza [260,324].

For the above mentioned reasons, there is an increased need to study the interactions between host immune responses and IAV intrinsic properties. The ferret model is a useful model for the study of human IAV induced pneumonia, for the reasons outlined in the introduction. In addition, ferrets, as outbreed animals, exhibit differentially individual susceptibilities to viral infection. The severity of infection in ferrets can range from a sublethal infection with mild symptoms, to lethality rates of 30-50% [74,167,201]. This variability suggests the importance of the influences of both differences in viral strain capacities and individual host variability, as occurs in humans [163,259]. These observations make the ferret a very interesting animal model for the study of such interactions. Nevertheless, *in vivo* assessments of immune function following IAV infection have primarily been limited to murine models, owing to a lack of ferret-specific reagents, particularly those reagents used to study immunological

reactions. In addition, the immune system of ferrets has not been characterised and its genome has only been partially sequenced [190].

In order to address this problem, we standardized different techniques to study the immune response of ferrets infected with H1N1v viruses. Firstly, we standardized different IHC techniques for the detection of different immune cells in healthy ferret tissues. Our results identified different commercial antibodies which cross-react with ferret immune cells in FFPE and frozen tissues. These techniques let us phenotype B cells, T cells, HLA-DR antigen presenting cells, cytotoxic T cells, NK cells, macrophages, neutrophils and apoptotic cells. The distribution of immune cells in ferrets was similar to that of humans and other mammal species [221,229,231,234,236,246]. Interestingly, naïve B lymphocytes expressed the CD79α antigen intensely on their membrane, but this expression was downregulated during the maturation process. In contrast, the CD20 antigen was expressed on naïve B cells, but its expression increased as they matured, as described in other species [224,225,234]. In addition, we standardized a double IHC technique, allowing double detection of antigens within a cell. This technique led us to identify a subpopulation of B cells with macrophagic/dendritic morphology, as described in humans [246].

In addition, we also aimed to study the different expression of innate immune genes during H1N1v infection. For this purpose, we used several published primers for the detection of innate immune genes by RRT-PCR, and designed new primers for the detection of β-actin, IL-1α, CCL3, RIG-I, SELPLG, BAX, and Caspase 8 genes. Finally, in order to identify the different sources of cytokines during H1N1v infection, we standardized a laser microdissection technique, for the assessment of the genetic innate immune response dynamics in different anatomic lung compartments in FFPE ferret lungs.

Laser microdissection techniques have been widely used in various studies focused on neoplastic transformation, inflammation, or tissue repair, and its genetics in humans and animal models [325]. Although the first descriptions of the use of laser

light for microdissection of tissue were published in 1976 [326], it was not until the introduction of efficient analytical methods for small amounts of biological material in the late 90s that these techniques found widespread use [325]. Because LCM helps to collect determinable cells under controlled conditions, its combination with methods such as RRT–PCR allows a more precise determination of cell specific gene expression, on a microscopic scale [327]. In contrast to DNA, mRNA is more sensitive to fixation, quickly degraded by ubiquitous RNases, and requires stringent RNase free conditions during specimen handling and preparation. Despite these limitations, several groups have recovered good quality mRNA from microdissected samples by RRT–PCR, down to a single cell level [327,328]. Several veterinary pathological reports have used LCM techniques for different purposes [329]. In addition, a study of influenza pathogenesis has been recently described in the swine model by studying the different genetic expression of bronchial epithelial cells in frozen tissues, at different stages of disease differentiation [330]. To the best of our knowledge, our study is the first report which uses the LCM technique in ferret FFPE tissues. Although most authors used frozen tissue, successful mRNA amplification by RRT–PCR has also been reported for single cells isolated from FFPE tissue by LCM [325]. Nevertheless, frozen tissue yields higher quality mRNA and should be used whenever possible, to ensure optimal recovery of low abundance messages. Here, we tried repeatedly to perform the technique from frozen tissues. However, the security procedures needed to extract the samples from BSL-3 facilities, plus the transportation to the research centre with the LCM microscope, damaged the integrity and the final yield of RNA from frozen sectioned lung tissues, impeding us from performing the technique using those samples. Despite the chemical alterations induced by formalin, biomolecules can still be recovered and analyzed using specific molecular extraction protocols and downstream analysis, optimized for FFPE tissues [331,332]. Recently, technical improvements in mRNA extraction, and the introduction of commercial kits for RNA extraction from FFPE microdissected tissues (miRNeasy FFPE Kit, nº217504, Qiagen), have allowed gene expression analysis from LCM FFPE samples [329]. A typical LCM sample can provide between 50 and 300 ng total of RNA, depending on the amount of microdissected

cells. In addition, samples with an RNA integrity number (RIN) <5 can be used for Taqman and SYBR Green quantitative RRT-PCR assays (Life Technologies) [329]. In our study, we microdissected high numbers of cells and only used amplicons between 90 and 110 bp, in order to minimize the effects of fragmented and low RNA yield, caused by FFPE fixation. In addition, blocks used in this study were only fixated for a minimum of 24 to 48 h, with previously small, sectioned portions of lung tissue, to assure complete formalin penetration, as chemical alterations induced by formalin are time dependent.

Three experimental infections in the ferret model were performed taking into account viral genetic characteristics, and the host immune response towards infection. Firstly, we studied the virulent differences of two human viral isolates, presenting similar genetic characteristics, but resulting in different disease outcomes in human patients (death vs. mild symptoms). Secondly, we studied two human viral isolates with different genetic characteristics (one virus Wt and one virus with the H275Y mutation, conferring resistance to Oseltamivir antivirals) in patients who developed the same outcome of disease (death). Finally, we studied the innate immune genetic expression dynamics in different lung compartments, in ferrets infected with a human Wt H1N1v isolate, at early stages of infection.

In all three studies, H1N1v infection was associated with ferret lung damage. More severe lung lesions correlated with viral replication in alveolar areas, higher release of pro-inflammatory cytokines and higher lung inflammatory infiltrates, as observed in human patients [74,167,168,205]. Our results revealed that the presence of viral replication in alveolar areas was not only related with viral capacities, but also with the type of host immune response triggered against infection.

In the presence of viral mutations affecting viral growth, pathogenicity was related with viral kinetics. Viral strains possessing deleterious mutations, such as H275Y, presented a slower viral growth. This allowed the host to mount an efficient innate immune response, restricting viral infection to bronchiolar areas. This may be

the reason why OR viral strains are mainly isolated from immunocompromised patients [126,127,274,333], as was the case with the patient from whom the OR viral strain was isolated in this study. On the contrary, in the case of viral strains with similar viral capacities, the development of severe or mild disease depended on the type of immune response triggered by the host. Ferrets infected with H1N1v isolates presenting similar viral characteristics showed different pathological outcomes, depending on the type/magnitude of the host immune response, and independently of the viral strain inoculums. As observed in humans, high individual variability was observed in the outcome of disease after H1N1v infection in ferrets. Once the virus has arrived to alveolar areas, the host immune response triggers a proinflammatory immune response which is beneficial for the host as it allows viral clearance [59]. However, if the host proinflammatory response is dysregulated, it finally perpetuates the damage triggered to alveolar structures, causing severe lung damage [260].

Our studies revealed that severe lung lesions in ferrets infected with H1N1v correlated with higher expression of the proinflammatory cytokines IL-6, CXCL10, CCL5, CCL3, IL-8, TLR3, and the apoptotic markers (BAX and CASP8). This cytokine profiles correlated with the inflammatory phenotype observed in the lungs, characterised by high numbers of macrophages and neutrophils in apoptosis, accompanied by large numbers of CTLs and NK cells.

Similar to our findings, several studies have correlated phagocytic, NK and CD8 T lung infiltrates, and the upregulation of related immune molecules to the development of severe influenza infection, both in the early stages of influenza infection, and later in the viral clearance phase [94,153,162,261-263]. It is known that phagocytic inflammatory infiltrates can be detrimental for the resolution of viral pneumonia after IAV infection [79,84,153]. Moreover, it has recently been suggested that neutrophils coacting with monocytes are the main culprits in the development of alveolar lung damage, and lethality after H1N1v infection in a murine model [83]. The main mechanisms for damage by recently recruited macrophages and neutrophils are related to the release of TNFα. This induces the apoptosis of infected cells via TRAIL

[92,272,303], the release of lytic enzymes which cause further necrosis, and the induction of proinflammatory cytokines which exacerbate inflammatory cell migration [79,272]. The infiltration of NK and CTLs results in necrosis of infected epithelial cells which limits viral replication. However, the suppression of the early innate cell infiltration of NK and CD8 T cells has been shown to significantly increase mouse survival rates, without altering the kinetics of viral clearance. This suggests that the infiltration of these cells has a negative inflammatory role which is independent of viral kinetics [79,95,264,303].

In contrast, our studies revealed that animals developing milder lung lesions presented a higher expression of type I IFN genes, suggesting that IFN induction is beneficial for the host after H1N1v infection. Several studies have pointed out the protective role of type I IFN release after IAV, and other viral infections [59,71,265,266]. It is noteworthy than IAV viruses have adopted various strategies to evade the antiviral innate immune response, triggered by IFNs. In particular, the NS1 protein and the polymerase complex have evolved for the sake of reducing host cell gene expression of IFN by various means, such as blocking RIG-I signalling [75,334]. These observations point even more to the protective role of IFN induction, and the recognition of the virus by the host. The induction of IFN responses is triggered by the signalling of PRRs, like RIG-I and TLR3, which recognize different types of endocytosed viral RNA on target cells [63,267].

Interestingly, our studies have shown that IFN type I responses correlate with the expression of RIG-I, but not with the expression of TLR3. In fact, TLR3 expression was up-regulated in animals presenting severe disease, in contraposition with a lower induction of type I IFN genes. It is believed that TLR3 as a PRR would activate an antiviral state through the induction of type I IFN genes [267,269]. However, it was shown that TLR3 is not required for the initial cell-autonomous recognition of viral infection, and/or the induction of type I IFN release, but that is dependent on the recognition of RNA viruses, actively replicating by RIG-I [59,306,309] . Furthermore, aberrant TLR3 signalling has been shown to play a key role in mediating lung pathology, contributing to detrimental host inflammatory responses, through the induction of

proinflammatory molecules and the recruitment of CD8+, and phagocytic cells during IAV virus infection [65,78,153,267-269]. However, the mechanisms of TLR3 regulation and its contribution to lung pathology are not well understood and further studies focused in the signalling pathways of TLRs should be undertaken.

The innate immunity is like a two-edge sword with two distinct roles in the pathogenesis of IAV infection. As discussed above, the innate immune response is indispensable for the protection of the host against IAV infection. However, the unregulated response of several proinflammatory cytokines and chemokines can harm, rather than protect, respiratory organs. Why innate immune responses against H1N1v differ, and which events trigger the differentiations to detrimental or protective innate immune response, are unknown. It is known that cytokines are produced by leukocytes, the lung epithelium, and the lung endothelium through the signalling of PRRs, then the release of different cytokines regulate the inflammatory cell recruitment into the lungs, after infection [80,164,263,335]. Nonetheless, the relative contribution of lung cell mediated regulation of cytokines, and their dynamics in influenza pathogenesis have as yet, not been entirely elucidated [260,324].

For this reason, we studied the induction of different innate immune molecules at early stages of infection, in different lung anatomic compartments, aiming to discern the cytokine production of the main type cell present in each compartment (endothelial cells, epithelial bronchiolar cells and alveolar epithelial cells). However, the limitations of the technique did not allow us to completely individualize the target cells, so we studied the induction in the different compartments (vascular, alveolar and bronchiolar), as showed in (Figure 22).

Our results showed that bronchiolar areas expressed higher levels of IFNα and IL-6, at early stages of infection. These findings were expected, since the bronchiolar epithelium is one of the first targets after IAV infection [303]. Later, bronchiolar areas presented a higher expression of TNFα, BAX, and IFNγ, indicating that infected bronchial epithelial cells participate in the first influx of inflammatory cells, early on

postinfection. However, TLR3 production was mainly and unexpectedly observed on vascular and alveolar areas throughout the infection. This observation indicates that TLR3 recognize viral components in a different way to other PRRs, and certainly in a different manner to infected bronchiolar epithelial cells. Viral replication was not observed in vascular areas and only low viral antigen by IHC was detected in alveolar areas at early stages of infection, when TLR3 was highly upregulated. Interestingly, viral RNA was also detected in alveolar and vascular areas at the same time points, which may indicate that TLR3 is activated through the detection of viral RNA, or a crosstalk with infected, or phagocytic cells in the lungs. In this way, it would be interesting to analyze RIG-I expression in the different microdissected compartments, to further investigate these hypothesis.

Moreover, vascular and alveolar areas also accounted for the up-regulation of IL-6, amongst others. Vascular areas showed most of CCL2 expression, throughout the infection, and presented a higher expression of IFNγ at the time when large inflammatory infiltrates were observed in the lungs. CCL2 recruits macrophages to virus infected lungs, inducing alveolar epithelial cell apoptosis [59]. The detrimental role of increased CCL2 expression in IAV pathogenesis has been elucidated in a study in which CCR2 deficient mice infected with IAV inhibited macrophage migration to the lungs, increasing survival rates [88]. Interestingly, in the second study of this thesis, animals presenting severe lung lesions showed elevated expressions of IFNγ, whilst no differences in the expression CCL2 were observed between animals with severe and mild lesions. This uncouplement of results may be a consequence of the different time post infection, when samples were taken. Animals presenting severe lung lesions at 4 dpi (in study II) probably did not show differences in CCL2 expression in the total lung, because the first input of CCL2 occurs earlier during infection. Later, the inflammatory infiltrates perpetuate the induction of other innate immune molecules such as CXCL10, CCL3, or CCL5, amongst others. These induce the migration of further inflammatory cells. Nonetheless, the results obtained in study IV suggest that vascular cytokine expression accounts for the recruitment of phagocytic and cytotoxic cells into the

lungs, independently of active viral replication. However, more studies assessing the up-regulation of innate immune genes such as CCL5 and IL-8 are needed, in order to clarify this hypothesis.

In summary, our results identified host immune responses as key participants in the development of severe and mild lung lesions, after H1N1v infection. The detrimental host immune profile was characterised by the upregulation of several cytokines and chemokines, inducing the recruitment of phagocytic and cytotoxic cells into the lungs, and related with a higher induction of TLR3. In contrast, type I IFN response and the induction of RIG-I was shown to be protective against viral pneumonia. Finally, bronchial areas were identified as major sources of cytokines, whilst our results identified vascular activation as contributing to the inflammatory response, through the recruitment of inflammatory cells into the lungs, independently of active viral replication, at early stages of infection.

We believe that this thesis provides new data to clarify the role of the host innate immune response and its interactions with viral characteristics in the divergent pathogenesis observed in H1N1v infection. Moreover, it contributes to the standardization of several techniques in the ferret model, which may help in the diagnosis of, and research into, different infectious and non-infectious diseases in ferrets, and viral studies using the ferret model, like SARS, cystic fibrosis and Influenza virus infection. Additionally, understanding host immune response in viral infections is important for the future development of therapeutic strategies, designed to the control of the host immune response. In this way, the modulation of the host immune response will have the potential advantage of exerting less selective pressure on viral populations, an important factor in the development of IAV infection therapies.

CHAPTER 8: CONCLUSIONS

1. Ferrets and humans share a similar distribution of immune system cells throughout lymphoid, and non-lymphoid organs, corroboring the suitability of the ferret model for the study of different infectious, and non-infectious human diseases, related with immunological processes.

2. Experimental infection of ferrets with Wt H1N1v virus with similar genetic characteristics, results in the development of severe or mild disease, independently of the viral strain. Severe lung lesions correlate with the infection of alveolar epithelial cells and an exacerbated pro-inflammatory host immune response in the lung.

3. In absence of compensatory mutations in the NA protein of OR virus, Wt H1N1v is more virulent than OR H1N1v virus in the ferret model. Higher virulence of the Wt virus is related with higher viral titres in alveolar areas, and early proinflammatory immune response.

4. Innate immune responses with higher expression of RIG-I and IFNα are beneficial for the host and correlate with H1N1v replication, limited to bronchial and bronchiolar areas. In contrast, innate immune responses with higher expression of IL-6, CXCL10, IL-8, TLR3, CCL3, and CCL5, correlated with higher viral titres in alveolar areas, and the development of severe lung lesions, in the ferret model.

5. The bronchiolar compartment is the major source of antiviral (IFNα) and proinflammatory cytokines (IL-6, TNFα) at early stages of H1N1v infection in the ferret model, in accordance with extensive viral replication in the bronchiolar epithelium. The vascular compartment also contributes to the induction of the innate immune response through the upregulation of TLR3, CCL2, and to a lesser extent, IL-6 and IFNγ, independently of active viral replication in this area.

REFERENCES

1. Cunha, B.A. Influenza: historical aspects of epidemics and pandemics. *Infect Dis Clin North Am* **18**, 141-155 (2004).

2. Beveridge, W.I. The chronicle of influenza epidemics. *Hist Philos Life Sci* **13**, 223-234 (1991).

3. Crosby, A. Influenza. in *The Cambridge world history of human disease* (ed. KF, K.) 807–811. (Cambridge University Press, New York, 1993).

4. Potter, C.W. Chronicle of influenza pandemics. in *Textbook of Influenza* (ed. K.G. Nicholson, R.F.W.a.A.J.H.) 3-18 (Blackwell Science Ltd., Oxford, 1998).

5. Molineux, T. Dr. Molineux's historical account of the late general coughs and colds; with some observation on other epidemic distemper. *Philosophic Transactions of the Royal Society of London* **18**, 105-109 (1694).

6. Hirsch, A. *Handbook of Geographical and Historical Pathology*, (London, 1883).

7. Creighton, C. *A History of Epidemics in Britain.* , (Cambridge University Press, London, 1894).

8. Smith, W., Andrewes, C. & Laidlaw, P. A virus obtained from influenza patients. *Lancet* **ii**, 66-68 (1933).

9. Cox, N.J. & Subbarao, K. Global epidemiology of influenza: past and present. *Annu Rev Med* **51**, 407-421 (2000).

10. Wright, P. & Webster, R. *Orthomyxoviruses*, (Lippincott Williams and Wilkins, Philadelphia, 2001).

11. Palese, P. & Shaw, M. *Orthomyxoviridae: the viruses and their replication.*, (Lippincott, Williams &Wilkins, Philadelphia, 2007).

12. Wright, P., Neumann, G. & Kawaoka, Y. *Orthomyxoviridae: the viruses and their replication.*, (Lippincott, Williams &Wilkins, Philadelphia, 2007).

13. Webster, R.G., Bean, W.J., Gorman, O.T., Chambers, T.M. & Kawaoka, Y. Evolution and ecology of influenza A viruses. *Microbiol Rev* **56**, 152-179 (1992).

14. Simonsen, L. The global impact of influenza on morbidity and mortality. *Vaccine* **17 Suppl 1**, S3-10 (1999).

15. Mehle, A. Unusual influenza A viruses in bats. *Viruses* **6**, 3438-3449 (2014).

16. Krauss, S*., et al.* Influenza A viruses of migrating wild aquatic birds in North America. *Vector Borne Zoonotic Dis* **4**, 177-189 (2004).

17. Munster, V.J*., et al.* Spatial, temporal, and species variation in prevalence of influenza A viruses in wild migratory birds. *PLoS Pathog* **3**, e61 (2007).

18. Taubenberger, J.K. & Kash, J.C. Influenza virus evolution, host adaptation, and pandemic formation. *Cell Host Microbe* **7**, 440-451 (2010).

19. Ghedin, E.*, et al.* Unseasonal transmission of H3N2 influenza A virus during the swine-origin H1N1 pandemic. *J Virol* **84**, 5715-5718 (2010).

20. Costa, T.*, et al.* Distribution patterns of influenza virus receptors and viral attachment patterns in the respiratory and intestinal tracts of seven avian species. *Vet Res* **43**, 28 (2012).

21. Christman, M.C., Kedwaii, A., Xu, J., Donis, R.O. & Lu, G. Pandemic (H1N1) 2009 virus revisited: an evolutionary retrospective. *Infect Genet Evol* **11**, 803-811 (2011).

22. Cros, J.F. & Palese, P. Trafficking of viral genomic RNA into and out of the nucleus: influenza, Thogoto and Borna disease viruses. *Virus Res* **95**, 3-12 (2003).

23. Neumann, G., Noda, T. & Kawaoka, Y. Emergence and pandemic potential of swine-origin H1N1 influenza virus. *Nature* **459**, 931-939 (2009).

24. Bouvier, N.M. & Palese, P. The biology of influenza viruses. *Vaccine* **26 Suppl 4**, D49-53 (2008).

25. Perez, J.T.*, et al.* Influenza A virus-generated small RNAs regulate the switch from transcription to replication. *Proc Natl Acad Sci U S A* **107**, 11525-11530 (2010).

26. Barman, S., Ali, A., Hui, E.K., Adhikary, L. & Nayak, D.P. Transport of viral proteins to the apical membranes and interaction of matrix protein with glycoproteins in the assembly of influenza viruses. *Virus Res* **77**, 61-69 (2001).

27. O'Neill, R.E., Talon, J. & Palese, P. The influenza virus NEP (NS2 protein) mediates the nuclear export of viral ribonucleoproteins. *EMBO J* **17**, 288-296 (1998).

28. Matrosovich, M.N., Matrosovich, T.Y., Gray, T., Roberts, N.A. & Klenk, H.D. Neuraminidase is important for the initiation of influenza virus infection in human airway epithelium. *J Virol* **78**, 12665-12667 (2004).

29. Taubenberger, J.K. & Morens, D.M. Influenza: the once and future pandemic. *Public Health Rep* **125 Suppl 3**, 16-26 (2010).

30. Chen, R. & Holmes, E.C. Avian influenza virus exhibits rapid evolutionary dynamics. *Mol Biol Evol* **23**, 2336-2341 (2006).

31. Murphy, B.R. & Clements, M.L. The systemic and mucosal immune response of humans to influenza A virus. *Curr Top Microbiol Immunol* **146**, 107-116 (1989).

32. Dugan, V.G.*, et al.* The evolutionary genetics and emergence of avian influenza viruses in wild birds. *PLoS Pathog* **4**, e1000076 (2008).

33. Holmes, E.C., Taubenberger, J.K. & Grenfell, B.T. Heading off an influenza pandemic. *Science* **309**, 989 (2005).

34. Landolt, G.A. & Olsen, C.W. Up to new tricks - a review of cross-species transmission of influenza A viruses. *Anim Health Res Rev* **8**, 1-21 (2007).

35. Flint, J., Enquist, L., Krug, R., Racaniello, V. & Skalka, A. Appendix, structure, genomic organization, and infectious cycles of selected animal viruses discussed in this book. in *Virology, molecular biology, pathogenesis and control* 759-761 (American Society for Microbiology Press, Washington, DC, 2000).

36. Taubenberger, J.K. & Morens, D.M. Pandemic influenza--including a risk assessment of H5N1. *Rev Sci Tech* **28**, 187-202 (2009).

37. Suarez, D. Influenza A virus. in *Avian Influenza* (ed. DE, S.) 3-22 (Blackwell Publishing, Iowa, 2008).

38. Shors, T. H5N1 virus (bird flu) controversy. (ed. AccessScience, I.) (McGraw-Hill Education, Chicago, 2013).

39. Hilleman, M.R. Realities and enigmas of human viral influenza: pathogenesis, epidemiology and control. *Vaccine* **20**, 3068-3087 (2002).

40. Jones, J.C.*, et al.* Possible role of songbirds and parakeets in transmission of influenza A(H7N9) virus to humans. *Emerg Infect Dis* **20**, 380-385 (2014).

41. Gibbs, A.J., Armstrong, J.S. & Downie, J.C. From where did the 2009 'swine-origin' influenza A virus (H1N1) emerge? *Virol J* **6**, 207 (2009).

42. Fasina, F.O., Ifende, V.I. & Ajibade, A.A. Avian influenza A(H5N1) in humans: lessons from Egypt. *Euro Surveill* **15**, 19473 (2010).

43. Wang, Q.*, et al.* Serological and Virological Surveillance of Avian Influenza A Virus H9N2 Subtype in Humans and Poultry in Shanghai, China, Between 2008 and 2010. *Zoonoses Public Health* (2014).

44. Liu, J.*, et al.* H7N9: a low pathogenic avian influenza A virus infecting humans. *Curr Opin Virol* **5**, 91-97 (2014).

45. de Wit, E. & Fouchier, R.A. Emerging influenza. *J Clin Virol* **41**, 1-6 (2008).

46. Garten, W. & Klenk, H.D. Understanding influenza virus pathogenicity. *Trends Microbiol* **7**, 99-100 (1999).

47. Horimoto, T. & Kawaoka, Y. Pandemic threat posed by avian influenza A viruses. *Clin Microbiol Rev* **14**, 129-149 (2001).

48. Steinhauer, D.A. Role of hemagglutinin cleavage for the pathogenicity of influenza virus. *Virology* **258**, 1-20 (1999).

49. Kawaoka, Y. & Webster, R.G. Sequence requirements for cleavage activation of influenza virus hemagglutinin expressed in mammalian cells. *Proc Natl Acad Sci U S A* **85**, 324-328 (1988).

50. Tscherne, D.M. & Garcia-Sastre, A. Virulence determinants of pandemic influenza viruses. *J Clin Invest* **121**, 6-13.

51. Josset, L., Tisoncik-Go, J. & Katze, M.G. Moving H5N1 studies into the era of systems biology. *Virus Res* **178**, 151-167 (2013).

52. de Wit, E.*, et al.* Molecular determinants of adaptation of highly pathogenic avian influenza H7N7 viruses to efficient replication in the human host. *J Virol* **84**, 1597-1606 (2010).

53. Tumpey, T.M.*, et al.* A two-amino acid change in the hemagglutinin of the 1918 influenza virus abolishes transmission. *Science* **315**, 655-659 (2007).

54. Liu, Y.*, et al.* Altered receptor specificity and cell tropism of D222G hemagglutinin mutants isolated from fatal cases of pandemic A(H1N1) 2009 influenza virus. *J Virol* **84**, 12069-12074 (2010).

55. Salomon, R. & Webster, R.G. The influenza virus enigma. *Cell* **136**, 402-410 (2009).

56. Gabriel, G.*, et al.* Differential polymerase activity in avian and mammalian cells determines host range of influenza virus. *J Virol* **81**, 9601-9604 (2007).

57. Gabriel, G., Herwig, A. & Klenk, H.D. Interaction of polymerase subunit PB2 and NP with importin alpha1 is a determinant of host range of influenza A virus. *PLoS Pathog* **4**, e11 (2008).

58. Mehle, A. & Doudna, J.A. Adaptive strategies of the influenza virus polymerase for replication in humans. *Proc Natl Acad Sci U S A* **106**, 21312-21316 (2009).

59. Fukuyama, S. & Kawaoka, Y. The pathogenesis of influenza virus infections: the contributions of virus and host factors. *Curr Opin Immunol* **23**, 481-486 (2011).

60. Garcia-Sastre, A. Inhibition of interferon-mediated antiviral responses by influenza A viruses and other negative-strand RNA viruses. *Virology* **279**, 375-384 (2001).

61. Crisci, E., Mussa, T., Fraile, L. & Montoya, M. Review: influenza virus in pigs. *Mol Immunol* **55**, 200-211 (2013).

62. Pang, I.K. & Iwasaki, A. Inflammasomes as mediators of immunity against influenza virus. *Trends Immunol* **32**, 34-41 (2011).

63. Opitz, B., van Laak, V., Eitel, J. & Suttorp, N. Innate immune recognition in infectious and noninfectious diseases of the lung. *Am J Respir Crit Care Med* **181**, 1294-1309 (2010).

64. Lund, J.M.*, et al.* Recognition of single-stranded RNA viruses by Toll-like receptor 7. *Proc Natl Acad Sci U S A* **101**, 5598-5603 (2004).

65. Guillot, L.*, et al.* Involvement of toll-like receptor 3 in the immune response of lung epithelial cells to double-stranded RNA and influenza A virus. *J Biol Chem* **280**, 5571-5580 (2005).

66. Takeuchi, O. & Akira, S. Innate immunity to virus infection. *Immunol Rev* **227**, 75-86 (2009).

67. Imai, Y.*, et al.* Identification of oxidative stress and Toll-like receptor 4 signaling as a key pathway of acute lung injury. *Cell* **133**, 235-249 (2008).

68. Van Hoeven, N.*, et al.* Pathogenesis of 1918 pandemic and H5N1 influenza virus infections in a guinea pig model: antiviral potential of exogenous alpha interferon to reduce virus shedding. *J Virol* **83**, 2851-2861 (2009).

69. Strieter, R.M., Belperio, J.A. & Keane, M.P. Cytokines in innate host defense in the lung. *J Clin Invest* **109**, 699-705 (2002).

70. Zimmerman, G.A.*, et al.* Endothelial activation in ARDS. *Chest* **116**, 18S-24S (1999).

71. Svitek, N., Rudd, P.A., Obojes, K., Pillet, S. & von Messling, V. Severe seasonal influenza in ferrets correlates with reduced interferon and increased IL-6 induction. *Virology* **376**, 53-59 (2008).

72. Garcia-Sastre, A.*, et al.* The role of interferon in influenza virus tissue tropism. *J Virol* **72**, 8550-8558 (1998).

73. Perrone, L.A., Plowden, J.K., Garcia-Sastre, A., Katz, J.M. & Tumpey, T.M. H5N1 and 1918 pandemic influenza virus infection results in early and excessive infiltration of macrophages and neutrophils in the lungs of mice. *PLoS pathogens* **4**, e1000115 (2008).

74. Itoh, Y.*, et al.* In vitro and in vivo characterization of new swine-origin H1N1 influenza viruses. *Nature* **460**, 1021-1025 (2009).

75. van de Sandt, C.E., Kreijtz, J.H. & Rimmelzwaan, G.F. Evasion of influenza A viruses from innate and adaptive immune responses. *Viruses* **4**, 1438-1476 (2012).

76. Worthen, G.S., Schwab, B., 3rd, Elson, E.L. & Downey, G.P. Mechanics of stimulated neutrophils: cell stiffening induces retention in capillaries. *Science* **245**, 183-186 (1989).

77. Doerschuk, C.M., Mizgerd, J.P., Kubo, H., Qin, L. & Kumasaka, T. Adhesion molecules and cellular biomechanical changes in acute lung injury: Giles F. Filley Lecture. *Chest* **116**, 37S-43S (1999).

78. Bradley, L.M., Douglass, M.F., Chatterjee, D., Akira, S. & Baaten, B.J. Matrix metalloprotease 9 mediates neutrophil migration into the airways in response to influenza virus-induced toll-like receptor signaling. *PLoS pathogens* **8**, e1002641 (2012).

79. van den Brand, J.M., Haagmans, B.L., van Riel, D., Osterhaus, A.D. & Kuiken, T. The pathology and pathogenesis of experimental severe acute respiratory syndrome and influenza in animal models. *J Comp Pathol* **151**, 83-112 (2014).

80. To, K.K.*, et al.* Delayed clearance of viral load and marked cytokine activation in severe cases of pandemic H1N1 2009 influenza virus infection. *Clin Infect Dis* **50**, 850-859 (2010).

81. Bermejo-Martin, J.F.*, et al.* Host adaptive immunity deficiency in severe pandemic influenza. *Crit Care* **14**, R167 (2010).

82. Lee, N.*, et al.* Cytokine response patterns in severe pandemic 2009 H1N1 and seasonal influenza among hospitalized adults. *PLoS One* **6**, e26050 (2011).

83. Brandes, M., Klauschen, F., Kuchen, S. & Germain, R.N. A systems analysis identifies a feedforward inflammatory circuit leading to lethal influenza infection. *Cell* **154**, 197-212 (2013).

84. van den Brand, J.M.*, et al.* Comparison of temporal and spatial dynamics of seasonal H3N2, pandemic H1N1 and highly pathogenic avian influenza H5N1 virus infections in ferrets. *PLoS One* **7**, e42343 (2012).

85. McGill, J., Heusel, J.W. & Legge, K.L. Innate immune control and regulation of influenza virus infections. *J Leukoc Biol* **86**, 803-812 (2009).

86. Snelgrove, R.J.*, et al.* A critical function for CD200 in lung immune homeostasis and the severity of influenza infection. *Nat Immunol* **9**, 1074-1083 (2008).

87. Lin, K.L., Suzuki, Y., Nakano, H., Ramsburg, E. & Gunn, M.D. CCR2+ monocyte-derived dendritic cells and exudate macrophages produce influenza-induced pulmonary immune pathology and mortality. *J Immunol* **180**, 2562-2572 (2008).

88. Dawson, T.C., Beck, M.A., Kuziel, W.A., Henderson, F. & Maeda, N. Contrasting effects of CCR5 and CCR2 deficiency in the pulmonary inflammatory response to influenza A virus. *Am J Pathol* **156**, 1951-1959 (2000).

89. Herold, S.*, et al.* Alveolar epithelial cells direct monocyte transepithelial migration upon influenza virus infection: impact of chemokines and adhesion molecules. *J Immunol* **177**, 1817-1824 (2006).

90. Kim, H.M.*, et al.* Alveolar macrophages are indispensable for controlling influenza viruses in lungs of pigs. *J Virol* **82**, 4265-4274 (2008).

91. van Riel, D.*, et al.* Highly pathogenic avian influenza virus H5N1 infects alveolar macrophages without virus production or excessive TNF-alpha induction. *PLoS Pathog* **7**, e1002099 (2011).

92. Herold, S.*, et al.* Lung epithelial apoptosis in influenza virus pneumonia: the role of macrophage-expressed TNF-related apoptosis-inducing ligand. *J Exp Med* **205**, 3065-3077 (2008).

93. Jost, S.*, et al.* Changes in cytokine levels and NK cell activation associated with influenza. *PLoS One* **6**, e25060 (2011).

94. Lee, K.Y., Rhim, J.W. & Kang, J.H. Hyperactive immune cells (T cells) may be responsible for acute lung injury in influenza virus infections: a need for early immune-modulators for severe cases. *Med Hypotheses* **76**, 64-69 (2011).

95. Abdul-Careem, M.F.*, et al.* Critical role of natural killer cells in lung immunopathology during influenza infection in mice. *J Infect Dis* **206**, 167-177 (2012).

96. Oxford, J.S. Influenza A pandemics of the 20th century with special reference to 1918: virology, pathology and epidemiology. *Rev Med Virol* **10**, 119-133 (2000).

97. Pyle, G. *The Diffusion of Influenza : Patterns and paradigms*, (Rowan &Littlefeld, New Jersey, 1986).

98. Finkler, D. Influenza in twentieth century practice. in *An International Encyclopaedia of Modern Medical Science* (ed. Shipman, T.L.) 21-32 (Sampson Law & Marston London, 1899).

99. Patterson, K.D. *Pandemic Influenza 1700-1900; A Study in Historical Epidemiology*, (Rowman & Littlefeld, New Jersey, 1987).

100. Pyle, G.F. & Patterson, K.D. *Influenza diffusion in European history: patterns and paradigms. Ecology of Disease* (1984).

101. Rabadan, R., Levine, A.J. & Robins, H. Comparison of avian and human influenza A viruses reveals a mutational bias on the viral genomes. *J Virol* **80**, 11887-11891 (2006).

102. Taubenberger, J.K. The virulence of the 1918 pandemic influenza virus: unraveling the enigma. *Arch Virol Suppl*, 101-115 (2005).

103. Johnson, N.P. & Mueller, J. Updating the accounts: global mortality of the 1918-1920 "Spanish" influenza pandemic. *Bull Hist Med* **76**, 105-115 (2002).

104. Morens, D.M., Taubenberger, J.K. & Fauci, A.S. Predominant role of bacterial pneumonia as a cause of death in pandemic influenza: implications for pandemic influenza preparedness. *J Infect Dis* **198**, 962-970 (2008).

105. Morens, D.M., Taubenberger, J.K. & Fauci, A.S. The persistent legacy of the 1918 influenza virus. *N Engl J Med* **361**, 225-229 (2009).

106. Kilbourne, E. *The Influenza Viruses and Influenza*, (Academic Press, London, 1975).

107. Scholtissek, C., Rohde, W., Von Hoyningen, V. & Rott, R. On the origin of the human influenza virus subtypes H2N2 and H3N2. *Virology* **87**, 13-20 (1978).

108. Kawaoka, Y., Krauss, S. & Webster, R.G. Avian-to-human transmission of the PB1 gene of influenza A viruses in the 1957 and 1968 pandemics. *J Virol* **63**, 4603-4608 (1989).

109. Kilbourne, E.D. Influenza pandemics of the 20th century. *Emerg Infect Dis* **12**, 9-14 (2006).

110. Smith, G.J.*, et al.* Origins and evolutionary genomics of the 2009 swine-origin H1N1 influenza A epidemic. *Nature* **459**, 1122-1125 (2009).

111. Peiris, J.S., Poon, L.L. & Guan, Y. Emergence of a novel swine-origin influenza A virus (S-OIV) H1N1 virus in humans. *J Clin Virol* **45**, 169-173 (2009).

112. WHO. Statement to the press by WHO Director-General Dr. Margaret Chan. (2009).

113. Dawood, F.S.*, et al.* Emergence of a novel swine-origin influenza A (H1N1) virus in humans. *N Engl J Med* **360**, 2605-2615 (2009).

114. WHO. Statement to the press by WHO Director-General Dr. Margaret Vol. 2010 (2010).

115. Garten, R.J.*, et al.* Antigenic and genetic characteristics of swine-origin 2009 A(H1N1) influenza viruses circulating in humans. *Science* **325**, 197-201 (2009).

116. Dunham, E.J.*, et al.* Different evolutionary trajectories of European avian-like and classical swine H1N1 influenza A viruses. *J Virol* **83**, 5485-5494 (2009).

117. Tumpey, T.M.*, et al.* Pathogenicity and immunogenicity of influenza viruses with genes from the 1918 pandemic virus. *Proc Natl Acad Sci U S A* **101**, 3166-3171 (2004).

118. Chang, L.Y., Shih, S.R., Shao, P.L., Huang, D.T. & Huang, L.M. Novel swine-origin influenza virus A (H1N1): the first pandemic of the 21st century. *J Formos Med Assoc* **108**, 526-532 (2009).

119. Shinde, V.*, et al.* Triple-reassortant swine influenza A (H1) in humans in the United States, 2005-2009. *N Engl J Med* **360**, 2616-2625 (2009).

120. CDC. Updated Interim Recommendations for the Use of Antiviral Medications in the Treatment and Prevention of Influenza for the 2009-2010 Season. (ed. CDC) (2009).

121. Moscona, A. Neuraminidase inhibitors for influenza. *N Engl J Med* **353**, 1363-1373 (2005).

122. Meijer, A.*, et al.* Oseltamivir-resistant influenza virus A (H1N1), Europe, 2007-08 season. *Emerg Infect Dis* **15**, 552-560 (2009).

123. WHO. Summary of influenza antiviral susceptibility surveillance findings, September 2010 - March 2011. (2011).

124. Baz, M., Abed, Y., Nehme, B. & Boivin, G. Activity of the oral neuraminidase inhibitor A-322278 against the oseltamivir-resistant H274Y (A/H1N1) influenza virus mutant in mice. *Antimicrob Agents Chemother* **53**, 791-793 (2009).

125. Le, Q.M.*, et al.* A community cluster of oseltamivir-resistant cases of 2009 H1N1 influenza. *N Engl J Med* **362**, 86-87 (2010).

126. Govorkova, E.A. Consequences of resistance: in vitro fitness, in vivo infectivity, and transmissibility of oseltamivir-resistant influenza A viruses. *Influenza Other Respir Viruses* **7 Suppl 1**, 50-57 (2012).

127. Hurt, A.C*., et al.* Antiviral resistance during the 2009 influenza A H1N1 pandemic: public health, laboratory, and clinical perspectives. *Lancet Infect Dis* **12**, 240-248 (2012).

128. Hurt, A.C*., et al.* Assessing the viral fitness of oseltamivir-resistant influenza viruses in ferrets, using a competitive-mixtures model. *J Virol* **84**, 9427-9438 (2010).

129. Ison, M.G., Mishin, V.P., Braciale, T.J., Hayden, F.G. & Gubareva, L.V. Comparative activities of oseltamivir and A-322278 in immunocompetent and immunocompromised murine models of influenza virus infection. *J Infect Dis* **193**, 765-772 (2006).

130. Hamelin, M.E*., et al.* Oseltamivir-resistant pandemic A/H1N1 virus is as virulent as its wild-type counterpart in mice and ferrets. *PLoS pathogens* **6**, e1001015 (2010).

131. Duan, S*., et al.* Oseltamivir-resistant pandemic H1N1/2009 influenza virus possesses lower transmissibility and fitness in ferrets. *PLoS pathogens* **6**, e1001022 (2010).

132. Kiso, M*., et al.* Characterization of oseltamivir-resistant 2009 H1N1 pandemic influenza A viruses. *PLoS pathogens* **6**, e1001079 (2010).

133. Girard, M.P., Tam, J.S., Assossou, O.M. & Kieny, M.P. The 2009 A (H1N1) influenza virus pandemic: A review. *Vaccine* **28**, 4895-4902 (2010).

134. Apolloni, A., Poletto, C. & Colizza, V. Age-specific contacts and travel patterns in the spatial spread of 2009 H1N1 influenza pandemic. *BMC Infect Dis* **13**, 176 (2013).

135. WHO. Weekly update, Global anert and Response WHO. Vol. 2010 (2010).

136. WHO. Acute Respiratory Infections (Update September 2009). (2009).

137. Harms, P.W*., et al.* Autopsy findings in eight patients with fatal H1N1 influenza. *Am J Clin Pathol* **134**, 27-35 (2010).

138. Punpanich, W. & Chotpitayasunondh, T. A review on the clinical spectrum and natural history of human influenza. *Int J Infect Dis* **16**, e714-723 (2012).

139. Jain, S*., et al.* Hospitalized patients with 2009 H1N1 influenza in the United States, April-June 2009. *N Engl J Med* **361**, 1935-1944 (2009).

140. Plessa, E*., et al.* Clinical features, risk factors, and complications among pediatric patients with pandemic influenza A (H1N1). *Clin Pediatr (Phila)* **49**, 777-781 (2010).

141. Pebody, R.G*., et al.* Pandemic Influenza A (H1N1) 2009 and mortality in the United Kingdom: risk factors for death, April 2009 to March 2010. *Euro Surveill* **15**(2010).

142. Ison, M.G. Influenza in hospitalized adults: gaining insight into a significant problem. *J Infect Dis* **200**, 485-488 (2009).

143. Ikonen, N.*, et al.* High frequency of cross-reacting antibodies against 2009 pandemic influenza A(H1N1) virus among the elderly in Finland. *Euro Surveill* **15**(2010).

144. Hancock, K.*, et al.* Cross-reactive antibody responses to the 2009 pandemic H1N1 influenza virus. *N Engl J Med* **361**, 1945-1952 (2009).

145. De Groot, A.S., Ardito, M., McClaine, E.M., Moise, L. & Martin, W.D. Immunoinformatic comparison of T-cell epitopes contained in novel swine-origin influenza A (H1N1) virus with epitopes in 2008-2009 conventional influenza vaccine. *Vaccine* **27**, 5740-5747 (2009).

146. Maines, T.R.*, et al.* Transmission and pathogenesis of swine-origin 2009 A(H1N1) influenza viruses in ferrets and mice. *Science* **325**, 484-487 (2009).

147. Yamagishi, T.*, et al.* Onset and duration of symptoms and timing of disease transmission of 2009 influenza A (H1N1) in an outbreak in Fukuoka, Japan, June 2009. *Jpn J Infect Dis* **63**, 327-331 (2010).

148. Siau, C.*, et al.* Influenza A H1N1 (2009): clinical spectrum of disease among adult patients admitted to a regional hospital in Singapore. *Singapore Med J* **52**, 475-480 (2011).

149. Ong, A.K.*, et al.* Improving the clinical diagnosis of influenza--a comparative analysis of new influenza A (H1N1) cases. *PLoS One* **4**, e8453 (2009).

150. Lee, C.S. & Lee, J.H. Dynamics of clinical symptoms in patients with pandemic influenza A (H1N1). *Clin Microbiol Infect* **16**, 389-390 (2010).

151. Kumar, A.*, et al.* Critically ill patients with 2009 influenza A(H1N1) infection in Canada. *JAMA* **302**, 1872-1879 (2009).

152. Soto-Abraham, M.V.*, et al.* Pathological changes associated with the 2009 H1N1 virus. *N Engl J Med* **361**, 2001-2003 (2009).

153. Mauad, T.*, et al.* Lung pathology in fatal novel human influenza A (H1N1) infection. *Am J Respir Crit Care Med* **181**, 72-79 (2010).

154. Gill, J.R.*, et al.* Pulmonary pathologic findings of fatal 2009 pandemic influenza A/H1N1 viral infections. *Arch Pathol Lab Med* **134**, 235-243 (2010).

155. Shieh, W.J.*, et al.* 2009 pandemic influenza A (H1N1): pathology and pathogenesis of 100 fatal cases in the United States. *Am J Pathol* **177**, 166-175 (2010).

156. Taubenberger, J.K. & Morens, D.M. The pathology of influenza virus infections. *Annu Rev Pathol* **3**, 499-522 (2008).

157. Keynan, Y., Malik, S. & Fowke, K.R. The role of polymorphisms in host immune genes in determining the severity of respiratory illness caused by pandemic H1N1 influenza. *Public Health Genomics* **16**, 9-16 (2013).

158. Horby, P., Nguyen, N.Y., Dunstan, S.J. & Baillie, J.K. The role of host genetics in susceptibility to influenza: a systematic review. *PLoS One* **7**, e33180 (2012).

159. Kuiken, T. & Taubenberger, J.K. Pathology of human influenza revisited. *Vaccine* **26 Suppl 4**, D59-66 (2008).

160. Xu, L.*, et al.* Genomic polymorphism of the pandemic A (H1N1) influenza viruses correlates with viral replication, virulence, and pathogenicity in vitro and in vivo. *PLoS One* **6**, e20698 (2011).

161. Meunier, I.*, et al.* Virulence differences of closely related pandemic 2009 H1N1 isolates correlate with increased inflammatory responses in ferrets. *Virology* **422**, 125-131 (2012).

162. La Gruta, N.L., Kedzierska, K., Stambas, J. & Doherty, P.C. A question of self-preservation: immunopathology in influenza virus infection. *Immunol Cell Biol* **85**, 85-92 (2007).

163. Bautista, E.*, et al.* Clinical aspects of pandemic 2009 influenza A (H1N1) virus infection. *N Engl J Med* **362**, 1708-1719 (2010).

164. Bermejo-Martin, J.F.*, et al.* Th1 and Th17 hypercytokinemia as early host response signature in severe pandemic influenza. *Crit Care* **13**, R201 (2009).

165. To, K.K.*, et al.* Concurrent comparison of epidemiology, clinical presentation and outcome between adult patients suffering from the pandemic influenza A (H1N1) 2009 virus and the seasonal influenza A virus infection. *Postgrad Med J* **86**, 515-521 (2010).

166. Marcelin, G.*, et al.* Fatal outcome of pandemic H1N1 2009 influenza virus infection is associated with immunopathology and impaired lung repair, not enhanced viral burden, in pregnant mice. *J Virol* **85**, 11208-11219 (2011).

167. Maines, T.R.*, et al.* Local innate immune responses and influenza virus transmission and virulence in ferrets. *J Infect Dis* **205**, 474-485 (2012).

168. Rowe, T.*, et al.* Modeling host responses in ferrets during A/California/07/2009 influenza infection. *Virology* **401**, 257-265 (2010).

169. Fezeu, L.*, et al.* Obesity is associated with higher risk of intensive care unit admission and death in influenza A (H1N1) patients: a systematic review and meta-analysis. *Obes Rev* **12**, 653-659 (2011).

170. Horby, P., Nguyen, N.Y., Dunstan, S.J. & Baillie, J.K. An updated systematic review of the role of host genetics in susceptibility to influenza. *Influenza Other Respir Viruses* **7 Suppl 2**, 37-41 (2013).

171. Keynan, Y.*, et al.* Chemokine receptor 5 big up tri, open32 allele in patients with severe pandemic (H1N1) 2009. *Emerg Infect Dis* **16**, 1621-1622 (2010).

172. Esposito, S.*, et al.* Toll-like receptor 3 gene polymorphisms and severity of pandemic A/H1N1/2009 influenza in otherwise healthy children. *Virol J* **9**, 270 (2012).

173. Antonopoulou, A.*, et al.* Role of tumor necrosis factor gene single nucleotide polymorphisms in the natural course of 2009 influenza A H1N1 virus infection. *Int J Infect Dis* **16**, e204-208 (2012).

174. Everitt, A.R.*, et al.* IFITM3 restricts the morbidity and mortality associated with influenza. *Nature* **484**, 519-523 (2012).

175. Gordon, C.L.*, et al.* Association between severe pandemic 2009 influenza A (H1N1) virus infection and immunoglobulin G(2) subclass deficiency. *Clin Infect Dis* **50**, 672-678 (2010).

176. Zuniga, J.*, et al.* Genetic variants associated with severe pneumonia in A/H1N1 influenza infection. *Eur Respir J* **39**, 604-610 (2012).

177. Lim, J.K.*, et al.* Genetic deficiency of chemokine receptor CCR5 is a strong risk factor for symptomatic West Nile virus infection: a meta-analysis of 4 cohorts in the US epidemic. *J Infect Dis* **197**, 262-265 (2008).

178. Kindberg, E.*, et al.* A deletion in the chemokine receptor 5 (CCR5) gene is associated with tickborne encephalitis. *J Infect Dis* **197**, 266-269 (2008).

179. Shapira, S.D.*, et al.* A physical and regulatory map of host-influenza interactions reveals pathways in H1N1 infection. *Cell* **139**, 1255-1267 (2009).

180. Hidaka, F.*, et al.* A missense mutation of the Toll-like receptor 3 gene in a patient with influenza-associated encephalopathy. *Clin Immunol* **119**, 188-194 (2006).

181. Berri, F., Le, V.B., Jandrot-Perrus, M., Lina, B. & Riteau, B. Switch from protective to adverse inflammation during influenza: viral determinants and hemostasis are caught as culprits. *Cell Mol Life Sci* **71**, 885-898 (2014).

182. Yao, D.*, et al.* Thermal instability of compound variants of carnitine palmitoyltransferase II and impaired mitochondrial fuel utilization in influenza-associated encephalopathy. *Hum Mutat* **29**, 718-727 (2008).

183. Zhou, J.*, et al.* A functional variation in CD55 increases the severity of 2009 pandemic H1N1 influenza A virus infection. *J Infect Dis* **206**, 495-503 (2012).

184. Lin, T.Y. & Brass, A.L. Host genetic determinants of influenza pathogenicity. *Curr Opin Virol* **3**, 531-536 (2013).

185. Vivier, E., Tomasello, E., Baratin, M., Walzer, T. & Ugolini, S. Functions of natural killer cells. *Nat Immunol* **9**, 503-510 (2008).

186. La, D*., et al.* Enrichment of variations in KIR3DL1/S1 and KIR2DL2/L3 among H1N1/09 ICU patients: an exploratory study. *PLoS One* **6**, e29200 (2011).

187. Konig, R*., et al.* Human host factors required for influenza virus replication. *Nature* **463**, 813-817 (2010).

188. WHO. Public Health Research Agenda for Influenza. (ed. Organisation, W.H.) (Geneva, 2009).

189. Barnard, D.L. Animal models for the study of influenza pathogenesis and therapy. *Antiviral Res* **82**, A110-122 (2009).

190. Belser, J.A., Katz, J.M. & Tumpey, T.M. The ferret as a model organism to study influenza A virus infection. *Dis Model Mech* **4**, 575-579 (2011).

191. Kuiken, T., van den Brand, J., van Riel, D., Pantin-Jackwood, M. & Swayne, D.E. Comparative pathology of select agent influenza a virus infections. *Vet Pathol* **47**, 893-914 (2010).

192. de Graaf, M. & Fouchier, R.A. Role of receptor binding specificity in influenza A virus transmission and pathogenesis. *EMBO J* **33**, 823-841 (2014).

193. van Riel, D*., et al.* Human and avian influenza viruses target different cells in the lower respiratory tract of humans and other mammals. *Am J Pathol* **171**, 1215-1223 (2007).

194. Lange, E*., et al.* Pathogenesis and transmission of the novel swine-origin influenza virus A/H1N1 after experimental infection of pigs. *J Gen Virol* **90**, 2119-2123 (2009).

195. Lipatov, A.S*., et al.* Domestic pigs have low susceptibility to H5N1 highly pathogenic avian influenza viruses. *PLoS pathogens* **4**, e1000102 (2008).

196. van der Laan, J.W*., et al.* Animal models in influenza vaccine testing. *Expert Rev Vaccines* **7**, 783-793 (2008).

197. Thangavel, R.R. & Bouvier, N.M. Animal models for influenza virus pathogenesis, transmission, and immunology. *J Immunol Methods* **410**, 60-79 (2014).

198. Ibricevic, A*., et al.* Influenza virus receptor specificity and cell tropism in mouse and human airway epithelial cells. *J Virol* **80**, 7469-7480 (2006).

199. Otte, A. & Gabriel, G. 2009 pandemic H1N1 influenza A virus strains display differential pathogenicity in C57BL/6J but not BALB/c mice. *Virulence* **2**, 563-566 (2011).

200. Herfst, S*., et al.* Pandemic 2009 H1N1 influenza virus causes diffuse alveolar damage in cynomolgus macaques. *Vet Pathol* **47**, 1040-1047 (2010).

201. Munster, V.J*., et al.* Pathogenesis and transmission of swine-origin 2009 A(H1N1) influenza virus in ferrets. *Science* **325**, 481-483 (2009).

202. Svitek, N. & von Messling, V. Early cytokine mRNA expression profiles predict Morbillivirus disease outcome in ferrets. *Virology* **362**, 404-410 (2007).

203. von Messling, V., Springfeld, C., Devaux, P. & Cattaneo, R. A ferret model of canine distemper virus virulence and immunosuppression. *J Virol* **77**, 12579-12591 (2003).

204. Bossart, K.N.*, et al.* A neutralizing human monoclonal antibody protects against lethal disease in a new ferret model of acute nipah virus infection. *PLoS Pathog* **5**, e1000642 (2009).

205. Kang, Y.M., Song, B.M., Lee, J.S., Kim, H.S. & Seo, S.H. Pandemic H1N1 influenza virus causes a stronger inflammatory response than seasonal H1N1 influenza virus in ferrets. *Arch Virol* **156**, 759-767 (2011).

206. Maines, T.R.*, et al.* Lack of transmission of H5N1 avian-human reassortant influenza viruses in a ferret model. *Proc Natl Acad Sci U S A* **103**, 12121-12126 (2006).

207. Maher, J.A. & DeStefano, J. The ferret: an animal model to study influenza virus. *Lab Anim (NY)* **33**, 50-53 (2004).

208. Zitzow, L.A.*, et al.* Pathogenesis of avian influenza A (H5N1) viruses in ferrets. *J Virol* **76**, 4420-4429 (2002).

209. van den Brand, J.M.*, et al.* Severity of pneumonia due to new H1N1 influenza virus in ferrets is intermediate between that due to seasonal H1N1 virus and highly pathogenic avian influenza H5N1 virus. *J Infect Dis* **201**, 993-999 (2010).

210. de Jong, M.D.*, et al.* Fatal outcome of human influenza A (H5N1) is associated with high viral load and hypercytokinemia. *Nat Med* **12**, 1203-1207 (2006).

211. Bouvier, N.M. & Lowen, A.C. Animal Models for Influenza Virus Pathogenesis and Transmission. *Viruses* **2**, 1530-1563 (2010).

212. Cameron, C.M.*, et al.* Gene expression analysis of host innate immune responses during Lethal H5N1 infection in ferrets. *J Virol* **82**, 11308-11317 (2008).

213. Fang, Y.*, et al.* Molecular characterization of in vivo adjuvant activity in ferrets vaccinated against influenza virus. *J Virol* **84**, 8369-8388 (2010).

214. Rutigliano, J.A.*, et al.* Screening monoclonal antibodies for cross-reactivity in the ferret model of influenza infection. *J Immunol Methods* **336**, 71-77 (2008).

215. Martel, C.J. & Aasted, B. Characterization of antibodies against ferret immunoglobulins, cytokines and CD markers. *Vet Immunol Immunopathol* **132**, 109-115 (2009).

216. Ochi, A.*, et al.* Cloning, expression and immunoassay detection of ferret IFN-gamma. *Dev Comp Immunol* **32**, 890-897 (2008).

217. Belser, J.A*., et al.* Pathogenesis and transmission of triple-reassortant swine H1N1 influenza viruses isolated before the 2009 H1N1 pandemic. *J Virol* **85**, 1563-1572 (2011).

218. Nakata, M., Itou, T. & Sakai, T. Quantitative analysis of inflammatory cytokines expression in peripheral blood mononuclear cells of the ferret (Mustela putorius furo) using real-time PCR. *Vet Immunol Immunopathol* **130**, 88-91 (2009).

219. Ammersbach, M*., et al.* Laboratory findings, histopathology, and immunophenotype of lymphoma in domestic ferrets. *Vet Pathol* **45**, 663-673 (2008).

220. Hammer, A.S., Williams, B., Dietz, H.H. & Hamilton-Dutoit, S.J. High-throughput immunophenotyping of 43 ferret lymphomas using tissue microarray technology. *Vet Pathol* **44**, 196-203 (2007).

221. Chianini, F., Majo, N., Segales, J., Dominguez, J. & Domingo, M. Immunohistological study of the immune system cells in paraffin-embedded tissues of conventional pigs. *Vet Immunol Immunopathol* **82**, 245-255 (2001).

222. Domenech, N*., et al.* Identification of porcine macrophages with monoclonal antibodies in formalin-fixed, paraffin-embedded tissues. *Vet Immunol Immunopathol* **94**, 77-81 (2003).

223. Ezquerra, A*., et al.* Porcine myelomonocytic markers and cell populations. *Dev Comp Immunol* **33**, 284-298 (2009).

224. Jubala, C.M*., et al.* CD20 expression in normal canine B cells and in canine non-Hodgkin lymphoma. *Vet Pathol* **42**, 468-476 (2005).

225. Engel, P., Gomez-Puerta, J.A., Ramos-Casals, M., Lozano, F. & Bosch, X. Therapeutic targeting of B cells for rheumatic autoimmune diseases. *Pharmacol Rev* **63**, 127-156 (2011).

226. Chaves, A.J*., et al.* Neuropathogenesis of a highly pathogenic avian influenza virus (H7N1) in experimentally infected chickens. *Vet Res* **42**, 106 (2011).

227. van der Loos, C.M. Multiple immunoenzyme staining: methods and visualizations for the observation with spectral imaging. *J Histochem Cytochem* **56**, 313-328 (2008).

228. Li, Z*., et al.* Cloned ferrets produced by somatic cell nuclear transfer. *Dev Biol* **293**, 439-448 (2006).

229. Stevens, A.L., J. (ed.) *Human Histology*, 464 (Elsevier, 25005).

230. Canfield, P.J., Day, M.J., Gavier-Widen, D., Hewinson, R.G. & Chambers, M.A. Immunohistochemical characterization of tuberculous and non-tuberculous lesionsin naturally infected European badgers (Meles meles). *J Comp Pathol* **126**, 254-264 (2002).

231. Abbas, A.K.L., A. H. (ed.) *Cellular and molecular Immunology*, (Elsevier, 2004).

232. Kipar, A.*, et al.* Morphologic features and development of granulomatous vasculitis in feline infectious peritonitis. *Vet Pathol* **42**, 321-330 (2005).

233. Uchida, J.*, et al.* Mouse CD20 expression and function. *Int Immunol* **16**, 119-129 (2004).

234. Rehg, J.E., Bush, D. & Ward, J.M. The utility of immunohistochemistry for the identification of hematopoietic and lymphoid cells in normal tissues and interpretation of proliferative and inflammatory lesions of mice and rats. *Toxicol Pathol* **40**, 345-374 (2012).

235. Banchereau, J. & Steinman, R.M. Dendritic cells and the control of immunity. *Nature* **392**, 245-252 (1998).

236. Munoz-Fernandez, R.*, et al.* Follicular dendritic cells are related to bone marrow stromal cell progenitors and to myofibroblasts. *J Immunol* **177**, 280-289 (2006).

237. Cunningham, A.C.*, et al.* Constitutive expression of MHC and adhesion molecules by alveolar epithelial cells (type II pneumocytes) isolated from human lung and comparison with immunocytochemical findings. *J Cell Sci* **107 (Pt 2)**, 443-449 (1994).

238. Holling, T.M., Schooten, E. & van Den Elsen, P.J. Function and regulation of MHC class II molecules in T-lymphocytes: of mice and men. *Hum Immunol* **65**, 282-290 (2004).

239. Shortman, K. & Liu, Y.J. Mouse and human dendritic cell subtypes. *Nat Rev Immunol* **2**, 151-161 (2002).

240. Unanue, E.R. & Allen, P.M. The basis for the immunoregulatory role of macrophages and other accessory cells. *Science* **236**, 551-557 (1987).

241. Perez, J.*, et al.* Immunohistochemical characterization of hemangiopericytomas and other spindle cell tumors in the dog. *Vet Pathol* **33**, 391-397 (1996).

242. Pileri, S.A.*, et al.* Tumours of histiocytes and accessory dendritic cells: an immunohistochemical approach to classification from the International Lymphoma Study Group based on 61 cases. *Histopathology* **41**, 1-29 (2002).

243. Fend, F.*, et al.* Phenotype and topography of human thymic B cells. An immunohistologic study. *Virchows Arch B Cell Pathol Incl Mol Pathol* **60**, 381-388 (1991).

244. Finke, D., Baribaud, F., Diggelmann, H. & Acha-Orbea, H. Extrafollicular plasmablast B cells play a key role in carrying retroviral infection to peripheral organs. *J Immunol* **166**, 6266-6275 (2001).

245. Isaacson, P.G., Norton, A.J. & Addis, B.J. The human thymus contains a novel population of B lymphocytes. *Lancet* **2**, 1488-1491 (1987).

246. Marafioti, T.*, et al.* Phenotype and genotype of interfollicular large B cells, a subpopulation of lymphocytes often with dendritic morphology. *Blood* **102**, 2868-2876 (2003).

247. Denzer, K.*, et al.* Follicular dendritic cells carry MHC class II-expressing microvesicles at their surface. *J Immunol* **165**, 1259-1265 (2000).

248. Brandtzaeg, P., Dale, I. & Gabrielsen, T.O. The leucocyte protein L1 (calprotectin): usefulness as an immunohistochemical marker antigen and putative biological function. *Histopathology* **21**, 191-196 (1992).

249. Louie, J.K.*, et al.* Factors associated with death or hospitalization due to pandemic 2009 influenza A(H1N1) infection in California. *JAMA* **302**, 1896-1902 (2009).

250. Rodriguez, A.*, et al.* Characterization in vitro and in vivo of a pandemic H1N1 influenza virus from a fatal case. *PLoS One* **8**, e53515 (2013).

251. Blazejewska, P.*, et al.* Pathogenicity of different PR8 influenza A virus variants in mice is determined by both viral and host factors. *Virology* **412**, 36-45 (2011).

252. Juno, J., Fowke, K.R. & Keynan, Y. Immunogenetic factors associated with severe respiratory illness caused by zoonotic H1N1 and H5N1 influenza viruses. *Clin Dev Immunol* **2012**, 797180 (2012).

253. Reed, L.J.a.M., H. A simple method of estimating fifty per cent endpoints. *American Journal of Higiene* **27**, 493-497 (1938).

254. Haines, D.M. & Chelack, B.J. Technical considerations for developing enzyme immunohistochemical staining procedures on formalin-fixed paraffin-embedded tissues for diagnostic pathology. *J Vet Diagn Invest* **3**, 101-112 (1991).

255. Busquets, N.*, et al.* Experimental infection with H1N1 European swine influenza virus protects pigs from an infection with the 2009 pandemic H1N1 human influenza virus. *Vet Res* **41**, 74 (2010).

256. Fronhoffs, S.*, et al.* A method for the rapid construction of cRNA standard curves in quantitative real-time reverse transcription polymerase chain reaction. *Mol Cell Probes* **16**, 99-110 (2002).

257. NCBI. NCBI nucleotide database

258. Belser, J.A.*, et al.* Pathogenesis of pandemic influenza A (H1N1) and triple-reassortant swine influenza A (H1) viruses in mice. *J Virol* **84**, 4194-4203 (2010).

259. Baumeister, E.*, et al.* Molecular characterization of severe and mild cases of influenza A (H1N1) 2009 strain from Argentina. *Medicina (B Aires)* **70**, 518-523 (2010).

260. Tisoncik, J.R.*, et al.* Into the eye of the cytokine storm. *Microbiol Mol Biol Rev* **76**, 16-32 (2012).

261. Seki, M.*, et al.* Critical role of IL-1 receptor-associated kinase-M in regulating chemokine-dependent deleterious inflammation in murine influenza pneumonia. *J Immunol* **184**, 1410-1418 (2010).

262. Monsalvo, A.C*., et al.* Severe pandemic 2009 H1N1 influenza disease due to pathogenic immune complexes. *Nat Med* **17**, 195-199 (2011).

263. Teijaro, J.R*., et al.* Endothelial cells are central orchestrators of cytokine amplification during influenza virus infection. *Cell* **146**, 980-991 (2011).

264. Nakamura, R*., et al.* Interleukin-15 is critical in the pathogenesis of influenza a virus-induced acute lung injury. *J Virol* **84**, 5574-5582 (2010).

265. Beilharz, M.W., Cummins, J.M. & Bennett, A.L. Protection from lethal influenza virus challenge by oral type 1 interferon. *Biochem Biophys Res Commun* **355**, 740-744 (2007).

266. Haagmans, B.L*., et al.* Pegylated interferon-alpha protects type 1 pneumocytes against SARS coronavirus infection in macaques. *Nat Med* **10**, 290-293 (2004).

267. Vercammen, E., Staal, J. & Beyaert, R. Sensing of viral infection and activation of innate immunity by toll-like receptor 3. *Clin Microbiol Rev* **21**, 13-25 (2008).

268. Le Goffic, R*., et al.* Detrimental contribution of the Toll-like receptor (TLR)3 to influenza A virus-induced acute pneumonia. *PLoS pathogens* **2**, e53 (2006).

269. Lee, N*., et al.* Role of human Toll-like receptors in naturally occurring influenza A infections. *Influenza Other Respir Viruses* **7**, 666-675 (2013).

270. Majde, J.A., Kapas, L., Bohnet, S.G., De, A. & Krueger, J.M. Attenuation of the influenza virus sickness behavior in mice deficient in Toll-like receptor 3. *Brain Behav Immun* **24**, 306-315 (2010).

271. Yang, P*., et al.* Characterization of the 2009 pandemic A/Beijing/501/2009 H1N1 influenza strain in human airway epithelial cells and ferrets. *PLoS One* **7**, e46184 (2012).

272. Moret, I*., et al.* Increased lung neutrophil apoptosis and inflammation resolution in nonresponding pneumonia. *Eur Respir J* **38**, 1158-1164 (2011).

273. Bordon, J.M*., et al.* Cytokines and neutrophils responses in influenza pneumonia. *Infection* **41**, 1021-1024 (2013).

274. Hurt, A.C. The epidemiology and spread of drug resistant human influenza viruses. *Curr Opin Virol* **8C**, 22-29 (2014).

275. Krumbholz, A*., et al.* High prevalence of amantadine resistance among circulating European porcine influenza A viruses. *J Gen Virol* **90**, 900-908 (2009).

276. Yi, H*., et al.* Oseltamivir-resistant pandemic (H1N1) 2009 virus, South Korea. *Emerg Infect Dis* **16**, 1938-1942 (2010).

277. Herlocher, M.L*., et al.* Influenza viruses resistant to the antiviral drug oseltamivir: transmission studies in ferrets. *J Infect Dis* **190**, 1627-1630 (2004).

278. Ives, J.A.*, et al.* The H274Y mutation in the influenza A/H1N1 neuraminidase active site following oseltamivir phosphate treatment leave virus severely compromised both in vitro and in vivo. *Antiviral Res* **55**, 307-317 (2002).

279. Moscona, A. Global transmission of oseltamivir-resistant influenza. *N Engl J Med* **360**, 953-956 (2009).

280. Bloom, J.D., Gong, L.I. & Baltimore, D. Permissive secondary mutations enable the evolution of influenza oseltamivir resistance. *Science* **328**, 1272-1275 (2010).

281. Hurt, A.C.*, et al.* Characteristics of a widespread community cluster of H275Y oseltamivir-resistant A(H1N1)pdm09 influenza in Australia. *J Infect Dis* **206**, 148-157 (2012).

282. Takashita, E.*, et al.* A community cluster of influenza A(H1N1)pdm09 virus exhibiting cross-resistance to oseltamivir and peramivir in Japan, November to December 2013. *Euro Surveill* **19**(2014).

283. Kwon, D., Shin, K., Kim, S.J., Lee, J.Y. & Kang, C. Mammalian pathogenesis of oseltamivir-resistant pandemic (H1N1) 2009 influenza virus isolated in South Korea. *Virus Res* **185**, 41-46 (2014).

284. Seibert, C.W.*, et al.* Oseltamivir-resistant variants of the 2009 pandemic H1N1 influenza A virus are not attenuated in the guinea pig and ferret transmission models. *J Virol* **84**, 11219-11226 (2010).

285. Memoli, M.J.*, et al.* Multidrug-resistant 2009 pandemic influenza A(H1N1) viruses maintain fitness and transmissibility in ferrets. *J Infect Dis* **203**, 348-357 (2010).

286. Poole, E., Elton, D., Medcalf, L. & Digard, P. Functional domains of the influenza A virus PB2 protein: identification of NP- and PB1-binding sites. *Virology* **321**, 120-133 (2004).

287. Tarendeau, F.*, et al.* Host determinant residue lysine 627 lies on the surface of a discrete, folded domain of influenza virus polymerase PB2 subunit. *PLoS pathogens* **4**, e1000136 (2008).

288. Asano, Y. & Ishihama, A. Identification of two nucleotide-binding domains on the PB1 subunit of influenza virus RNA polymerase. *Journal of biochemistry* **122**, 627-634 (1997).

289. Guu, T.S., Dong, L., Wittung-Stafshede, P. & Tao, Y.J. Mapping the domain structure of the influenza A virus polymerase acidic protein (PA) and its interaction with the basic protein 1 (PB1) subunit. *Virology* **379**, 135-142 (2008).

290. Ye, Q., Krug, R.M. & Tao, Y.J. The mechanism by which influenza A virus nucleoprotein forms oligomers and binds RNA. *Nature* **444**, 1078-1082 (2006).

291. Sriwilaijaroen, N. & Suzuki, Y. Molecular basis of the structure and function of H1 hemagglutinin of influenza virus. *Proceedings of the Japan Academy. Series B, Physical and biological sciences* **88**, 226-249 (2012).

292. Shtyrya, Y.A., Mochalova, L.V. & Bovin, N.V. Influenza virus neuraminidase: structure and function. *Acta naturae* **1**, 26-32 (2009).

293. Leang, S.K.*, et al.* Influenza antiviral resistance in the Asia-Pacific region during 2011. *Antiviral Res* **97**, 206-210 (2013).

294. Okomo-Adhiambo, M.*, et al.* Drug susceptibility surveillance of influenza viruses circulating in the United States in 2011-2012: application of the WHO antiviral working group criteria. *Influenza Other Respir Viruses* **8**, 258-265 (2013).

295. Goka, E.A., Vallely, P.J., Mutton, K.J. & Klapper, P.E. Mutations associated with severity of the pandemic influenza A(H1N1)pdm09 in humans: a systematic review and meta-analysis of epidemiological evidence. *Arch Virol* **159**, 3167-3183 (2014).

296. Renzette, N.*, et al.* Evolution of the influenza A virus genome during development of oseltamivir resistance in vitro. *J Virol* **88**, 272-281 (2014).

297. Butler, J.*, et al.* Estimating the fitness advantage conferred by permissive neuraminidase mutations in recent oseltamivir-resistant A(H1N1)pdm09 influenza viruses. *PLoS pathogens* **10**, e1004065 (2014).

298. Gabay, C. & Kushner, I. Acute-phase proteins and other systemic responses to inflammation. *N Engl J Med* **340**, 448-454 (1999).

299. Huang, Y.*, et al.* Innate and adaptive immune responses in patients with pandemic influenza A(H1N1)pdm09. *Arch Virol* **158**, 2267-2272 (2013).

300. Huang, S.S.*, et al.* Differential pathological and immune responses in newly weaned ferrets are associated with a mild clinical outcome of pandemic 2009 H1N1 infection. *J Virol* **86**, 13187-13201 (2012).

301. Kuiken, T., Riteau, B., Fouchier, R.A. & Rimmelzwaan, G.F. Pathogenesis of influenza virus infections: the good, the bad and the ugly. *Curr Opin Virol* **2**, 276-286 (2012).

302. Huang, Y.*, et al.* Temporal dynamics of host molecular responses differentiate symptomatic and asymptomatic influenza a infection. *PLoS Genet* **7**, e1002234 (2011).

303. Short, K.R., Kroeze, E.J., Fouchier, R.A. & Kuiken, T. Pathogenesis of influenza-induced acute respiratory distress syndrome. *Lancet Infect Dis* **14**, 57-69 (2014).

304. Sanders, C.J., Doherty, P.C. & Thomas, P.G. Respiratory epithelial cells in innate immunity to influenza virus infection. *Cell Tissue Res* **343**, 13-21 (2011).

305. Vidana, B.*, et al.* Heterogeneous pathological outcomes after experimental pH1N1 influenza infection in ferrets correlate with viral replication and host immune responses in the lung. *Vet Res* **45**, 85 (2014).

306. Iwasaki, A. & Pillai, P.S. Innate immunity to influenza virus infection. *Nat Rev Immunol* **14**, 315-328 (2014).

307. Alexopoulou, L., Holt, A.C., Medzhitov, R. & Flavell, R.A. Recognition of double-stranded RNA and activation of NF-kappaB by Toll-like receptor 3. *Nature* **413**, 732-738 (2001).

308. Edelmann, K.H.*, et al.* Does Toll-like receptor 3 play a biological role in virus infections? *Virology* **322**, 231-238 (2004).

309. Akira, S., Uematsu, S. & Takeuchi, O. Pathogen recognition and innate immunity. *Cell* **124**, 783-801 (2006).

310. Pichlmair, A.*, et al.* RIG-I-mediated antiviral responses to single-stranded RNA bearing 5'-phosphates. *Science* **314**, 997-1001 (2006).

311. Wisskirchen, C., Ludersdorfer, T.H., Muller, D.A., Moritz, E. & Pavlovic, J. The cellular RNA helicase UAP56 is required for prevention of double-stranded RNA formation during influenza A virus infection. *J Virol* **85**, 8646-8655 (2011).

312. Fischer, S.*, et al.* Extracellular RNA promotes leukocyte recruitment in the vascular system by mobilising proinflammatory cytokines. *Thromb Haemost* **108**, 730-741 (2012).

313. Yao, L., Korteweg, C., Hsueh, W. & Gu, J. Avian influenza receptor expression in H5N1-infected and noninfected human tissues. *FASEB J* **22**, 733-740 (2008).

314. Klenk, H.D. Infection of the endothelium by influenza viruses. *Thromb Haemost* **94**, 262-265 (2005).

315. Armstrong, S.M., Mubareka, S. & Lee, W.L. The lung microvascular endothelium as a therapeutic target in severe influenza. *Antiviral Res* **99**, 113-118 (2013).

316. Armstrong, S.M., Darwish, I. & Lee, W.L. Endothelial activation and dysfunction in the pathogenesis of influenza A virus infection. *Virulence* **4**, 537-542 (2013).

317. Armstrong, S.M.*, et al.* Influenza infects lung microvascular endothelium leading to microvascular leak: role of apoptosis and claudin-5. *PLoS One* **7**, e47323 (2012).

318. Hiyoshi, M.*, et al.* Influenza A virus infection of vascular endothelial cells induces GSK-3beta-mediated beta-catenin degradation in adherens junctions, with a resultant increase in membrane permeability. *Arch Virol* **160**, 225-234 (2015).

319. Wang, S.*, et al.* Influenza virus-cytokine-protease cycle in the pathogenesis of vascular hyperpermeability in severe influenza. *J Infect Dis* **202**, 991-1001 (2010).

320. Sumikoshi, M.*, et al.* Human influenza virus infection and apoptosis induction in human vascular endothelial cells. *J Med Virol* **80**, 1072-1078 (2008).

321. Frensing, T., Pflugmacher, A., Bachmann, M., Peschel, B. & Reichl, U. Impact of defective interfering particles on virus replication and antiviral host response in cell culture-based influenza vaccine production. *Appl Microbiol Biotechnol* **98**, 8999-9008 (2014).

322. Tscherne, D.M. & Garcia-Sastre, A. Virulence determinants of pandemic influenza viruses. *J Clin Invest* **121**, 6-13 (2011).

323. Garcia-Sastre, A. Induction and evasion of type I interferon responses by influenza viruses. *Virus Res* **162**, 12-18 (2011).

324. Oshansky, C.M. & Thomas, P.G. The human side of influenza. *J Leukoc Biol* **92**, 83-96 (2012).

325. Fend, F. & Raffeld, M. Laser capture microdissection in pathology. *J Clin Pathol* **53**, 666-672 (2000).

326. Isenberg, G., Bielser, W., Meier-Ruge, W. & Remy, E. Cell surgery by laser micro-dissection: a preparative method. *J Microsc* **107**, 19-24 (1976).

327. Fink, L.*, et al.* Real-time quantitative RT-PCR after laser-assisted cell picking. *Nat Med* **4**, 1329-1333 (1998).

328. Hiller, T., Snell, L. & Watson, P.H. Microdissection RT-PCR analysis of gene expression in pathologically defined frozen tissue sections. *Biotechniques* **21**, 38-40, 42, 44 (1996).

329. Liu, H.*, et al.* Laser capture microdissection for the investigative pathologist. *Vet Pathol* **51**, 257-269 (2014).

330. Hicks, D.J.*, et al.* Cytokine Expression at Different Stages of Influenza A(H1N1)pdm09 Virus Infection in the Porcine Lung, Using Laser Capture Microdissection. *Transbound Emerg Dis* (2014).

331. Patel, V.*, et al.* Proteomic analysis of laser-captured paraffin-embedded tissues: a molecular portrait of head and neck cancer progression. *Clin Cancer Res* **14**, 1002-1014 (2008).

332. Chung, J.Y. & Hewitt, S.M. An optimized RNA extraction method from archival formalin-fixed paraffin-embedded tissue. *Methods Mol Biol* **611**, 19-27 (2010).

333. Dharan, N.J.*, et al.* Infections with oseltamivir-resistant influenza A(H1N1) virus in the United States. *JAMA* **301**, 1034-1041 (2009).

334. Gack, M.U.*, et al.* Influenza A virus NS1 targets the ubiquitin ligase TRIM25 to evade recognition by the host viral RNA sensor RIG-I. *Cell Host Microbe* **5**, 439-449 (2009).

335. Steinberg, B.E., Goldenberg, N.M. & Lee, W.L. Do viral infections mimic bacterial sepsis? The role of microvascular permeability: A review of mechanisms and methods. *Antiviral Res* **93**, 2-15 (2012).

ANNEX

Table 1: Primer sequences.

Gene		Primer Sequence (5´- 3´)	Publication source
pH1N1 (2009)	M+25 M-124 human09 M+64:	F:AGATGAGTCTTCTAACCGAGGTCG R:TGCAAAGACACTTTCCAGTCTCTG Probe:FAM[a]- TCAGGCCCCCTCAAAGCCGA-TAMRA[b]	[255]
	IFNα	F:TCTCCATGTGACAAACCAGAAGA R:CAGAAAGTCCTGAGCACAATTCC	[213]
	IFNγ	F: TCAAAGTGATGAATGATCTCTCACC R: GCCGGGAAACACACTGTGAC	”
	TNFα	F: CCAGATGGCCTCCAACTAATCA R: GGCTTGTCACTTGGAGTTCGA	”
	IL-6	F: AGTGGCTGAAACACGTAACAATTC R: ATGGCCCTCAGGCTGAACT	”
	CCL5	F: GCTGCTTTGCCTACATTTCC R: CCCATTTCTTCTGTGGGTTG	”
	IL8	F: AAGCAGGAAAACTGCCAAGAGA R: GCCAGAAGAAACCTGACCAAAG	”
	CXCL10	F: TTTGAACCAAAGTGCTGTTCTTATC R: CGTGTAGTTCTAGAGAGAGGTACTC	”
	TLR3	F: GATGACCTCCCAGCAAACAT R: GCACAATTCTGGCTCCAGTT	”
	CCL2	F:GCTCCCTATTCACTTGCTGTTTC R:GATTCGATAGCCCTCCAGCTT	[168]
	IFNβ	F: GGTGTATCCTCCAAACTGCTCTCC R: CACTCCACACTGCTGCTGCTTAG	[167]

Gene	Primer Sequence (5´- 3´)	NCBI accession n°
β-actin	F: GCAGGTCATCACCATCG R: TGGAGTTGAAGGTGGTCT	[Genbank: AF038150]
IL-1α	F: GGGAAACTACCTCATGGC R: TAGAGTCACAGGAAATTTAGAATCTT	[Genbank:JP011578]
CCL3	F: GGTCTTCTCTGCACCAT R: CCAGGCTTGGAGCATTG	[Genbank:JP007133]
CASP8	F: TTATGACTTTAGCATAGCACGGA R: GTCTCTGAAAGGCACGAT	[Genbank:JP006891]
BAX	F: CTGGACAGTAACATGGAGTTACA R: CAAAGTAGAAGAGGGCAACGA	[Genbank:JP006358]
RIG-I	F: AGAGCACTTGTGGACGCTTT R: TGCAATGTCAATGCCTTCAT	[Genbank: EU836024.1]
SELPLG	F: CCGCATCCCTGTGAAAC R: GTGATTCTTGCGGGAGAG	[Genbank:XM4824948.1]